Heterogenization of Schiff base complexes on mesoporous silica and their application as catalysts in the oxidative transformation of alcohols

By

Corli Joubert

A dissertation submitted in fulfilment of the requirements for the degree of M.Sc. in Chemistry in the Department of Chemistry and Polymer Science,
Stellenbosch University

Supervisor: Prof. S. F. Mapolie

December 2012

DECLARATION

I, Corli Joubert, declare that **"Heterogenization of Schiff base complexes on mesoporous silica and their application as catalysts in the oxidative transformation of alcohols"** is my own work and that all sources I have used or quoted have been acknowledged by means of complete references.

……

Corli Joubert

ABSTRACT

In this thesis the synthesis of a range of model and siloxane functionalized salicylaldimine ligands and [N-(*n*-propyl)-(2-pyridyl)] diimine ligands are described. The functionalized ligands were obtained by the reaction of salicylaldehyde and 2-pyridinecarboxaldehyde with 3-aminopropyltriethyoxysilane. All ligands were characterized by FT-IR and ^{1}H NMR spectroscopy. The salicylaldimine ligands were reacted with either Cu(II) or Pd(II) salts to form both the model and functionalized Cu(II) and Pd(II) complexes. The Cu(II) complexes were characterized using FT-IR, EPR and UV-VIS spectroscopy while the Pd(II) complexes were characterized using FT-IR, ^{1}H NMR and ^{13}C{^{1}H} NMR spectroscopy. The diimine ligands were reacted with Cu(II) salts to form functionalized pyridinyl complexes which were characterized used FT-IR spectroscopy.

Two mesoporous silica supports, MCM-41 and SBA-15 were synthesized. The siloxane functionalized salicylaldimine Cu(II) and Pd(II) complexes were immobilized onto these supports to produce heterogenized catalysts. These catalysts were characterized using a range of solid-state techniques: BET nitrogen adsorption/desorption, scanning electron microscopy (SEM), thermal gravimetric analysis (TGA), ICP-AES, and powder X-ray diffraction (XRD) analysis. The powder XRD and SEM analysis showed that the structural integrity of the catalyst supports was kept intact during the immobilization process. BET analysis and ICP-AES showed that the complexes had been attached to the silica supports.

Both the model complexes and heterogenized catalyst systems were tested in the oxidation of benzyl alcohol to benzaldehyde. The model copper catalyst showed high activity in this reaction with molecular oxygen used as oxidant and the (2,2,6,6-tetramethylpiperidin-1-yl)oxyl radical as co-oxidant. The immobilized copper complexes showed low activity in the same reaction. This was attributed to steric hindrance around the active site dye to its entrapment with the silica matrix thus hindering the formation of a key intermediate in the oxidation cycle due to steric hindrance. The palladium complexes were not active in the oxidation reaction when molecular oxygen was used as oxidant, but showed slight activity when hydrogen peroxide was used.

OPSOMMING

In hierdie tesis word die sintese van ‘n reeks model sowel as gefunksioneerde salisielaldemien ligande en [N-(n-propiel)-(2-piridiel)] di-imien ligande beskryf. Die gefunksioneerde ligande is verkry deur die reaksie van salisielaldehied en en 2-piridienaldehied met 3-aminopropieltriëtoksiesilaan. Al die ligande is gekarakteriseer deur FT-IR en ^{1}H-KMR spektroskopie. Die salisielaldimien ligande is met óf Cu(II) óf Pd(II) soute reageer om beide die model en gefunksioneerde Cu(II) en Pd(II) komplekse te vorm. Die Cu(II) komplekse is gekarakteriseer deur FT-IR, EPR en UV-Vis spektroskopie terwyl die Pd(II) komplekse deur FT-IR, ^{1}H-KMR en ^{13}C{^{1}H}-KMR spektroskopie gekarakteriseer is. Die di-imien ligande is met Cu(II) soute reageer om gefunksioneerde piridinielkompekse te vorm wat deur FT-IR spektroskopie gekarakteriseer is.

Twee mesoporeuse silika draers, MCM-41 en SBA-15 is gesintetiseer. Die siloksaan-gefunksioneerde salisielaldemien Cu(II) en Pd(II) komplekse is op hierdie draers geimobiliseer om geheterogeniseerde katalisatore te vorm. Hierdie katalisatore is gekarakteriseer deur van ‘n wye reeks vaste toestand tegnieke gebruik te maak: BET stikstof adsorpsie/desorpsie, skandeer elektron mikroskopie (SEM), termiese gravimetriese analise (TGA), ICP-AES en poeier-XRD analise. Die poeier-XRD en SEM analisies het aangetoon dat die strukturele integriteit van die katalisator draers behoue gebly het tydens die immobiliseringsproses. BET analise en ICP-AES het aangetoon dat die komplekse aan die silika draers geheg is.

Beide die model komplekse en geimobiliseerde katalisators is getoets in die oksidasie van bensielalkohol na bensaldehied. Die model Cu(II) katalisator het hoë aktiwiteit in hierdie reaksie getoon met molekulêre suurstof as oksideermiddel en die (2,2,6,6-tetrametielpipiridien-1-iel)oksiel radikaal as ko-oksideermiddel. Die geimobiliseerde Cu(II) komplekse het lae aktiwiteit in dieselfde reaksie getoon. Dit is toegeskryf aan steriese hindernis rondom die aktiewe sentrum as gevolg van die verstrikking binne die silika matrys, wat die vorming van ‘n belangrike tussentoestand in die oksidasie-siklus verhinder. Die Pd(II) komplekse was nie aktief in die oksidasie-reaksie in die geval waar molekulêre suurstof as oksideermiddel gebruik is nie, maar het effense aktiwiteit getoon waneer waterstofperoksied gebruik is.

ACKNOWLEDGEMENTS

I would like to thank my supervisor, Prof Selwyn Mapolie, for his patient guidance and support during this project.

I would also like to thank my past and present colleagues from the Organometallic Research Group at Stellenbosch University for their friendship and support within and outside of the academic environment: Hennie Kotze, Derik Wilbers, Danie van Niekerk, Andrew Swarts, Angelique Blanckenberg, Manana Moletsane and Drs Douglas Onyancha, Gangadhar Bagihalli, Jane Mugo and Feng Zheng.

I would like to thank to the staff and technical assistants of the Department of Chemistry and Polymer Science of Stellenbosch University, especially the CAF group for assisting with various analytical techniques. A special word of thanks also goes to Mr Malcolm Taylor for his invaluable assistance.

I would like to thank my mentor at Sasol, Elzet Grobler, for her interest and guidance for the duration of this project. I would also like to thank Sasol for financial support.

Lastly I would like to thank my family and friends, especially Jedri Visser, for their encouragement and support throughout the project.

CONFERENCE CONTRIBUTIONS

Corli Joubert and Selwyn Mapolie

Oral Presentation Titled: **Heterogenization of Schiff base complexes on mesoporous silica and their application as catalysts in the oxidative transformation of alcohols**

Catalysis Society of South Africa (CATSA), Cape Town (Club Mykonos), South Africa, 2012.

TABLE OF CONTENT

LIST OF FIGURES

Chapter One

Chapter Two

Chapter Three

Chapter Four

LIST OF SCHEMES

Chapter One

Chapter Two

Chapter Three

Chapter Four

LIST OF TABLES

Chapter Two

Chapter Three

ABBREVIATIONS

µM	micromolar
Å	Ångstrom
ATR	attenuated total reflectance
BET	Brunauer-Emmett-Teller
bis-phen	bis-phenanthroline
BJH	Barret-Joyner-Halenda
cm^{-1}	wavenumber
CP	cross polarization
CTAB	cetyl trimethylammonium bromide
d	doublet
DCM	dichloromethane
EPR	electron paramagnetic resonance
ESI	electronspray ionization
EtOH	ethanol
FT-IR	Fourier Transform infrared spectroscopy
g	grams
GC	gas chromatography
h	hours

HPLC	high performance liquid chromatography
HPWA	phosphotungstic acid
Hz	Hertz
ICP-AES	inductively coupled plasma atomic emission spectroscopy
m	multiplet
MAS	magic angle spinning
MCM	Mobil crystalline material
mL	milliliters
MLCT	metal-to-ligand charge transfer
min.	minute
mmol	millimole
mol	mole
MS	mass spectrometery
MSU	Michigan State University
nm	nanometer
NMR	nuclear magnetic resonance
PEG	polyethyleneglycol
ppm	chemical shift
RCM	ring-closing metathesis
ROMP	ring-opening metathesis polymerization

s	singlet
SBA	Santa Barbara amorphous
SEM	scanning electron microscopy
sol-gel	solution/gelation
t	triplet
TEMPO	2,2,6,6-tetramethylpiperidin-1-yl)oxyl
TEOS	tetraethylorthosilicate
THF	tetrahydrofuran
TEM	transmission electron microscopy
TEOS	tetra-ethylorthosilicate
TGA	thermogravimetric analysis
TOF	turnover frequency
UV/Vis	ultraviolet/visible
VPI	Virginia Polytechnic Institute
XRD	X-ray diffraction

Chapter 1: Literature Review of Immobilized Catalysts

1. Introduction

Numerous chemical synthesis pathways rely on a catalytic transformation in one or more steps. The shift towards green chemistry and the environmental impact of chemical processes has recently become an important factor in the design of catalyst systems.[1,2] In particular, the reuseability and ease of recovery of a catalyst can minimize the impact of the process on the environment.[3]

The synthesis of fine chemicals, in particular, utilize homogeneous catalyst systems, since the yield and selectivity obtained using homogeneous catalysts are usually superior to that of heterogeneous catalysts. However, homogeneous systems suffer from two major drawbacks: The separation of the catalyst from the product mixture and the subsequent recovery and re-use of the catalyst. In the process of separating the desired product from the catalyst, organic solvents are commonly used and chemical waste is created. This is in contrast with the first and fifth principles of green chemistry, which focus on the minimization of waste and auxiliary substances.[1] As an added drawback, the catalyst is usually destroyed in this process.

A possible solution to this problem is to use heterogeneous systems instead of homogeneous systems. Heterogeneous catalyst systems have indeed been used for years because of the ease of separation and the ability to regenerate of these systems. There is, however, a major drawback when using these systems: the conversion and selectivity of heterogeneous systems is lower than what can be accomplished when using homogeneous systems.[4]

Over the past two decades, an alternative solution to these problems has been developed – taking a homogeneous catalyst, and 'heterogenizing' it. The idea behind this approach is to have a catalyst system with the desirable characteristics of both homogeneous and heterogeneous catalyst systems. Since the active catalytic site would still be homogeneous in nature, the selectivity and conversion would be comparable with normal homogeneous systems. On the other hand, since the homogeneous catalyst is immobilized on a solid support, the separation and regeneration of the catalyst would be much easier than in a normal homogeneous system. This process, known as heterogenization, has received much attention in recent times.[5]

1.1 Heterogenization of homogeneous catalysts

Considering the advantages of heterogenized catalyst systems, it should come as no surprise that considerable interest in this field has been shown in both academia and industry over the past few decades.[6,7] Various types of materials have been used as supports for homogeneous catalysts in heterogenized systems. These usually fall into one of three groups: inorganic, organic or hybrid materials. Examples of inorganic supports found in the literature include silica and clay, while dendrimers and polymeric ligands are examples of organic supports.[8,9]

The manner in which homogeneous catalysts are immobilized onto these supports can vary. Several methods of non-covalent immobilization are known, but the most used method involves the covalent tethering of homogeneous catalysts to the supports. This method is used with silica supports, as the silanol groups on the surface of the material provides reactive sites for covalent bonding to take place with catalysts functionalized with silane groups.

1.1.1 Non-covalent interaction

1.1.1.1 Adsorption

Catalysts immobilized by adsorption rely on van der Waals interactions. Since these interactions are very weak, leaching into the reaction medium can easily occur. The stability of the system can be improved by modifying the catalyst as well as the support surface to allow the occurrence of hydrogen bonding. Adsorption is often used to immobilize enzymes onto solid supports, as the immobilization of enzymes requires mild conditions to avoid denaturation.[10]

1.1.1.2 Electrostatic interaction

Many porous solids can act as ions exchangers and this presents an opportunity to immobilize catalysts through electrostatic interaction. The amount of leaching that takes place when immobilization occurs through electrostatic interactions rather than simple adsorption is greatly diminished.[11] Figure 1.1 shows an example of a complex heterogenized by electrostatic interaction.

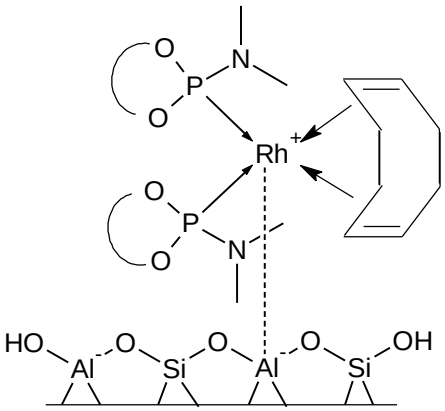

Figure 1.1 Immobilization of a Rh complex through electrostatic interactions[11]

Ion-exchange resins based on polystyrene-divinylbenzene copolymers is an example of a support that can be used. The functional groups on these resins can be modified to allow the immobilization of both anionic and cationic metal complexes.[12]

1.1.1.3 Encapsulation

Encapsulation involves the entrapment of a catalyst in pore spaces where the opening to the pore is smaller than the catalyst itself, making it impossible for the catalyst to be removed from the pore while intact, and would therefore prevent leaching. The encapsulation of catalysts makes it possible to mimic the homogeneous process without having to alter the catalyst structure to have direct interaction with the support.

The supported catalyst can be prepared by either assembling the catalyst inside the pores of the support, or by assembling the support around the already formed catalyst. The approach taken depends on the stability and ease of synthesis of the catalyst. If the catalyst is easy to synthesize, assembling the catalyst inside the support is preferred. If the catalyst is more difficult to make, the support is assembled around the catalyst, provided that the catalyst is stable enough.[13]

A third approach that has gained attention recently is to encapsulate homogeneous catalysts in a sol-gel support.[14] The sol-gel process is a well-known technique that is used in the fields of material science, bioengineering and ceramics.[15,16] It involves the synthesis of materials starting from a chemical solution (known as a sol) which forms an integrated network (known as a gel) of particles or polymers. Metal alkoxides such as $Si(OEt)_4$ are often used as precursors for metal oxides in the sol-gel process.

The sol-gel process can occur in either aqueous or non-aqueous solvents, depending on the solubility of the dopant. If the aqueous route is followed, the solvents used are usually water and an alcohol. Tetrahydrofuran is popular as a solvent for the non-aqueous route. The metal alkoxide and catalyst is

dissolved in the appropriate solvent, and the gel is subsequently formed. This happens as a result of the gel precursors being hydrolyzed and condensed. In the case of silica, the gel consists of a three-dimensional network with nanometer-sized pores.[17]

The catalyst can be at one of three positions in the formed structure: in an accessible pore, in an inaccessible pore or on the surface. Catalyst on the surface can be removed by washing the silica with a good solvent for the catalyst. In one particular study where rhodium-, ruthenium and iridium-phosphine catalysts were encapsulated, a decrease in the catalyst activity was seen after several catalytic runs; this was attributed to clogging of the pores (thus creating more inaccessible pores) and catalytic activity was restored by washing the silica with water and an organic solvent.[18]

1.1.1.4 Covalent tethering

Ordered mesoporous silicas contain silanol groups on the silica surface. These groups make it possible to covalently bind metal complexes to the silica support. Two distinct approaches are used to bind the catalysts to the support: the sequential and the convergent approaches. In the sequential synthesis shown in Scheme 1.1, a carbon tether, such as 3-aminopropyltriethoxysilane, is anchored to the silica support. The ligand is then attached to the tether, followed by the coordination of the metal. A drawback of this method is the difficulty of characterizing the final material. It is therefore not always clear whether it is the actual catalyst or some by-product that has deposited onto the silica performing the reaction.[5]

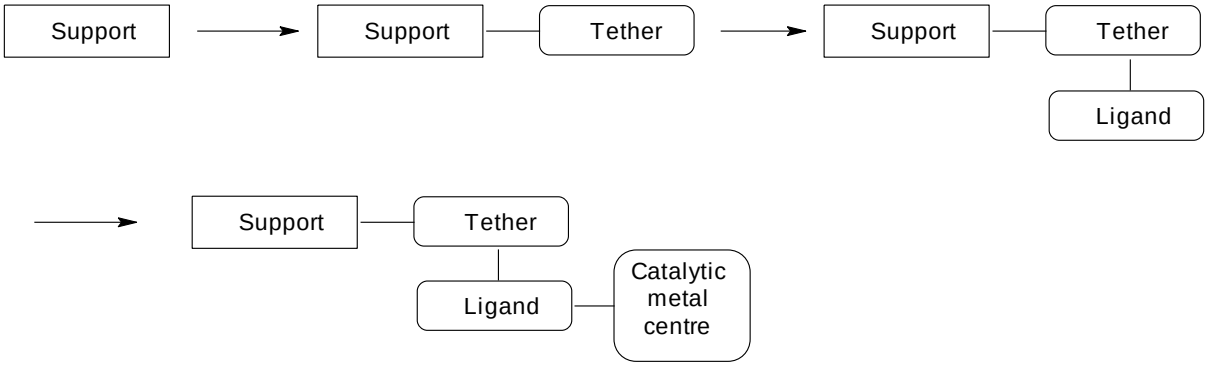

Scheme 1.1 Sequential heterogenization

The convergent approach avoids this problem by following the opposite route. A ligand is functionalized so that it contains a trimethoxy- or triethoxy-silyl group, which can be used to react with the silanol groups. The metal is then coordinated to the ligand. The catalytic species can be purified using conventional methods, and is only then immobilized onto the support. Using this

approach, one can be much more confident of the structure of the actual catalytic centre. This approach is illustrated in Scheme 1.2.

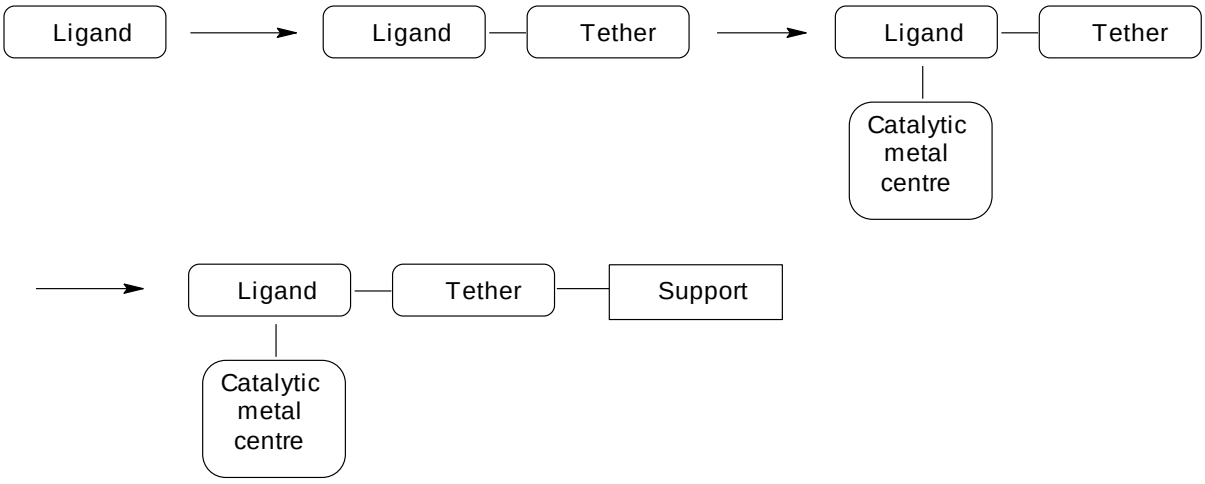

Scheme 1.2 Convergent heterogenization

1.2 Ordered mesoporous silica

Ordered mesoporous silicas are considered as excellent catalyst supports, due to their high surface area, large pore volumes and well ordered arrangement of pores.[19] Two of the most well known ordered mesoporous silicas are MCM-41 and SBA-15. These silicas are synthesized in the presence of surfactants which act as templates around which the silica condenses. The silica can come from various sources such as sodium silicate or tetraethylorthosilicate (TEOS). Reaction conditions such as surfactant type, pH, the silica source used, temperature and reaction time all have an influence on the final silica product. By using different conditions, the nanostructure and mesostructure of the material can be altered.[20]

The silanol groups on the surface of the mesoporous silica make it an excellent material to use as a support in the heterogenization of homogeneous catalysts. The silanol groups on the surface of the silica can be present in three different configurations shown in Figure 1.2.[21]

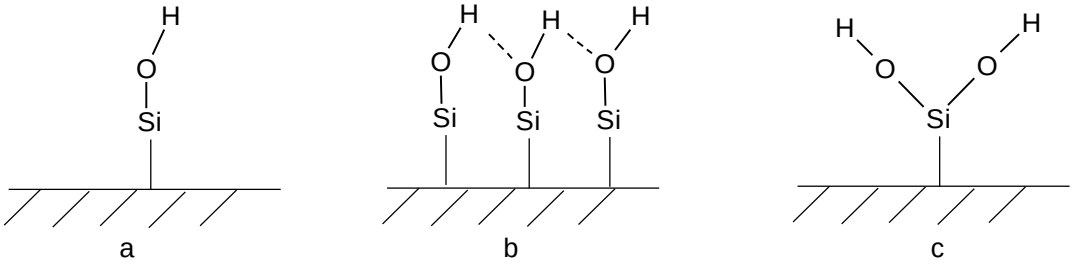

Figure 1.2 Silanol groups present on the surface of a silica support: (a) single, (b) hydrogen bonded and (c) geminal silanol groups[21]

1.2.1 Synthesis of ordered mesoporous silica

One of the earliest types of mesoporous silicas was synthesized in 1992 by the Mobil Corporation. These materials have a periodic structure and were name Mobil Crystalline Materials, or MCM.[22] MCM-41 is the most well known of these materials. Widespread interest in the surfactant template synthesis of mesoporous materials has been shown because of the use of these materials in catalysis and separation technology. Another well known type of mesoporous silica was synthesized some years later at the University of California in Santa Barbara. These materials have larger pores than MCM materials, and are known as Santa Barbara Amorphous or SBA materials.[23]

The synthesis of mesoporous materials has been well studied and reported in literature and is outlined in Scheme 1.3. The formation of the hexagonal pore structure relies on the template molecule having hydrophobic and hydrophilic properties. When an appropriate template molecule is dissolved in water, it forms a micelle with the hydrophobic tails facing inwards and the hydrophilic heads forming the outside surface of the micelle. The micelles then arrange to form a micellar rod. The rods themselves arrange to form a hexagonal array. At this time, a silicate source is added to the reaction mixture and forms a layer on the outside of the micellar rods. After completion of the reaction, the product is washed to get rid of the excess template, dried, and calcined at 500 to 600°C to decompose the template.[24]

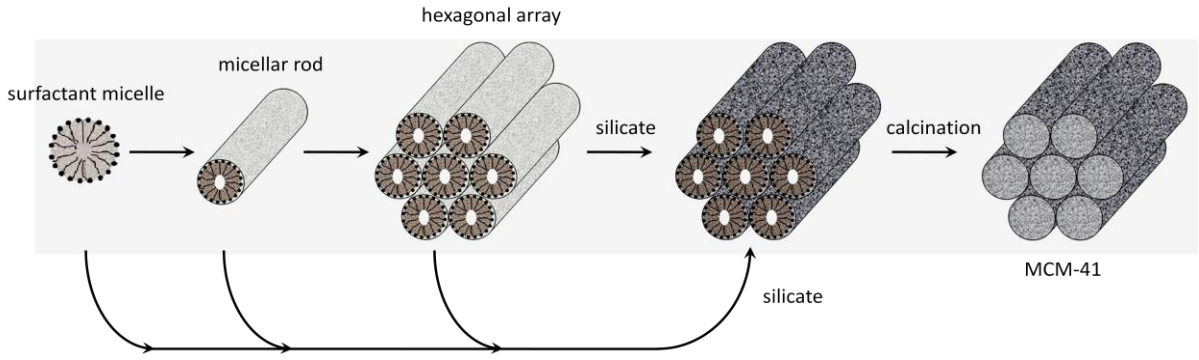

Scheme 1.3 Template synthesis of mesoporous silica

There are some slight differences between the synthesis of MCM-41 and SBA-15 which in the end lead to the different structures of these two materials. The surfactant used in the synthesis of MCM-41 is cetyl trimethylammonium bromide, while SBA-15 uses a poly ethylene glycol block copolymer. There is also a difference in the pH used in the synthesis; MCM-41 is synthesized under basic conditions and SBA-15 under acidic conditions.

1.2.2 Applications of mesoporous materials

Mesoporous silicas have found uses in a wide range of fields, from chemistry and materials science to biology. They are used as supports for enzymes and biocatalysts, as agents for drug delivery, as template agents for mesoporous carbon synthesis, in electrochemical chemistry, as nanoparticle supports and as supports for the heterogenization of homogeneous catalysts.

1.2.2.1 Adsorption of enzymes

Several different proteins have been adsorbed onto ordered mesoporous silica materials with the aim to using these systems as biocatalysts. Adsorbing enzymes onto mesoporous silica can improve the stability of the enzymes under strenuous conditions. Enzymes are usually immobilized *via* non-covalent interactions, since modification of the enzyme to allow covalent bonding can negatively influence the reactive site and lower the enzyme activity. If, however, immobilization *via* covalent bonding is possible without lowering enzyme activity, it will be the preferred method since the probability of leaching will be lower.[25]

It has been shown by Takahashi and coworkers that size-matching of the enzyme and silica pore is an important factor to consider when immobilizing enzymes onto silica.[26] They showed that the loading of horseradish peroxidase (with an approximate diameter of 4.8 nm) was much higher on MCM-41 and FSM-16 (with pore diameters of 5.1 nm and 5.0 nm respectively) than on SBA-15 (with a pore diameter of 9.2 nm). The study goes on to show that enzymatic activity and thermal stability is also higher when the enzyme size matches the pore size.

1.2.2.2 Drug delivery

The regular pores and well-defined surface properties of ordered mesoporous materials make them excellent candidates for use in drug delivery. Both large and small drug molecules can be entrapped in mesoporous silica and liberated *via* a diffusion-controlled mechanism.[25] MCM-41- as well as SBA-15-systems have been studied in this regard.[27,28]

A study by Qu *et al*. has shown that drug loading on MCM-41 could be correlated to BET surface area of the silica as well as the surface hydrophilicity and hydrophobicity of the surface. The release

profile of the water-soluble drug Captopril could be controlled by altering the surface properties and pore size. It was found that the release rate was slower with lesser degree of silylation. Since the degree of silylation can easily be controlled, the drug release rate can be altered so that it takes place over the necessary time period.[29] Several other studies have also pointed to surface modification as a contributing factor to more sustained drug release.[30,31]

1.2.2.3 Template agent for carbon synthesis

Carbon materials with different pore sizes can be synthesized by using microporous and mesoporous materials as templates. The synthesis of ordered mesoporous carbon materials by using a mesoporous silica material as hard template was first reported in 1999.[32] MCM-48, the silica template, was impregnated with sucrose and sulfuric acid. The material was then heated and the sucrose converted to carbon. Finally, the silica template was removed by dissolution to yield the mesoporous carbon.

Since then, different types of mesoporous carbon have been synthesized by making use of various mesoporous silica materials together with different carbon sources, with SBA-15 being particularly prominent as template.[33] The silica template can also undergo pre-treatment, for example hydrothermal treatment or doping with metals, to influence the type of carbon that will form.

1.2.2.4 Use in catalysis

Porous materials have been used as both catalysts and as catalyst supports. Porous materials are classified into one of three types according to pore size: microporous (pore size < 2 nm), mesoporous (2-50 nm) or macroporous (> 50 nm).[34] Zeolites, porous materials with a very well defined pore structure and narrow pore size distribution, have been well studied as catalysts. Among their applications is in the petrochemical industry where they are used as solid acid catalysts, replacing traditional liquid acid catalysts for environmental reasons. Processes where zeolites catalysts are used include fluid catalytic cracking, hydrocracking and various isomerization reactions. Zeolites do have some limitations as catalysts, mainly caused by the small size of the pores. When reactant molecules of a larger size are involved in the catalysis, only the active sites on the outer surface of the zeolites can be involved in the reaction. Attempts have been made to either influence the structure of zeolites during synthesis, or modifying the zeolites after synthesis to overcome these limitations.[35]

Mesoporous materials provide a good alternative to zeolites in cases where the size of the reactants becomes a problem. MCM-41 (pore size 2-3 nm) and SBA-15 (pore size 9 nm) are examples of two well-studied types of mesoporous materials with regards to their use in catalysis. The catalysts systems are either formed by immobilizing a homogeneous catalyst on the support, or by impregnating the support with a metal precursor. There are numerous reports of mesoporous silica

being used as catalyst support in the literature. A few recent examples will be discussed to show the wide scope of mesoporous materials in catalysis.

Karthikeyan and Pandurangan studied supported solid acid catalysts in the synthesis of xanthenediones, which are molecules with important medicinal use. [36] These molecules are usually synthesized from active methylene carbonyl compounds and aldehydes using mineral acids as catalysts, and the aim of the study was to find a more environmentally friendly alternative. They synthesized MCM-41 impregnated with the heteropolyacid HPWA by stirring the desired amount of HPWA and silica gently in water. The HPWA/MCM-41 systems were characterized using XRD, nitrogen adsorption, FT-IR spectroscopy, pyridine-adsorped FT-IR spectroscopy, ^{31}P-MAS-NMR and TEM. Scheme 1.4 shows the synthesis of a xanthenedione.

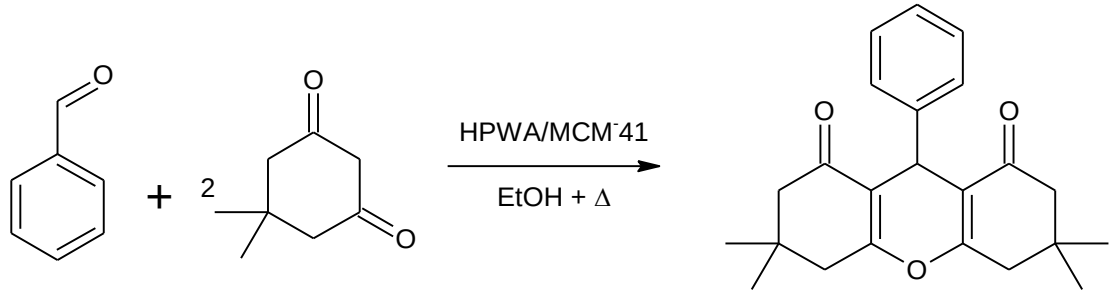

Scheme 1.4 Reaction of benzaldehyde and dimedone[36]

The catalyst systems were then evaluated in the reaction of two mole equivalents of dimedone with one mole equivalent of an aromatic aldehyde in a selected solvent. They found a number of factors influencing the reaction, including the aldehyde used, the solvent, the molar ratio of the reactants and the amount of HPWA impregnated on the MCM-41. For our purposes we will focus only on the latter. The most active catalyst system was impregnated with 20 wt% of HPWA with a yield of 94% of product. The authors reasoned that this amount generates enough active catalytic sites (compared to 10 wt% which gives 71% yield) while still keeping the pore sizes large enough (compared to 30 wt% which gives a yield of 85%). When bulk HPWA was used, the yield was only 75%; the supported catalyst therefore improves upon the yield of the bulk catalyst. The catalyst system shows sufficient recyclability and reusability, with yields of 84% obtained after four uses.

Mesoporous silicas are also used as supports for metal nanoparticles with catalytic properties. Riout *et al.*[37] studied the immobilization of platinum nanoparticles on SBA-15 as catalysts for ethylene hydrogenation and ethane hydrogenolysis. Platinum nanoparticles in a range of 1.7 – 7 nm were synthesized by alcohol reduction methods. These nanoparticles were stabilized on a polymer and characterized by XRD en TEM. The nanoparticles were incorporated into SBA-15 by using low-power sonication. The material was then calcined to remove the supporting polymer. The supported

nanoparticles were characterized by XRD, TEM and gas adsorption methods. TEM images showed a very good dispersion of the particles in the channels of the SBA-15, even for the largest nanoparticles. This was possible due to the relatively large pore size (9 nm) of the channels in SBA-15. They also determined that long sonication times was essential in order to achieve good dispersion of the nanoparticles by varying the sonication times and studying the resulting TEM images.

The activity of these materials were then determined in an ethylene hydrogenation test reaction and the activity compared to that of previously synthesized catalysts. The turnover rates using the Pt/SBA-15 catalyst were identical to a Pt/SiO_2 catalyst synthesized previously. The Pt/SBA-15 catalysts were then tested in an ethane hydrogenolysis reaction. The rates for these reactions were comparable with those obtained using Pt powder and a Pt/ SiO_2 catalyst and it was observed that using smaller particles led to higher turnover frequencies. The thermal stability of the Pt/SBA-15 was excellent under the studied catalytic conditions and the activation energy for the reaction was lower than what was necessary when Pt powder or the Pt/ SiO_2 catalyst was used. The authors also conclude that the synthesis method followed was a good general procedure than can be followed to study various metal/support catalysis systems.

The heterogenization of Rh and Au (NHC)NN-pincer complexes *via* immobilization onto MCM-41 was studied by del Pozo *et al*.[38] These complexes have proven to be excellent catalysts for the hydrogenation of alkenes when used as homogeneous catalysts. A variety of Rh and Au complexes were synthesized with some containing an alkoxide linker group. An example of such a complex is shown in Figure 1.3. These complexes were refluxed in toluene with MCM-41 for 16 hours. The silica underwent a colour change, indicating that immobilization had taken place. Soxhlet extraction for 24 hours ensured that any remaining complex that was not immobilized, was removed. These materials were characterized used SEM, CP/MAS-NMR spectroscopy, FTIR-spectroscopy, elemental analysis and ICP-MS.

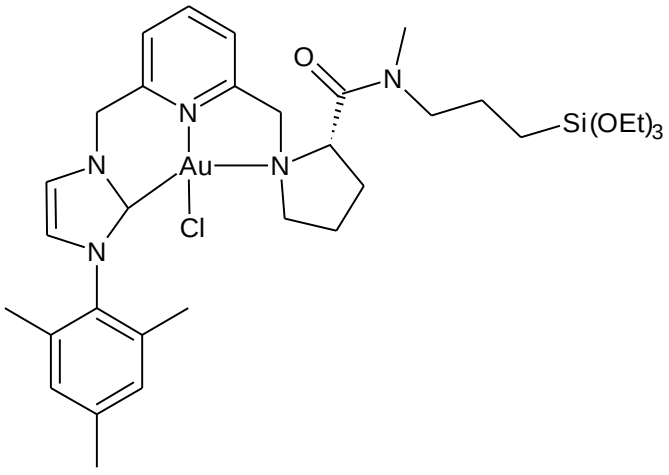

Figure 1.3 Example of a Au(NHC)NN complex with alkoxide linker molecule[38]

The heterogenized systems were tested in the hydrogenation of diethyl itaconate and (E)-diethyl 2-benzylidenesuccinate under standard conditions (EtOH as solvent, 4 atm H_2, 40°C). All the immobilized catalyst systems showed turnover frequencies higher than that of the equivalent homogeneous system for both substrates. It was also observed that the enantioselectivity increased when using the immobilized complexes as opposed to the homogenous catalyst. This led to a conclusion that the confinement effect in the mesoporous support was responsible for the higher enantioselectivity. Recyclability of the catalyst was tested as well. The catalyst showed excellent conversion and enantiomeric selectivity even after four catalytic runs, and no metal leaching was observed.

These few examples illustrate the application of immobilized catalysts in a variety of systems. They highlight the advantages of using immobilized catalysts, and specifically catalysts immobilized on mesoporous silica, over using homogeneous systems. It can be seen that conversion and selectivity can sometimes be improved after immobilization of catalysts. The examples also illustrate some of the problems that can be experienced when using immobilized catalysts. The examples given here are only a very small part of a wide range of similar reports available on this subject in the literature.

1.3 Immobilization of complexes

The covalent immobilization of a complex onto a silica support makes use of the silanol groups that are present on the surface of mesoporous silica materials. An alkoxysilane group is incorporated into the complex that is to be immobilized. The functionality undergoes a condensation reaction with the surface silanol groups, and a covalent bond is formed to complete the immobilization of the complex.

1.3.1 Methods of immobilization

There are numerous reports of both the sequential and convergent method of immobilization of metal complexes onto silica. The method chosen for our investigation is the convergent synthesis method. Both these methods are explained in the following sections, and the reasons for our choice of method will become apparent when one looks at the synthesis methods involved.

1.3.1.1 Sequential immobilization

Sequential immobilization involves the functionalization of the support surface with a tether molecule. This tether molecule contains both the siloxane functionality needed to react with the support surface and the necessary functionality to react with the chosen ligand. After immobilization of the tether molecule, the ligand molecule is added and the immobilized ligand is formed. Finally the

appropriate metal salt is added to form the immobilized metal complex which is then used as a catalyst.

The drawback of using this method is that it is difficult to fully characterize the final catalyst. The particular problem lies with the last step, the addition of the metal salt. It is not possible to know with certainty whether the metal salt reacts with the ligand to form the desired complex or whether it is physically adsorbed onto the surface and in the pores of the support. One cannot, therefore, say with certainty whether the catalysis is facilitated by the metal complex or simply by the adsorbed metal salt. An example of sequential immobilization is shown in Scheme 1.5.

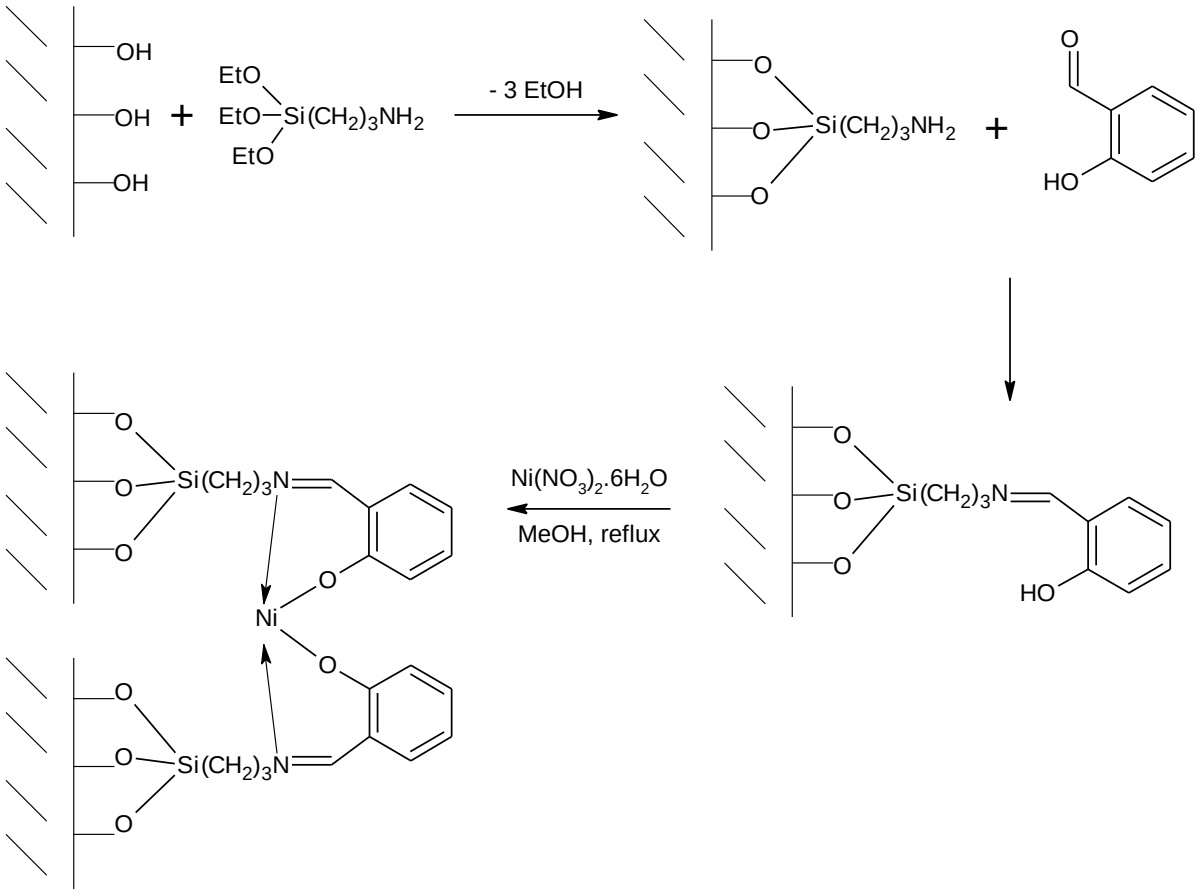

Scheme 1.5 Sequential immobilization as used by Bhunia and Koner[39]

1.3.1.2 Convergent immobilization

The convergent immobilization method involves the synthesis of the functionalized metal complex first. Only after the complex has been characterized is it immobilized onto the silica support. Any metal facilitating catalysis in the system is therefore part of the metal complex system and no

uncoordinated metal is present on the support surface. An example of this type of immobilization can be seen in Scheme 1.6.

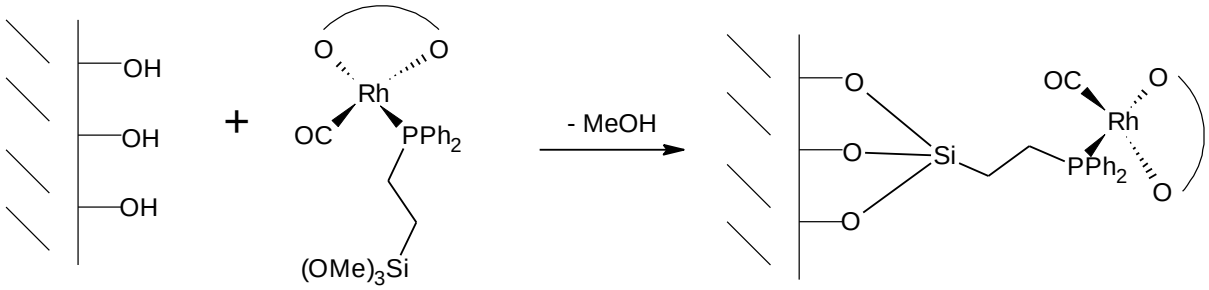

Scheme 1.6 Convergent immobilization as reported by Standfest-Hauser *et al.* [40]

1.3.1.3 Siloxane tethers

A common tethering molecule used in both the convergent and sequential approaches is 3-aminopropyltriethoxysilane, especially when the immobilized complex contains Schiff base ligands. This molecule, while useful, limits the scope of the possible complexes, especially with regards to the substitution of the chelating nitrogen atom.

1.3.2 Immobilized metal complexes as catalysts

A previous example[38] has shown how metal complexes immobilized on mesoporous silica supports can be used as catalyst systems which display the advantageous properties of both heterogeneous and homogeneous catalysts. A few more examples will be discussed to give a further idea of the scope of this type of heterogenized catalyst systems.

Komura and coworkers[41] developed a copper-free palladium catalyst for Sonogashira coupling supported on MCM-41. Previously, catalysts supported on silica gel and zeolites have been studied. The quinoline-2-carboimine palladium complexes are synthesized using the sequential method in which the ligands are first supported on the silica and $Pd(OAc)_2$ was added to this system. The catalyst system was characterized by XRD, nitrogen adsorption analysis and FT-IR.

The catalyst system was used in the reaction of various alkynes and aryl halides. The reaction with terminal alkynes showed very high conversion and selectivity at a temperature of 80°C. The turnover value calculated was found to be the highest amongst the previously reported heterogeneous Sonogashira catalysts. This was attributed to the fact that the catalytic site was essentially the same as that of a homogeneous Sonogashira catalyst as well as the high surface area of MCM-41 compared to silica gel and zeolites. Leaching of the catalyst was found to be minimal. This catalyst system could be recycled under aerobic conditions, making it easy to handle.

SBA-15-supported Hoveyda-Grubbs type ruthenium carbene complexes were synthesized by Bek *et al.*[42] They exchanged both of the halide ligands on the ruthenium centre with a trialkoxysilyl-substituted silver(I) carboxylate. This led to a catalyst that could easily be immobilized onto the surface of SBA-15 by reacting with the –OH groups, shown in Figure 1.4. The catalysts were characterized using nitrogen adsorption analysis and ^{13}C-MAS NMR spectroscopy.

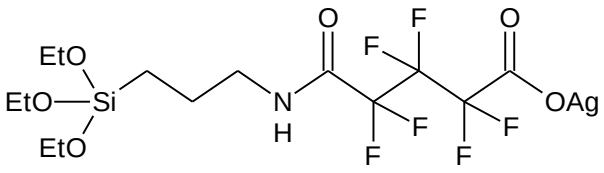

Figure 1.4 Silver(I) carboxylate ligand used as tether

The catalysts were used for both ring-closing metathesis (RCM) and ring-opening metathesis polymerization (ROMP). In the RCM of 1,7-octadiene, the reaction rate was slower than that of the homogeneous catalyst. This was ascribed to the low substrate or product diffusion rate in the mesoporous channels. The selectivity, however, was preserved. Some ruthenium leaching occurred and after the fourth catalytic run with the same catalyst, conversion fell to 85%. The ruthenium contamination found in the product was comparable to that of other heterogeneous systems, and much lower than what was reported in the literature for homogeneous ruthenium systems, even after special purification methods had been used. The same trends of lower reaction rates and lower catalyst contamination of the product was seen when the catalyst systems were used in ROMP.

Terry and Stack[43] studied a Mn(II) bis-phen complex which was immobilized onto SBA-15 *via* a metal-template/metal exchange method. Two routes were followed to immobilize the Mn(II)-complexes – the sequential method (referred to as the grafting method), and a metal-exchange method in which Cu(I)-complexes with the same ligands as the desired end product were grafted onto the SBA-15, followed by a metal exchange reaction in which the manganese replaces the copper. The second method allowed for more control over the amount of manganese loading. The loading was monitored by determining the ligand to metal ratio.

These catalyst systems were then tested in the epoxidation of vinylcyclohexane using peracetic acid as oxidant. The catalyst systems obtained *via* the metal template method showed higher activity and selectivity than both the homogeneous catalyst and the catalyst systems obtained by using the grafting method. The catalysts were used in the epoxidation of a wide variety of alkenes, and showed high conversion and selectivity. The advantage of using the immobilized systems became especially apparent in the epoxidation of electron-deficient olefins, as the immobilized catalyst systems showed almost double the conversion as well as better selectivity.

These examples illustrate that metal complexes immobilized on mesoporous silica can be utilized as catalysts for a wide variety of catalytic transformations, and that the immobilized systems can, in some cases, show improved catalytic activity over their homogeneous counterparts. The examples show both the sequential and convergent approaches to metal complex immobilization.

1.3.3 Metal complexes used for alcohol oxidation

Oxidation of alcohols to aldehydes has traditionally required stoichiometric amounts of metal salts such as Cr(IV) and Mn(VII) derivatives. The use of these types of oxidizing agents generates a lot of toxic waste and is harmful to the environment. A better approach would be to use molecular oxygen or air as oxidant, as this generates water as the only byproduct.[44] This approach requires the use of transition metal catalysts. Both homogeneous and heterogeneous catalyst systems have been developed for alcohol oxidation.

A number of transition metals have been used in alcohol oxidation. These include copper, ruthenium, palladium, gold, vanadium, iridium, osmium, iron, cobalt, manganese and nickel.[45, 46] Of these metals, two have attracted our interest – palladium, because of the many mechanistic studies that has appeared on this subject, and copper, since it is abundant in enzymes that catalyze oxidation reactions with molecular oxygen and is relatively cheap compared to the other metals used in oxidation reactions.[47, 48]

Arita and coworkers developed bifunctional Ir, Ru and Rh complexes bearing C-N ligands derived from primary benzylic amines.[49] These complexes were applied in the oxidation of secondary alcohols to ketones *via* hydrogen transfer reactions. The complexes showed high catalytic activity under mild reaction conditions (1 atm air, 30°C, 3 hours), with the Ir-complexes outperforming the Ru- and Rh-complexes. These complexes are both environmentally benign and easy to handle, offering a good opportunity to study the hydrogen-transfer protocol.

The first report on a homogeneous oxidation process catalyzed by ligand-supported gold with molecular oxygen as oxidant was published in 2005 by Guan *et al*.[50] This group speculated that alcohol oxidation was promoted by oxygenated gold species and that electron-donating ligands would help to generate these oxygenated species. They decided to use β-diketiminate anions as ligands, as these ions bear a negative charge, can be readily prepared and contain groups that can provide steric hindrance, leaving open coordination sites on the metal centre. This is shown in Scheme 1.7.

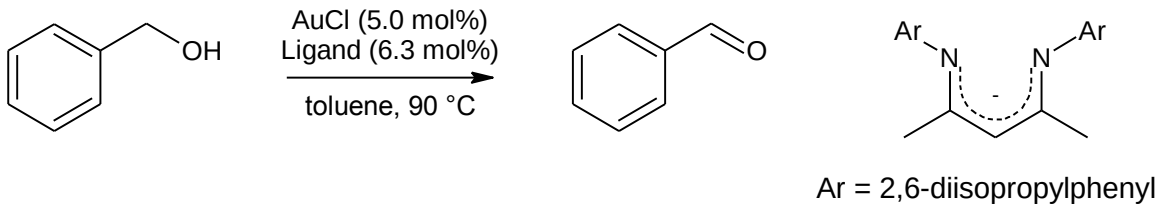

Scheme 1.7 Oxidation of benzyl alcohol to benzaldehyde using a gold catalyst[50]

The prepared complexes showed complete conversion of benzyl alcohol to benzaldehyde in molecular oxygen after 10 hours, and after 24 hours when air was used as oxidant. A wide variety of alcohols, including primary and secondary benzylic and allylic alcohols, were subsequently employed as substrates. No over-oxidation was observed. The complex could be detected during the reaction by using ESI-MS. This catalyst system has several advantages over the more commonly used gold nanoparticle systems. No additives are required when the gold complex was used, and the only byproduct in most cases was water.

Choudhary and co-workers prepared a series of palladium complexes bearing N-N, N-O and N-S chelating ligands. [51] These complexes were immobilized onto silica gel *via* the sequential method. The immobilized complexes were first tested in the oxidation of benzyl alcohol to benzaldehyde. Although all of the complexes, at 3 mol% of Pd, showed satisfactory yield of benzaldehyde after some time, one of the complexes bearing a N-N ligand stood out, giving 95% yield after 2.5 hours using molecular oxygen as oxidant. This complex is shown in Figure 1.5. The group reasoned that the alkyl group on the carbon adjacent to the imino nitrogen atom increases the stability of the catalyst by increasing the binding energy of the palladium with the nitrogen atoms.

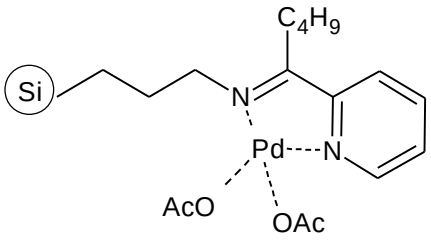

Figure 1.5 Complex found to be most active in study by Choudhary *et al*.[51]

To test whether the catalyst was a true heterogeneous catalyst, the oxidation reaction was carried out in the presence of the silica containing the catalyst until the conversion had reached 35%. The solid was then filtered off, and the filtrate allowed to react further with any catalyst still present in the system. No further significant conversion was seen. The reuseability of the systems was tested as well by carrying out consecutive catalytic runs. A slight decrease in conversion was seen until the 5th run, after which the conversion dropped dramatically.

The above examples illustrate some of the various metal complexes that have previously been studied as catalysts for alcohol oxidation. As stated, copper and palladium were chosen as the metals to be used in this study.

There are various types of ligand systems that have been shown to form effective catalyst systems for alcohol oxidation with copper and/or palladium. One well-studied ligand system involves a method called Schiff base condensation. Schiff bases are formed from the condensation of an aldehyde with an amine. This reaction was first described in 1864 by Hugo Schiff. Schiff bases act as ligands by coordinating to metals through the imine nitrogen and another heteroatom. The heteroatom normally forms part of the original aldehyde molecule and can be oxygen, nitrogen or phosphorous. Various types of Schiff base ligands are known. Salicylaldimine ligands are formed by the condensation of a primary amine with a hydroxybenzaldehyde group. If a diamine is used instead of a mono-functionalized amine, the resulting ligand is called a salen-type ligand. Both these systems coordinate to the metal through the imine nitrogen and a phenoxy group situated on the aldehyde and form a so-called N,O chelating complex. Figure 1.6 show a few examples of Schiff base ligands.

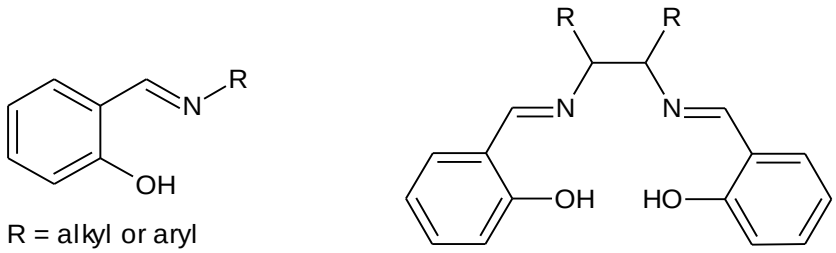

Figure 1.6 Examples of different Schiff base ligands

Copper- and palladium complexes of these ligands are well known and are used in various types of catalytic chemical transformations, including oxidation.

1.4 Conclusion and project objectives

1.4.1 Conclusions

Salicylaldimine complexes are suitable ligand systems to coordinate the transition metals copper and palladium, both of which are able to facilitate catalytic oxidation. These ligand systems can be functionalized in order to be able to immobilize the metal complexes onto a solid support. Mesoporous silicas are excellent catalyst supports due to their regular pores, high thermal and chemical stability and large surface areas. Catalyst systems of transition metal catalysts covalently bonded to mesoporous silica are able to retain the high activity of homogeneous catalysts while also possessing the easier separation and regeneration aspects of heterogeneous catalysts.

1.4.2 Project objectives

The aim of this project was to synthesize model and siloxane functionalized N,O Schiff base ligands and to use these ligands to form copper and palladium Schiff base complexes. The functionalized complexes were immobilized onto MCM-41 and SBA-15. Both the complexes and the heterogenized catalyst systems were characterized using various analytical techniques. The heterogenized catalyst systems were evaluated as oxidation catalysts and the activity of these systems compared to that of the model catalysts.

Chapter one serves as a summary of the synthesis and applications of mesoporous silica, especially with regards to the use of mesoporous silica as catalysts supports. Various ways of immobilizing metal complexes onto the silica is investigated. A brief overview of metal complexes used as alcohol oxidation catalysts is given as well.

In **Chapter two** the synthesis and characterization of the ligands and complexes is discussed. The ligands were synthesized used Schiff base condensation and characterized using FT-IR and ^{1}H NMR spectroscopy. The ligands were complexed with two different metal salts to yield the desired Cu(II) and Pd(II) complexes. The copper complexes were characterized using FT-IR and EPR spectroscopy while FT-IR, ^{1}H NMR and ^{13}C NMR spectroscopy was used to characterize the palladium complexes.

Chapter three deals with the synthesis and characterization of the silica supports, and the immobilization of the complexes onto these supports. Various solid state techniques were used to characterize the immobilized catalyst systems. Functionalized complexes of palladium and copper were immobilized onto MCM-41 and SBA-15. Model and functionalized complexes of copper were encapsulated or immobilized in sol-gel silica. These systems were fully characterized and the full characterization data is described.

Chapter four focuses on the application of both the model and immobilized catalyst systems in the oxidation of benzyl alcohol to benzaldehyde. The different catalysts were tested and the results were compared. GC-FID and HPLC were used to follow the reactions and determine the conversions.

Chapter five contains a summary of the most important results of this project, as well as some suggestions for possible future work.

1.5 References

1. Anastas, P. T.; Kirchoff, M. M. *Acc. Chem. Res.* **2002,** *35,* 686.

2. Li, C.-J.; Simon, M.-O. *Chem. Soc. Rev.* **2012,** *41,* 1415.

3. Dunn, P. J. *Chem. Soc. Rev.* **2012,** *41,* 1452.

4. Brintzinger, H. H.; Fischer, D.; Mülhaupt, R.; Rieger, B.; Waymouth, R. M. *Angew. Chem. Int. Ed.* **2003,** *34,* 1143.

5. Corma, A.; Garcia, H. *Adv. Synth. Catal.* **2006,** *348,* 1391.

6. Sankaranarayanapillai, S.; Volker, S.; Thiel, W. R. *Angew. Chem. Int. Ed.* **2010,** *49,* 3428.

7. Clark, J. H. *Pure Appl. Chem.* **2001,** *73,* 103.

8. De Vos, D. E.; Dams, M.; Sels, B. F.; Jacobs, P. A. *Chem. Rev.* **2002,** *102,* 3615.

9. McNamara, C. A.; Dixon, M. J.; Bradley, M. *Chem. Rev.* **2002,** *102,* 3275.

10. Goradia, D.; Cooney, J.; Hodnett., B. K.; Magner, E. *J. Mol. Catal. B-Enzym.* **2005,** *32,* 231.

11. Simons, C.; Hanefeld, U.; Arends, I. W. C. E.; Minnaard, A. J.; Maschmeyer, T.; Sheldon, R. A. *Chem. Commun.* **2004,** *24,* 2830.

12. Barbaro, P.; Liguori, F. *Chem. Rev.* **2009,** *109,* 515.

13. McMorn, P.; Hutching, G. J. *Chem. Soc. Rev.* **2004,** *33,* 108.

14. Gelman, F.; Blum, J.; Avnir, D. *J. Am. Chem. Soc.* **2002,** *124,* 14460.

15. Chen, A.; Holt-Hindle, P. *Chem. Rev.* **2010,** *110,* 3767.

16. Arcos, D.; Vallet-Regi, M. *Acta Biomater.* **2010,** *6,* 2874.

17. Marr, A. C.; Marr, P. C. *Dalton T.* **2011,** *40,* 20.

18. Sertchook, H.; Avnir, D.; Blum, J.; Joo, F.; Katho, A.; Schumann, H.; Weimann, R.; Wernik, S. *J. Mol. Catal. A-Chem* **1996,** *108,* 153.

19. Li, Y.; Feng, Z.; van Santen, R. A.; Hensen, E. J. M.; Li, C. . *J. Catal.* **2008,** *255,* 190.

20. Di Renzo, F.; Testa, F.; Chen, J. D.; Cambon, H.; Galarneau, A.; Plee, D.; Fajula, F. *Micropor. Mesopor. Mater.* **1999,** *28,* 437.

21. Ramirez, A.; Lopez, B. L.; Sierra, L. *J. Phys. Chem. B* **2003,** *107,* 9275.

22. Beck, J. S.; Vartuli, J. C.; Roth, W. J.; Leonowicz, M. E.; Kresge, C. T.; Schmitt, K. D.; Chu, C. T. W.; Olson, D. H.; Sheppard, E. W. *J. Am. Chem. Soc.* **1992,** *114,* 10834.

23. Zhao, D.; Feng, J.; Huo, Q.; Melosh, N.; Frederickson, G. H.; Chmelka, B. F.; Stucky, G. D. *Science* **1998,** *279,* 548.

24. Kresge, C. T.; Leonowicz, M. E.; Roth, W. J.; Vartuli, J. C.; Beck, J. S. *Nature* **1992,** *359,* 710.

25. Hartmann, M. *Chem. Mater.* **2005,** *17,* 4577.

26. Takahashi, H.; Sasaki, B. L. T.; Miyazaki, C.; Kajino, T.; Inagaki, S. *Micropor. Mesopor. Mat.* **2001,** *44,* 755.

27. Vallet-Regi, M.; Ramila, A.; del Real, R. P.; Perez-Pariente, J. *Chem. Mater.* **2001,** *13,* 308.

28. Doadrio, A. L.; Sousa, E. M. B.; Doadrio, J. C.; Perez-Pariente, J.; Izquierdo-Barba, I.; Vallet-Regi, M. *J. Control Release* **2004,** *97,* 125.

29. Qu, F.; Zhu, G.; Huang, S.; Li, S.; Qiu, S. *Chem. Phys. Chem.* **2006,** *7,* 400.

30. Munoz, B.; Ramila, A.; Perez-Pariente, J.; Diaz, I.; Vallet-Regi, M. *Chem. Mater.* **2003,** *15,* 500.

31. Doadri, J. C.; Sousa, E. M. B.; Izquierdo-Barba, I.; Doadrio, A. L.; Perez-Pariente, J.; Vallet-Regi, M. *J. Mater. Chem.* **2006,** *16,* 462.

32. Ryoo, R.; Joo, S. H.; Jun, S. *J. Phys. Chem. B* **1999,** *103,* 7743.

33. Lee, J.; Kim., J.; Taeghwan., H. *Adv. Mater.* **2006,** *18,* 2073.

34. Sing, K. S. W.; Everett, D. H.; Haul, R. A. W.; Moscou, L.; Pierotti, R. A.; Rouquerol, J.; Siemieniewska, T. *Pure Appl. Chem* **1985,** *57,* 603.

35. Martinez, C.; Avelino, C. *Coor. Chem. Rev.* **2011,** *255,* 1558.

36. Karthikeyan, G.; Pandurangan, A. *J. Mol. Cat. A: Chemical* **2009,** *311,* 36.

37. Rioux, R. M.; Song, H.; Hoefelmeyer, J. D.; Yang, P.; Somorjai, G. A. *J. Phys. Chem.* **2005,** *109,* 2192.

38. del Pozo, C.; Corma, A.; Iglesias, M.; Sanchez, F. *Organometallics* **2010,** *29,* 4491.

39. Bhunia, S.; Koner, S. *Polyhedron* **2011,** *30,* 1857.

40. Standfest-Hauser, C. M.; Lummerstorfer, T.; Schmid, R.; Hoffmann, H.; Kirchner, K.; Puchberger, M.; Trzeciak, A. M.; Mieczynska, E.; Tylus, W.; Ziolkowski, J. J. *J. Mol. Catal. A: Chem.* **2004,** *210,* 179.

41. Komura, K.; Nakamura, H.; Sugi, Y. *J. Mol. Cat. A: Chemical* **2008,** *293,* 72.

42. Bek, D.; Zilkova, N.; Dedecek, J.; Sedlacek, J.; Balcar, H. *Top. Catal.* **2010,** *53,* 200.

43. Terry, T. J.; Stack, T. D. P. *J. Am. Chem. Soc.* **2008,** *130,* 4945.

44. Bäckvall, J. *Modern Oxidation Methods;* Wiley-VCH, 2004.

45. Parmeggiani, C.; Cardona, F. *Green Chem.* **2012,** *14,* 547.

46. Gupta, K. C.; Sutar, A. K.; Lin, C. *Coord. Chem. Rev.* **2009,** *253,* 1926.

47. Stalh, S. S. *Angew. Chem., Int. Ed.* **2004,** *43,* 3400.

48. Wang, Y.; DuBois, J. L.; Hedman, B.; Hodgson, K. O.; T. D. P. Stack, T. P. D. *Science* **1998,** *279,* 537.

49. Arita, S.; Koike, T.; Kayaki, Y.; Ikariya, T. *Chem. Asian. J.* **2008,** *3,* 1479.

50. Guan, B.; Xing, D.; Cai, G.; Wan, X.; Yu, N.; Fang, Z.; Yang, L.; Shi, Z. *J. Am. Chem. Soc* **2005,** *127,* 18004.

51. Choudhary, D.; Paul, S.; Gupta, R.; Clark, J. H. *Green Chem.* **2006,** *8,* 479.

Chapter 2: Synthesis and Characterization of Schiff Base Ligands and Complexes

2. Introduction

Schiff bases, first described by Hugo Schiff in 1864, are compounds containing a carbon-nitrogen double bond. The nitrogen atom is bonded to an aryl or alkyl group. These compounds are usually formed by the condensation of a primary amine with an aldehyde. This reaction can take place in a wide range of solvents and under different reaction conditions, depending on the amine and aldehyde that is used.[1] Schiff base ligands can also be formed using ketones instead of aldehydes, but in this case the ligand formation occurs less readily.[2]

Schiff base compounds can easily coordinate transition metal ions. The coordination takes place through the lone pair of electrons on the imine nitrogen, as well as a second heteroatom combined with the imine, usually nitrogen or oxygen. Because of this method of coordination, Schiff base ligands can stabilize transition metal ions in a wide variety of oxidation states. The ease with which Schiff base condensation takes place allows for the design of new ligand systems which are selective to specific metal ions. A wide range of applications is therefore found for Schiff base complexes in the literature, ranging from the use of ligands as metal extracting agents, to the use of the complexes for antimicrobial applications and as polymerization initiators.[3,4] Transition metal complexes of Schiff bases are also widely used in catalysis. The uses include, to name but a few examples, the selective epoxidation of cyclohexene, the ring-opening polymerization of lactides and selective Suzuki cross- or homocoupling. [5,6]

Since Schiff base ligands form very readily, they are ideal precursors for the preparation of heterogenized catalyst systems. There are many examples in the literature of mesoporous silica being functionalized with an amine such as 3-aminopropyltriethoxysiloxane and then reacted with an aldehyde to form a Schiff base ligand. Finally, a metal salt is added to form a Schiff base complex which is then used as catalyst. One such system is described by Nandi *et al*.[7] These workers functionalized a mesoporous silica with 3-aminopropyltriethoxysilane (3-APTS). The functionalized silica was then reacted with 4-methyl-2,6-diformylphenol to form the heterogenized Schiff base ligand. The required metal salt was then added in order to synthesize the desired Schiff base complex. The complexes were employed in the epoxidation of olefins. Scheme 2.1 shows the preparation of the immobilized complexes.

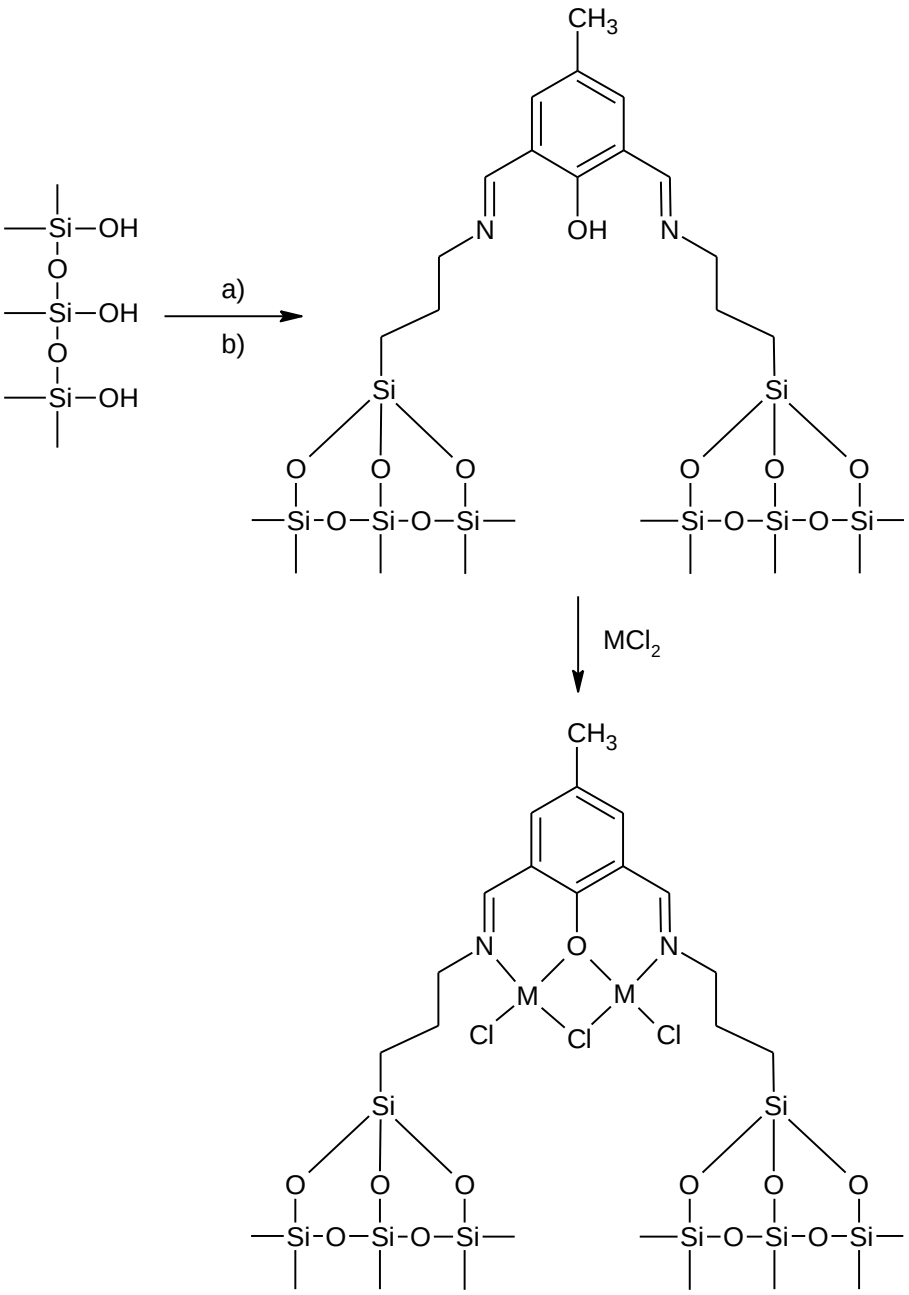

Scheme 2.1 Preparation of Cu and Ni heterogenized complexes. Functionalization with a) 3-APTS and b) 4-methyl-2,6-diformylphenol. M = Cu, Ni

One problem with this approach (in which the complex is synthesized after immobilization of the ligand) is the lack of evidence of complete complexation. IR data is often used to substantiate claims of complex formation; however, it is possible that some of the metal salt may remain on the support. Murphy *et al*. studied both these approaches (shown in Scheme 2.2) using electron paramagnetic resonance (EPR) spectroscopy.[8] Although they were successful in characterizing complexes formed by both methods, the characterization is time-consuming and complicated methods had to be followed. If the functionalized ligand is synthesized first, and the metal complex formed and

characterized before immobilization, there can be no doubt that all of the metal salt will be coordinated to the ligand. The convergent approach to the synthesis of heterogenized catalyst was therefore followed in our study – synthesis of the functionalized metal complexes, followed by immobilization onto the silica supports.

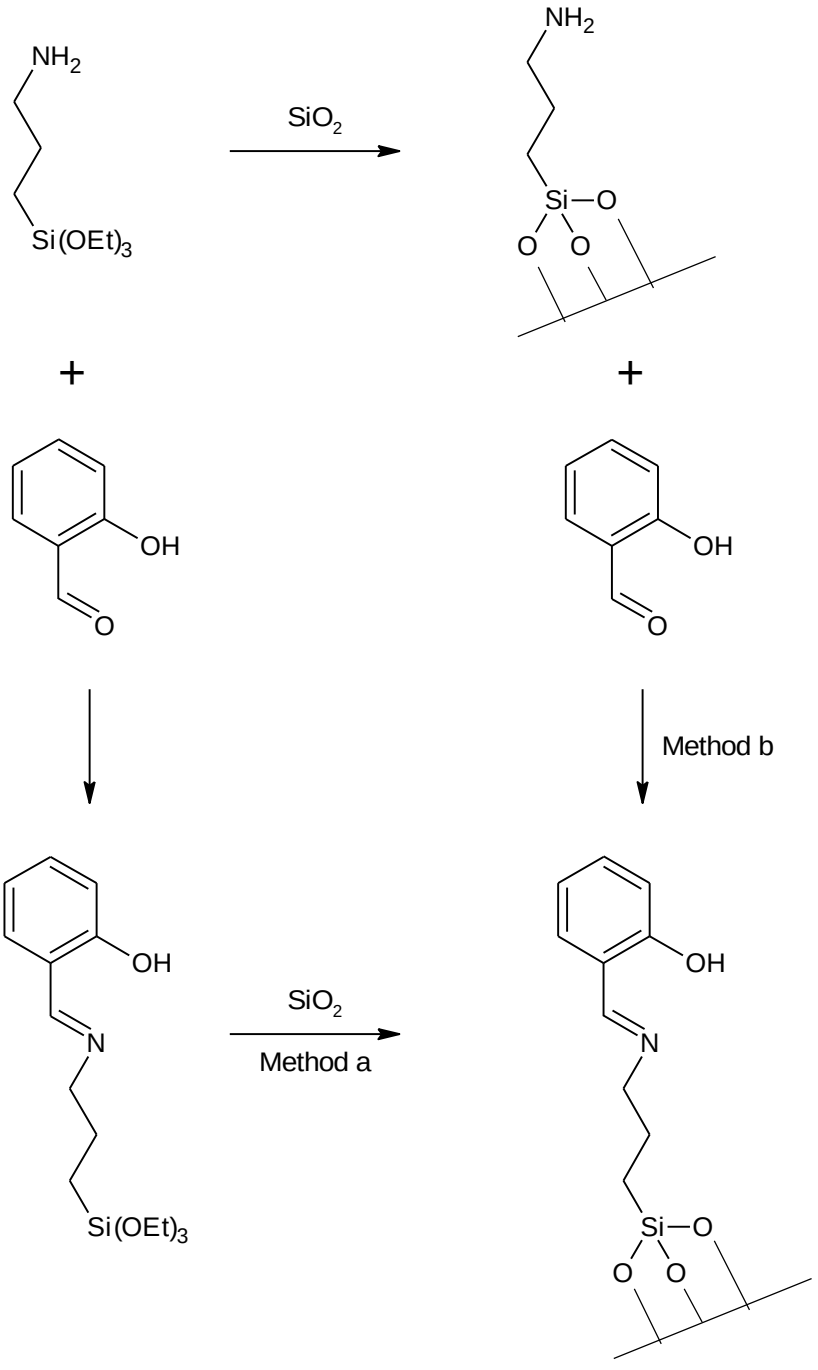

Scheme 2.2 Preparation and immobilization routes of salicylaldimine ligands

2.1 Synthesis and characterization of model salicylaldimine ligands and siloxane-functionalized salicylaldimine ligands

The model ligand was synthesized by a method adapted from Murphy *et al*.[8] All ligands were synthesized under nitrogen making using of standard Schlenk techniques. Salicylaldehyde and *n*-propylamine were reacted in a 1:1 ratio in dry diethyl ether at room temperature with added $MgSO_4$ to remove any formed water. In order to synthesize the functionalized ligand, *n*-propylamine was replaced with 3-aminopropyltriethoxysilane. It was observed that the reaction time for the functionalized ligand was shorter than for the model ligand. Both ligands were isolated as yellow oils. The general experimental procedure is shown in Scheme 2.3.

The model ligand was found to be stable in air and in solution and no hydrolysis of the imine bond was seen. For the functionalized ligand, hydrolysis of the siloxane bonds on the tail was found to occur when the compound was left to stand in air for an extended period of time. This ligand was therefore stored under nitrogen in a glovebox.

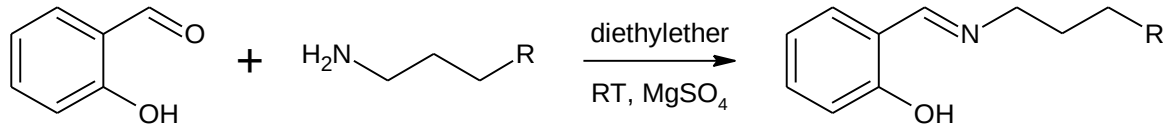

L1: R = H
L2: R = $Si(OEt)_3$

Scheme 2.3 General reaction scheme for the synthesis of salicylaldehyde model and functionalized ligands

2.1.1 Characterization of salicylaldimine ligands

All ligands were characterized by ^{1}H NMR and FT-IR spectroscopy

2.1.1.1 Characterization of ligands by means of ^{1}H NMR spectroscopy

The ^{1}H NMR spectra of both the ligand **L1** and **L2** show the expected resonances for the aliphatic (0.67 – 3.88 ppm) and the aromatic (6.85 – 8.35 ppm) regions. Both spectra also show a broad peak between δ 13.62 and 13.69 ppm which corresponds to the proton on the –OH group attached to the aromatic ring. For the siloxane-functionalized ligand **L2** (shown in Figure 2.1), five resonances are expected in the aliphatic as well as the aromatic region. The H-1 protons (nine protons in total) of the methyl group on the siloxane functionality resonate as a triplet at δ 1.24 ppm. The methylene (H-2) protons of the siloxane functionality (corresponding to 6 protons) resonate as a quartet at δ 3.85 ppm.

The methylene protons resonate more downfield than the methyl protons due to close proximity of the oxygen atom.

The resonances of the methylene protons on the propyl chain are found at δ 0.70 (H-3), δ 1.81 (H-4) and δ 3.61 (H-5) ppm respectively (each resonance integrates for 2 protons). H-3 resonates as a triplet and is the most upfield because of the proximity of the silicon atom. H-4 is seen as a multiplet, while H-5 resonates as a triplet and is the most downfield because of the deshielding effect of the nitrogen atom. The aromatic resonance found most upfield is the triplet due to H-8 at δ 6.88 ppm. The resonance due to H-7 is found as a doublet at δ 6.98 ppm. Both these resonances integrate to give 1 proton. The other two aromatic resonances (H-9 and H-10) overlap and appear as a "multiplet" (2 protons) at δ 7.28 ppm. The singlet (1 proton) found at δ 8.35 ppm is due to the proton on the imine carbon. The reason for the downfield position is the proximity of both the nitrogen atom and the aromatic ring. H-11 is found as a broad peak at δ 13.62 ppm due to proton exchange, which occurs because it is a phenolic proton.

The complete ^{1}H NMR data for ligands **L1** and **L2** are found in Table 2.1. The full ^{1}H NMR spectrum for **L2** is shown in Figure 2.1. The sample was run in chloroform-*d*.

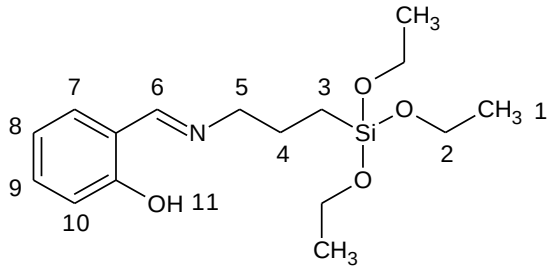

Figure 2.1 Siloxane-functionalized ligand L2

2.1.1.2 Characterization of ligands by means of FT-IR (ATR) spectroscopy

FT-IR spectroscopy was used to monitor the Schiff base condensation reactions. The disappearance of the aldehyde stretch of the salicylaldehyde and the subsequent formation of the imine stretch was used to follow the reaction progress. The aldehyde stretch of salicylaldehyde appears at 1672 cm^{-1}, while the formed imine is seen in the region between 1632 – 1631 cm^{-1}. Other important stretches are the ν(C=C) stretches of the aromatic ring, seen between 1494 – 1460 cm^{-1}, as well as the ν(C-O) where the hydroxyl group is attached to the aromatic ring, which is found between 1279-1276 cm^{-1}. In the infrared spectrum of the siloxane-functionalized ligand, very intense stretches are observed in the range 1099 – 1071 cm^{-1} and at 752 cm^{-1}. These vibrations are assigned to the Si-O bonds which form part of the siloxane tail of the functionalized ligand. Table 2.2 gives a summary for the important vibrations of ligands **L1** and **L2**.

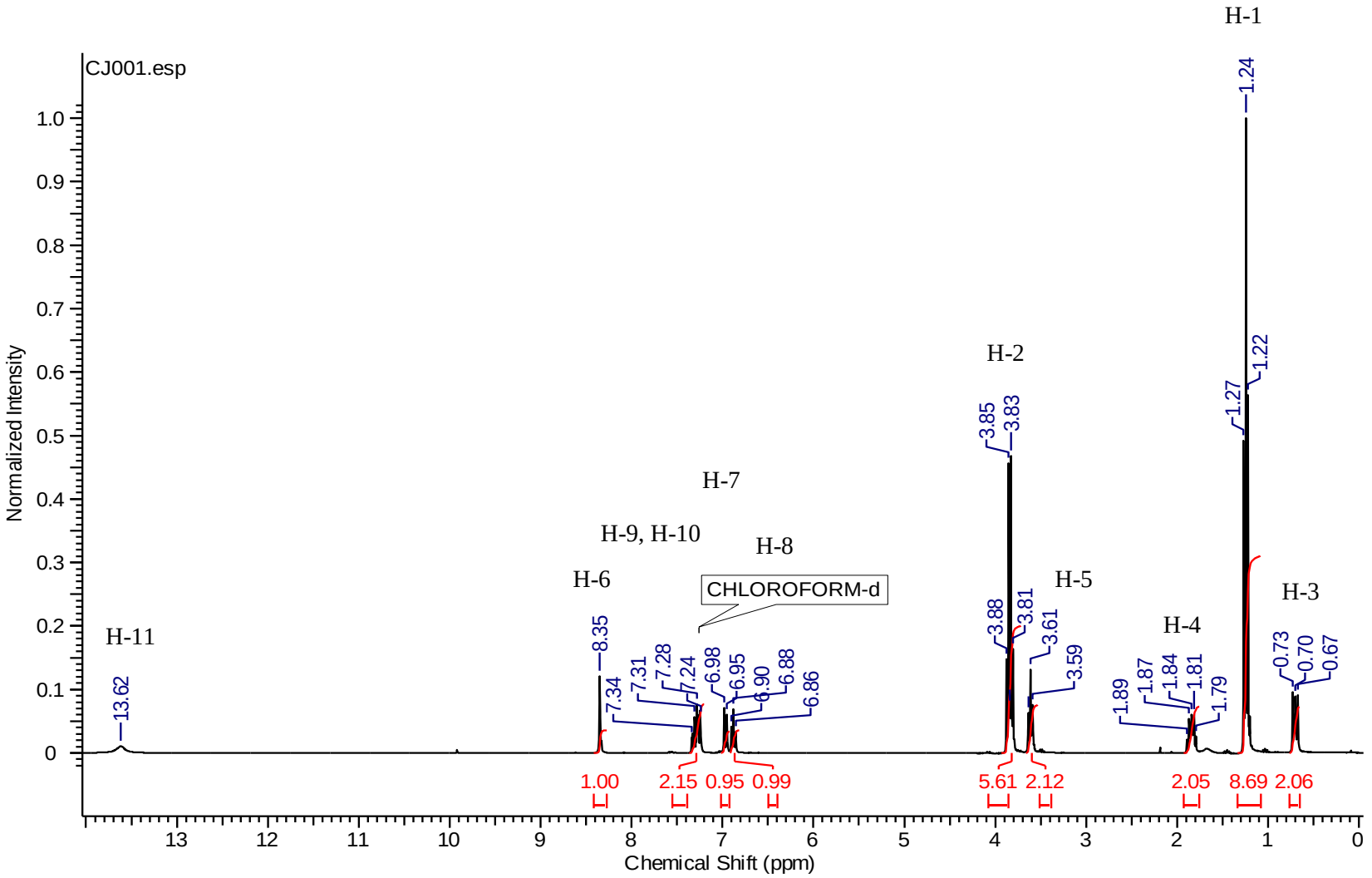

Figure 2.2 ^{1}H NMR spectrum of L2

Table 2.1 ^{1}H NMR data for model and siloxane-functionalized ligands L1 and L2[c]

Ligand	-O-CH_2-$C\underline{H}_3$	-Si-O-$C\underline{H}_2$-	[a]-CH_2-$C\underline{H}_3$ [b]-$C\underline{H}_2$-Si-	[a]–CH_2-$C\underline{H}_2$-CH_3 [b]-$C\underline{H}_2$-CH_2-Si-	-N-$C\underline{H}_2$-CH_2-	Ar-$\underline{H}$	Ar-O$\underline{H}$	-N=C$\underline{H}$
L1			1.00 (t, *J* = 7 Hz)	1.75 (m)	3.57 (t, *J* = 7 Hz)	7.28 (m) 6.99 (d, *J* = 8 Hz) 6.88 (t, *J* = 8 Hz)	13.69 (s)	8.34 (s)
L2	1.24 (t, *J* = 7 Hz)	3.85 (q, *J* = 7 Hz)	0.70 (t, *J* = 8 Hz)	1.84 (m)	3.61 (t, *J* = 6 Hz)	7.28 (m) 6.98 (d, *J* = 8 Hz) 6.88 (t, *J* = 8 Hz)	13.62 (s)	8.35 (s)

[a]**L1**
[b]**L2**
[c]Measured in chloroform-*d*

Table 2.2 Summary of IR vibrations of model and siloxane-functionalized ligands[a]

Ligand	ν(C=N) cm^{-1}	ν(C=C) cm^{-1}	ν(C-O) cm^{-1}	ν(Si-O-Si) cm^{-1}	ν(Si-OH) cm^{-1}
L1	1631	1495	1276	-	-
L2	1632	1496	1279	1071-1099	752

[a] Oils recorded as neat samples using ATR accessory

2.2 Synthesis and characterization of model and siloxane-functionalized salicylaldimine Cu(II) complexes

The copper salicylaldimine complexes were prepared using a method adapted from Singh *et al*.[9] Both the model and functionalized complexes were prepared by refluxing the appropriate ligand with copper acetate in a 2:1 mole ratio in dry ethanol under nitrogen. After removal of the solvent, an olive green solid was obtained for the model complex and a dark green residue for the functionalized complex. A general reaction scheme for the copper complex formation can be seen in Scheme 2.4.

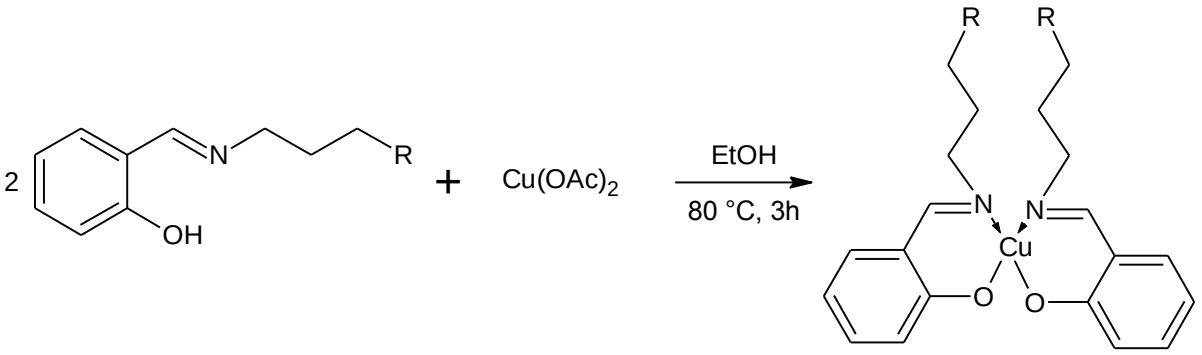

C1: R = H

C2: R = $Si(OEt)_3$

Scheme 2.4 General reaction scheme for the synthesis of model and functionalized copper complexes

2.2.1 Characterization of salicylaldimine Cu(II) complexes

All complexes were characterized by EPR spectroscopy, FT-IR (ATR) spectroscopy, UV-VIS spectroscopy and melting point analysis.

2.2.1.1 Characterization of salicylaldimine Cu(II) complexes by means of EPR spectroscopy

Electron paramagnetic resonance spectroscopy was used in order to study the electronic and chemical environment of the copper ions in the complexes. The EPR spectrum of the complexes shows the expected hyperfine splitting of four peaks. This is due to the nuclear spin of the Cu^{2+} ion, which is 3/2 as well as the chemical environment of the Cu^{2+} ion. The g-factor for the complex **C2** is 2.15. This value is in agreement with the complex structure, as it indicates a Cu^{2+} bonded to two neutral nitrogen and two charged oxygen atoms. The aromatic nature of the ligands causes a lowering of the g-factor.[10] The EPR spectrum of **C2** is shown in Figure 2.3.

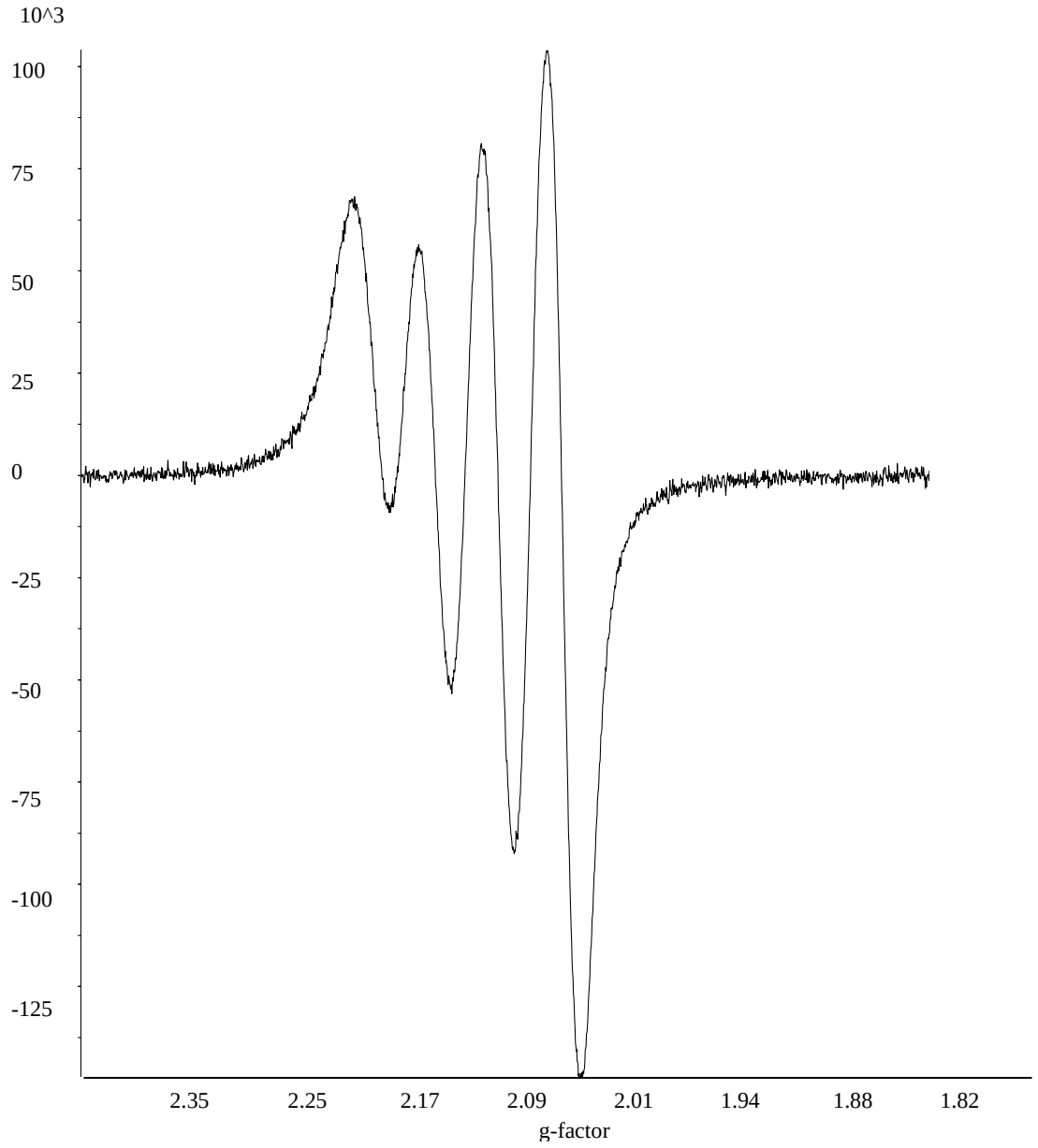

Figure 2.3: EPR spectrum of functionalized copper complex C2

2.2.1.2 Characterization of salicylaldimine Cu(II) complexes by means of FT-IR (ATR) spectroscopy

Infrared spectroscopy suggested the successful formation of metal complexes. A shift of 10 – 12 cm^{-1} to lower wavenumbers was observed in the imine vibration of the complexes when compared to the ligands. This indicates a change in the double bond character of the imine, and is compelling evidence for the coordination of the copper to the ligand. The siloxane peaks are still visible in the spectrum of the functionalized complex, confirming that no hydrolysis of the siloxane bonds had taken place during complexation. No other significant changes were observed in the infrared spectra. A summary of the important shifts are seen in Table 2.3.

Table 2.3 Summary of shifts for imine vibrations (ATR)[a]

Ligand/Complex	ν(C=N) cm^{-1}		Melting point of complex (^oC)
	Ligand	Complex	
1	1631	1621	116 – 120
2	1632	1620	232 - 240

[a]Solids recorded as neat samples using ATR accessory

2.2.1.3 Characterization of salicylaldimine Cu(II) complexes by means of UV-VIS spectroscopy

UV-VIS spectra of the copper complexes were recorded in methanol at concentrations of 10^{-2} M over the range 600 – 200 nm. The electronic spectra of these complexes are shown in Figure 2.4. The spectra for both **C1** and **C2** show five peaks in the region 200 nm – 600 nm. The data is summarized in Table 2.4. The four peaks between 221 nm and 312 nm are assigned to intra-ligand $\pi - \pi^*$ transitions. The peak at 361 nm and 368 nm for **C1** and **C2** respectively is due to metal to ligand charge transfer, specifically from the filled d-orbitals of the copper(II) to the antibonding orbitals of the phenolic residue.[11] This peak is typical for Schiff base copper(II) complexes.[12, 13]

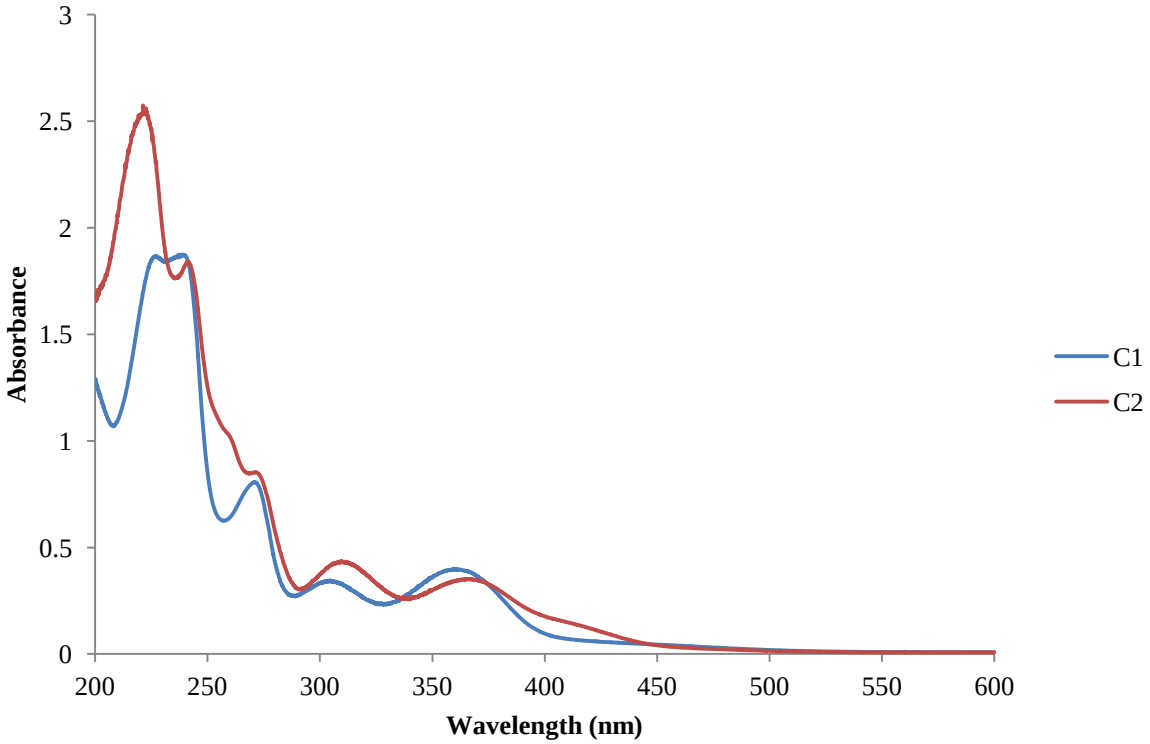

Figure 2.4: UV-VIS spectrum of copper salicylaldimine complexes

Table 2.4 Summary of UV-VIS data of C1 and C2

Complex	Intraligand transitions				Charge transfer
	$\pi - \pi^*$	$\pi - \pi^*$	$\pi - \pi^*$	$\pi - \pi^*$	$\pi - \pi^*$
1	225	241	274	308	361
2	221	243	274	312	368

2.3 Synthesis and characterization of model and siloxane salicylaldimine Pd(II) complexes

The palladium salicylaldimine complexes were prepared using a method previously employed in our group. Both the model and functionalized complexes were prepared by refluxing the appropriate ligand with palladium acetate in a 2:1 ratio in dry methanol under nitrogen. After removal of the solvent, a yellow powder was obtained in both cases. The powders were recrystallized from chloroform and ethanol and yielded bright yellow crystals. The yield was lower compared to the copper complexes, and some palladium black formation was observed. A general reaction scheme for the palladium complex formation can be seen in Scheme 2.5.

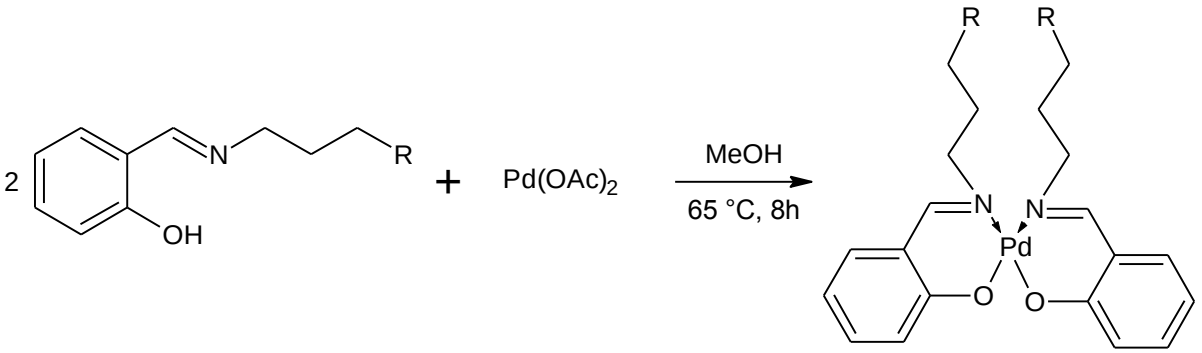

C3: R = H

C4: R = $Si(OEt)_3$

Scheme 2.5 General reaction scheme for the synthesis of model and functionalized palladium complexes

2.3.1 Characterization of salicylaldimine Pd(II) complexes

All complexes were characterized by ^{1}H NMR spectroscopy, ^{13}C NMR spectroscopy, FT-IR spectroscopy and melting point analysis.

2.3.1.1 Characterization of salicylaldimine Pd(II) complexes by means of ^{1}H NMR spectroscopy

All the palladium complexes were fully characterized by ^{1}H NMR spectroscopy. The expected peaks were seen for both the model and functionalized complexes and it was concluded that the desired complexes were successfully synthesized and characterized. Table 2.5 shows a summary of the ^{1}H NMR data for **C3** and **C4**. The most important resonance is found between δ 7.63 and 7.65 ppm. This resonance corresponds to the imine proton in the Schiff base ligand. A shift in this resonance indicates a change in the chemical environment of the imine proton – in this case, because of the ligand coordinating to the metal - and is evidence that complexation took place. In the model ligand, for example, the imine proton resonates at δ 8.34 ppm, while the resonance is found at δ 7.63 ppm in the complex.

2.3.1.2 Characterization of salicylaldimine Pd(II) complexes by means of ^{13}C NMR spectroscopy

The palladium complexes were also characterized by ^{13}C NMR spectroscopy. The expected number of peaks was found for both **C3** and **C4**. The imine carbon resonance is found downfield at δ 164 ppm in both cases. Six resonances, corresponding to the aromatic carbons, are found between δ 161 and 114 ppm. Three more signals, corresponding to the propyl functionality, are observed in the upfield region for **C3**, while the spectrum of **C4** shows these three signals as well as an additional two signals due to the ethoxy functionality. Table 2.6 shows a summary of these results.

2.3.1.3 Characterization of salicylaldimine Pd(II) complexes by means of FT-IR (ATR) spectroscopy

Infrared spectroscopy also gave some insight into the formation of the palladium complexes. A shift of 12 – 19 cm^{-1} to lower wavenumbers was observed in the imine bond vibration of the complexes compared to those of the ligands. This indicates a change in the double bond character of the imine and is evidence of the palladium coordinating to the ligand. The siloxane peaks are still visible in the spectrum of the functionalized complex, indicating that no hydrolysis of the Si-O bonds had taken place. No other significant shifts in wavenumber were observed in the spectra. A summary of these shifts are shown in Table 2.7.

The melting point of the functionalized complex is much lower than that of the model complex. The melting point is higher than that of the copper complex, indicating that the palladium complexes have better thermal stability. The melting points are shown in Table 2.7.

Table 2.5 ^{1}H NMR data for model and siloxane-functionalized palladium complexes C3 and C4[c]

Complex	-O-CH_2-CH_3	-Si-O-CH_2-	[a]-CH_2-CH_3 [b]-CH_2-Si-	[a]–CH_2-CH_2-CH_3 [b]-CH_2-CH_2-Si-	-N-CH_2-CH_2-	Ar-H	-N=CH
C3			0.99 (t, *J* = 7 Hz)	1.83 (m, *J* = 7 Hz)	3.70 (t, *J* = 7 Hz)	7.23 (m) 6.88 (d, *J* = 8 Hz) 6.58 (t, *J* = 7 Hz)	7.63 (s)
C4	1.20 (t, *J* = 7 Hz)	3.82 (q, *J* = 7 Hz)	0.70 (t, *J* = 8 Hz)	1.93 (m, *J* = 8 Hz)	3.72 (t, *J* = 7 Hz)	7.21 (m) 6.88 (d, *J* = 8 Hz) 6.58 (t, *J* = 7 Hz)	7.65 (s)

[a]**C3**
[b]**C4**
[c]Measured in chloroform-*d*

Table 2.6 ^{13}C NMR data for model and siloxane-functionalized palladium complexes C3 and C4[c]

Complex	-O-CH_2-CH_3	-Si-O-CH_2-	[a]-CH_2-CH_3 [b]-CH_2-Si-	[a]–CH_2-CH_2-CH_3 [b]-CH_2-CH_2-Si-	-N-CH_2-CH_2-	Aromatic carbons	-N=CH
C3			7.5	25.5	60.1	114.8, 120.2, 120.3, 134.0, 134.4, 161.5	164.5
C4	18.3	58.4	11.3	25.4	60.8	114.8, 120.1, 120.7, 134.0, 134.4, 161.8	164.5

[a]**C3**
[b]**C4**
[c]Measured in chloroform-*d*

Table 2.7 Summary of shifts for imine vibrations (ATR)[a]

Ligand/Complex	ν(C=N) cm^{-1}		Melting point of complex (^oC)
	Ligand	**Complex**	
1	1631	1613	191 - 194
2	1632	1619	98 - 104

[a]Solids recorded as neat samples using ATR accessory

2.4 Synthesis and characterization of model diimine ligands and siloxane-functionalized diimine ligands

The synthesis of the pyridinyl diimine ligands was adapted from work previously reported in the literature.[14] The ligands were synthesized by making use of normal Schlenk techniques under nitrogen atmosphere. **L3** was synthesized by the condensation of pyridine-2-carboxaldehyde with *n*-propylamine in a 1:1 ratio in dry diethyl ether. Anhydrous $MgSO_4$ was added to remove any water formed during the reaction. For the synthesis of **L4**, *n*-propylamine was replaced by 3-aminopropyltriethoxysilane. Both ligands were isolated as yellow oils. A general procedure is shown in Scheme 2.6.

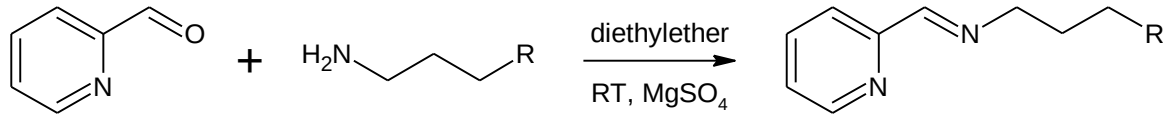

L3: R = H
L4: R = $Si(OEt)_3$

Scheme 2.6 General reaction scheme for the synthesis of model and functionalized diimine ligands

2.4.1 Characterization of diimine ligands

All ligands were characterized by ^{1}H NMR and FT-IR spectroscopy

2.4.1.1 Characterization of ligands by means of ^{1}H NMR spectroscopy

The ^{1}H NMR spectra of **L3** and **L4** show the expected resonances for both the aliphatic and aromatic regions. For the siloxane-functionalized ligand **L4**, Figure 2.5, five resonances are expected for the aliphatic as well as the aromatic region. The H-1 protons resonate as a triplet (corresponding to nine

protons) at δ 1.22 ppm, while the methylene protons on the siloxane functionality, H-2, resonate as a quartet at δ 3.83 ppm. The downfield shift of the H-2 protons is caused by the proximity of the oxygen atoms. The methylene protons of the propyl chain are found at δ 0.70 (H-3), δ 1.84 (H-4) and δ 3.67 ppm respectively. The upfield character of the H-3 triplet is caused by the silicon atom, while the nitrogen of the imine causes a downfield shift for the H-5 protons. H-10 found the furthest downfield as a doublet at δ 8.64 ppm due to its proximity to the nitrogen of the pyridine ring. The other three aromatic resonances are found at δ 7.30 (multiplet), δ 7.73 (triplet) and δ 7.98 ppm (doublet) respectively. The resonance of the proton on the imine carbon (H-6) is found as a singlet at δ 8.36 ppm.

A summary of the ^{1}H NMR shifts for **L3** and **L4** is shown in Table 2.8.

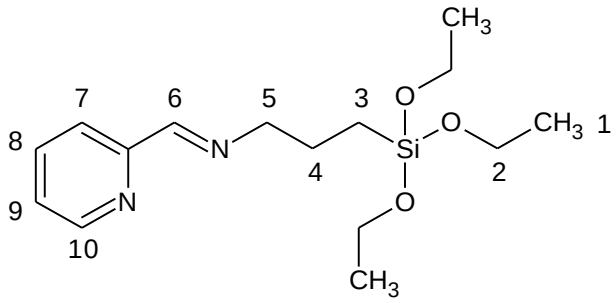

Figure 2.5 Siloxane-functionalized ligand L4

2.4.1.2 Characterization of ligands by means of FT-IR (ATR) spectroscopy

FT-IR was used to follow the Schiff-base condensation reaction. The disappearance of the aldehyde stretch and the formation of the imine stretch during the condensation reaction were monitored. The C=O stretch for pyridine-2-carboxaldehy appears at 1716 cm-1, whereas the C=N stretch can be seen at 1649 cm-1. Other important peaks are found between 1587-1567 cm-1 for the ν(C=N) vibrations of the pyridine ring, as well as between 1468-1435 cm-1 for the ν(C=C) vibrations of the ring. For **L4**, some intense stretches are observed at 1100-1074 cm-1 and 770 cm-1. These bands correspond to the Si-O vibrations of the siloxane tail. A summary of the FT-IR data is shown in Table 2.9.

Table 2.8 ^{1}H NMR data for model and siloxane-functionalized ligands L3 and L4[c]

Ligand	-O-CH_2-$C\underline{H}_3$	-Si-O-$C\underline{H}_2$-	[a]-CH_2-$C\underline{H}_3$ [b]-$C\underline{H}_2$-Si-	[a]–CH_2-$C\underline{H}_2$-CH_3 [b]-$C\underline{H}_2$-CH_2-Si-	-N-$C\underline{H}_2$-CH_2-	Ar-$\underline{H}$	-N=C$\underline{H}$
L3			0.92 (t, *J* = 7 Hz)	1.72 (m)	3.60 (t, *J* = 8 Hz)	7.25 (m) 7.69 (t, *J* = 8 Hz) 7.95 (d, *J* = 8 Hz) 8.60 (d, *J* = 5 Hz)	8.33 (s)
L4	1.22 (t, *J* = 7 Hz)	3.83 (q, *J* = 7 Hz)	0.70 (t, *J* = 8 Hz)	1.84 (m)	3.67 (t, *J* = 7 Hz)	7.30 (m) 7.73 (t, *J* = 8 Hz) 7.98 (d, *J* = 8 Hz) 8.64 (d, *J* = 5 Hz)	8.36 (s)

[a]**L3**
[b]**L4**
[c]Measured in chloroform-*d*

Table 2.9: FT-IR data for model and siloxane-functionalized ligands L3 and L4[a]

Ligand	ν(C=N) cm^{-1} imine	ν(C=N) cm^{-1}	ν(C=C) cm^{-1} pyridine ring	ν(Si-O-Si) cm^{-1}	ν(Si-OH) cm^{-1}
L3	1649	1567-1587	1437-1468	-	-
L4	1649	1567-1587	1437-1468	1073-1100	770

[a] Oils recorded as neat samples using ATR accessory

2.5 Synthesis and characterization of diimine model and siloxane-functionalized Cu(II) complexes

The synthesis of the diimine copper(II) complexes was attempted using a method similar to that used to synthesize the salicylaldimine complexes. Both the model and functionalized complexes were prepared by refluxing the appropriate ligand with copper chloride in a 2:1 ratio in dry methanol under nitrogen. After removal of the solvent, a light green solid was obtained for the model complex and a dark green oil for the functionalized complex. A general reaction scheme for the proposed copper complex formation can be seen in Scheme 2.7.

From the FT-IR spectroscopy, as explained in Section 2.5.1.1, it was concluded that the correct product had not formed. Instead of the ligand coordinating to the metal through both the pyridine and imine nitrogen atoms, coordination took place through the pyridine nitrogen atoms and the chlorine atoms of the copper salt. Some other copper salts – $Cu(ClO_4)_2$ and $Cu(OSOCF_3)_2$ - were used in an attempt to formed the desired complex. The complexes formed using these salts were similar to those obtained when $CuCl_2$ was used. The FT-IR data is summarized in Table 2.10.

2.5.1 Characterization of diimine model and siloxane-functionalized Cu(II) complexes

The complexes were characterized using FT-IR spectroscopy.

2.5.1.1 Characterization of diimine model and siloxane-functionalized Cu(II) complexes by means of FT-IR (ATR) spectroscopy

Three peaks were monitored in the FT-IR spectra of **C5** and **C6**, namely the imine C=N peak and the two C=N stretches of the pyridine ring. In the first reaction, using $CuCl_2$ as metal salt, it was observed that the imine C=N peak did not shift from 1649 cm^{-1}. One of the pyridine C=N stretches disappeared while the other shifted from 1586 to 1599 cm^{-1}. This lead to the conclusion that the imine nitrogen could not displace the chlorine ligands on the copper salt. Other copper salts gave similar results with the model ligand and this is summarized in Table 2.10.

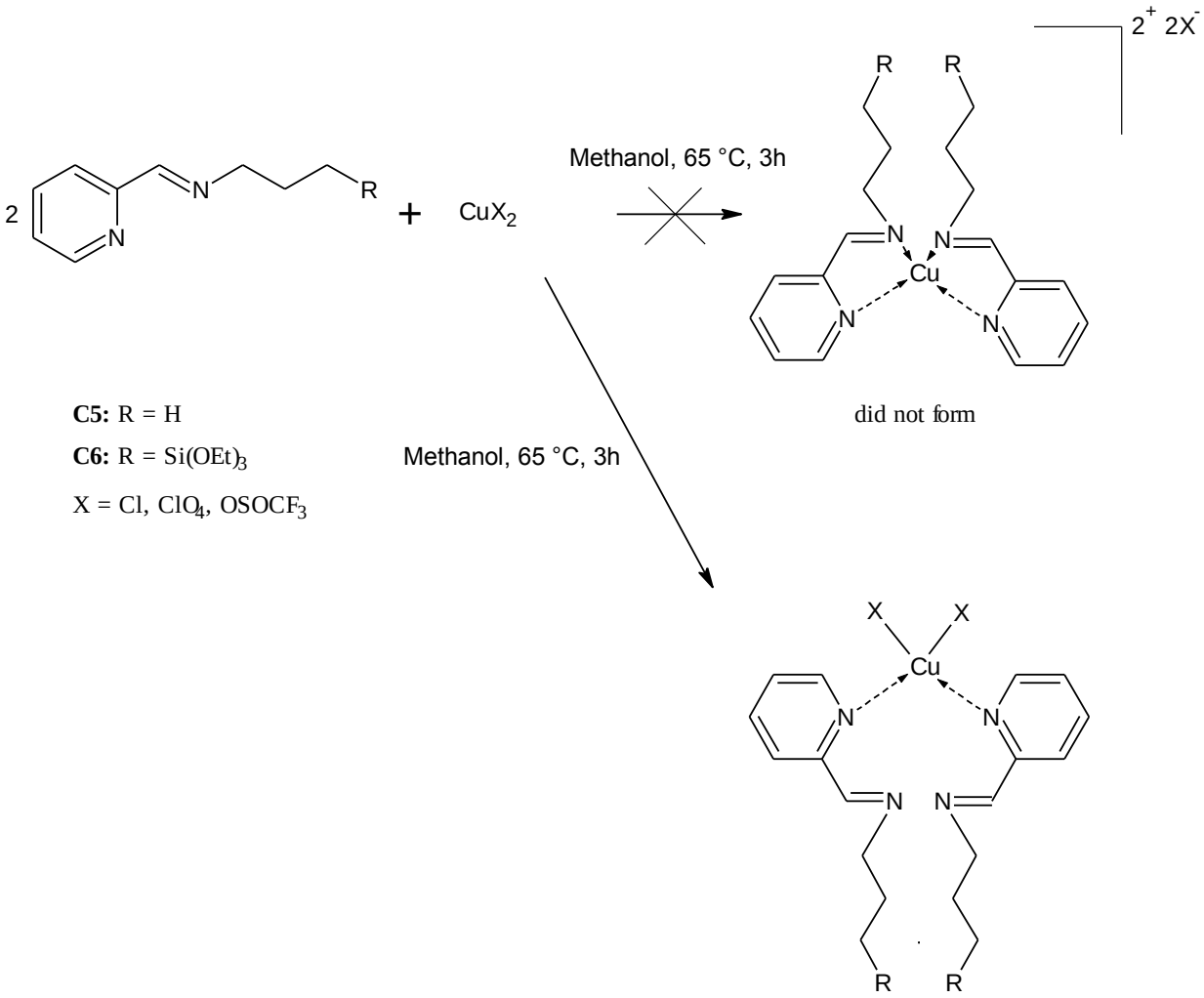

Scheme 2.7 General reaction scheme for the synthesis of diimine model and functionalized copper complexes

Table 2.10 FT-IR data for model diimine copper complexes[a]

Copper salt used	imine ν(C=N) cm^{-1}		pyridine ν(C=N) cm^{-1}	
	Ligand	**Complex**	**Ligand**	**Complex**
$CuCl_2$	1649	1649	1567, 1587	1599
$Cu(ClO_4)_2$	1649	1646	1567, 1587	1603
$Cu(OSOCF_3)_2$	1649	1649	1567, 1587	1602

[a] Oils recorded as neat samples using ATR accessory

2.6 Concluding remarks

A model and a siloxane-functionalized salicylaldimine ligand were prepared by Schiff base condensation reactions. The copper(II) and palladium(II) complexes of both ligands were prepared as well, giving four complexes in total. The model complexes were found to be stable in air and in solution, while the siloxane tails of the functionalized complexes were prone to hydrolysis in air after extended periods of time. The copper complexes were successfully characterized by FT-IR spectroscopy and EPR spectroscopy, while the palladium complexes were characterized by FT-IR spectroscopy, ^{1}H NMR spectroscopy and ^{13}C spectroscopy. A model and a siloxane-functionalized diimine ligands were prepared as well using Schiff base condensation reactions. An attempt was made to synthesize copper(II) complexes of these ligands, but the proposed products did not form.

2.7 Experimental section

2.7.1 General remarks and instrumentation

All reactions were carried out under nitrogen making use of standard Schlenk techniques. IR spectra were recorded using an ATR accessory on a Nicolet Avatar 330 FT-IR spectrometer. NMR spectra were recorded on a Varian Unity Inova instrument at 300 and 400 MHz for ^{1}H and 75 and 100 MHz for ^{13}C.

2.7.2 Materials

Reagents were purchased from Sigma-Aldrich and were used as received. Solvents were purchased from Sigma-Aldrich and Kimix Chemicals and were purified by refluxing them over the appropriate drying agents. Dichloromethane was dried over phosphorous pentoxide, hexane was dried over sodium wire, ethanol and methanol were dried over magnesium and diethyl ether over sodium wire with added benzophenone.

2.7.3 Synthesis of salicylaldimine model and functionalized Schiff base ligands

2.7.3.1 Model 2-Propyliminomethyl-phenol ligand

Propylamine (5 mmol, 0.296 g) in dry diethyl ether (10 mL) was added to a Schlenk tube containing salicylaldehyde (5 mmol, 0.611 g) dissolved in dry diethyl ether (10 ml), as well as a small amount of $MgSO_4$. The tube was flushed with nitrogen and the reaction was stirred at room temperature under nitrogen for 24 hours. The $MgSO_4$ was then filtered off and the solvent removed on a rotary evaporator. A bright yellow oil was obtained as product (0.742 g, 90%). This ligand was characterized by FT-IR (ATR) and ^{1}H NMR spectroscopy.

2.7.3.2 Functionalized 2-(3-triethoxysilanepropyliminomethyl)-phenol ligand

(3-Aminopropyl)-triethoxysilane (5 mmol, 1.111 g) in dry diethyl ether (10 mL) was added to a Schlenk tube containing salicylaldehyde (5 mmol, 0.611 g) dissolved in dry diethyl ether (10 mL), as well as a small amount of $MgSO_4$. The tube was flushed with nitrogen and the reaction was stirred under nitrogen for 3 hours. The $MgSO_4$ was then filtered off and the solvent removed on a rotary evaporator. A bright yellow oil was obtained as product (1.486 g, 91%). This ligand was characterized by FT-IR (ATR) and ^{1}H NMR spectroscopy.

Summaries of the ^{1}H NMR spectroscopy and FT-IR spectroscopy data for the ligands can be found in Tables 2.1 and 2.2 respectively.

2.7.4 Synthesis of model and functionalized Cu(II) complexes

2.7.4.1 Model 2-Propyliminomethyl-phenol Cu(II) complex C1

$Cu(OAc)_2$ (0.75 mmol, 0.115 g) was added to a solution of **L1 (**1.5 mmol, 0.488 g) dissolved in dry ethanol (10 mL). The solution was refluxed at 80°C under nitrogen for 3 hours. The solvent was removed on a rotary evaporator and an olive-green solid was obtained (0.348 g, 89%). This product was dried under vacuum and used without any further purification.

2.7.4.2 Functionalized 2-(3-triethoxysilanepropyliminomethyl)-phenol Cu (II) complex C2

$Cu(OAc)_2$ (0.75 mmol, 0.115 g) was added to a solution of **L2 (**1.5 mmol, 0.245 g) dissolved in dry ethanol (10 mL). The solution was refluxed at 80°C under nitrogen for 3 hours. The solvent was removed on a rotary evaporator and a dark green residue was obtained (0.569 g, 78%). This product was dried under vacuum and used without any further purification.

2.7.5 Synthesis of model and functionalized Pd(II) complexes

2.7.5.1 Model 2-Propyliminomethyl-phenol Pd(II) complex C3

A suspension of $Pd(OAc)_2$ (0.4 mmol, 0.090 g) in dry methanol (15 mL) was added to a solution of **L1** (0.8 mmol, 0.260 g) in dry methanol (30 mL). The reaction mixture was stirred under reflux for 8h. The mixture was cooled down to room temperature, and filtered. The solvent was removed from the filtrate, and a yellow powder was obtained. The product was recrystallized from chloroform and ethanol at low temperature to obtain yellow crystals (0.130 g, 40%).

2.7.5.2 Functionalized 2-(3-triethoxysilanepropyliminomethyl)-phenol Pd (II) complex C4

A suspension of $Pd(OAc)_2$ (0.4 mmol, 0.090 g) in dry methanol (15 mL) was added to a solution of **L2** (0.8 mmol, 0.130 g) in dry methanol (30 mL). The reaction mixture was stirred under reflux for

8h. The mixture was cooled down to room temperature, and filtered. The solvent was removed from the filtrate, and a yellow powder was obtained. The product was recrystallized from chloroform and ethanol at low temperature to obtain a yellow solid (0.150 g, 48%).

2.7.6 Synthesis of model and functionalized diimine ligands

2.7.6.1 Model [N-(*n*-propyl)-(2-pyridyl)] ligand L5

Propylamine (5 mmol, 0.296 g) in dry diethyl ether (10 mL) was added to a Schlenk tube containing 2-pyridinecarboxaldehyde (5 mmol, 0.536 g) dissolved in dry diethyl ether (10 ml), as well as a small amount of $MgSO_4$. The tube was flushed with nitrogen and the reaction was stirred at room temperature under nitrogen for 24 hours. The $MgSO_4$ was then filtered off and the solvent removed on a rotary evaporator. A yellow oil was obtained as product (0.599 g, 81%). This ligand was characterized by FT-IR (ATR) and ^{1}H NMR spectroscopy.

2.7.6.2 Functionalized [N-(3-aminopropyltriethoxysilane)-(2-pyridyl)] ligand L6

(3-Aminopropyl)-triethoxysilane (5 mmol, 1.111 g) in dry diethyl ether (10 mL) was added to a Schlenk tube containing 2-pyridinecarboxaldehyde (5 mmol, 0.536 g) dissolved in dry diethyl ether (10 mL), as well as a small amount of $MgSO_4$. The tube was flushed with nitrogen and the reaction was stirred under nitrogen for 3 hours. The $MgSO_4$ was then filtered off and the solvent removed on a rotary evaporator. A yellow oil was obtained as product (1.348 g, 86%). This ligand was characterized by FT-IR (ATR) and ^{1}H NMR spectroscopy.

Summaries of the ^{1}H NMR spectroscopy and FT-IR spectroscopy data for the ligands can be found in Tables 2.8 and 2.9 respectively.

2.7.7 Synthesis of model and functionalized diimine Cu(II) complexes

2.7.7.1 Model [N-(*n*-propyl)-(2-pyridyl)] Cu(II) using $CuCl_2$ as metal salt (C5)

$CuCl_2$ (0.75 mmol, 0.100 g) was dissolved in dry methanol (5 mL) and added to a solution of L5 (1.5 mmol, 0.222 g) in dry methanol (10 mL). The solution was refluxed at 65°C while stirring for 3 hours. The solvent was removed, yielding a light green solid (0.231 g, 71%).

2.7.7.2 Functionalized [N-(*n*-propyl)-(2-pyridyl)] Cu(II) using $CuCl_2$ as metal salt (C6)

$CuCl_2$ (0.75 mmol, 0.100 g) was dissolved in dry methanol (5 mL) and added to a solution of L6 (1.5 mmol, 0.466 g) in dry methanol (10 mL). The solution was refluxed at 65°C while stirring for 3 hours. The solvent was removed, yielding a dark green oil (0.585 g, 85%).

2.7.7.3 Model [N-(*n*-propyl)-(2-pyridyl)] Cu(II) using $Cu(ClO_4)_2$ as metal salt

$Cu(ClO)_2$ (0.75 mmol, 0.0.197 g) was dissolved in dry methanol (5 mL) and added to a solution of L5 (1.5 mmol, 0.222 g) in dry methanol (10 mL). The solution was refluxed at 65°C while stirring for 3 hours. The solvent was removed, yielding a green solid (0.550 g, 80%).

2.7.7.4 Model [N-(*n*-propyl)-(2-pyridyl)] Cu(II) using $Cu(OSOCF_3)_2$ as metal salt

$Cu(OSOCF_3)_2$ (0.75 mmol, 0.271 g) was dissolved in dry methanol (5 mL) and added to a solution of L5 (1.5 mmol, 0.222 g) in dry methanol (10 mL). The solution was refluxed at 65°C while stirring for 3 hours. The solvent was removed, yielding a green solid (0.495 g, 72%).

A summary of the FT-IR spectroscopy data for the complexes can be found in Table 2.10

2.8 References

1. Cozzi, P. G. *Chem. Soc. Rev.* **2004,** *33,* 410.

2. Gupta, K. C.; Sutar, A. K. *Coord. Chem. Rev.* **2004,** *252,* 1420.

3. Shamspur, T.; Sheikhshoaie, I.; Mashhadizadeh, M. H. *J. Anal. At. Spectrom.* **2005,** *20,* 476.

4. Chmura, A. J.; Cousins, D. M.; Davidson, M. G.; Jones, M. D.; Lunn, M. D.; Mahon, M. F. *Dalton T.* **2008,** *11,* 1437.

5. Pouralimardan, O.; Chamayou, A.; Janiak, C.; Hosseini-Mondared, H. *Inorg. Chim. Acta* **2007,** *360,* 1599.

6. Gonzalez-Arellano, C.; Corma, A.; Iglesias, M.; Sanchez, F. *J. Catal.* **2006,** *238,* 497.

7. Nandi, M.; Roy, P.; Uyama, H.; Bhaumik, A. *Dalton T.* **2011,** *40,* 12510.

8. Murphy, E. F.; Ferri, D.; Baiker, A.; Van Doorslaer, S.; Schweiger, A. *Inorg. Chem.* **2003,** *42,* 2559.

9. Singh, U. G.; Williams, R. T.; Hallam, K. R.; Allen, G. C. *J. Sol. Chem.* **2005,** *178,* 3405.

10. Peisach, J.; Blumberg, W. E. *Arch. Biochem. Biophys.* **1974,** *165,* 691.

11. Amundsen, A. R.; Whelan, J.; Bosnich, B. *J. Am. Chem. Soc.* **1997,** *99,* 6730.

12. Akkus, O.; Uzman, S. *Spectrosc. Lett.* **2000,** *33,* 445.

13. Losasda, J.; del Peso, I.; Beyer, L. *Inorg. Chim. Acta.* **2001,** *321,* 107.

14. Chen, R.; Basca, J.; Mapolie, S. F. *Polyhedron* **2003,** *22,* 2855.

15. Tumer, M.; Koksal, H.; Serin, S.; Digrak, M. *Trans. Met. Chem.* **1999,** *24,* 13.

16. Chen, H.; Tang, H.; Lin, C. *Macromolecules* **2006,** *39,* 3745.

Chapter 3: Synthesis and Characterization of Immobilized Catalysts

3. Introduction

In the late 1980's and early 1990's great effort was made to synthesize new mesoporous materials (pore sizes 2 – 50 nm) with pore sizes greater than 8 Å. This size was seen as a barrier since the largest naturally occurring zeolites as well as synthetic zeolites up to that point consisted of rings of 12 tetrahedral atoms and therefore had a pore diameter of 8 Å or less.[1,2] The first report of zeolites with a pore size greater than 8 Å was published by Davis *et al* in 1988.[3] This material was designated VPI-5 (Virginia Polytechnic Institute) and had a pore size of 13 Å. Another material, an alumina-silica hybrid, with a pore size of 9 Å, AIPO-8, was reported in 1990.[4] This material consisted of rings of 14 tetrahedral atoms.

In 1992 Beck and his research group at the Mobil Research and Development Corporation reported the successful synthesis of a new type of mesoporous silicate material.[5] They used the liquid crystal templating technique to synthesize a new family of materials, designated as M41S. By altering the template molecule the symmetry of the material could be varied from cubic to hexagonal, and the pore size could be altered to be from 15 Å to over 100 Å. One of the most well studied materials from this family, MCM-41, exhibits a hexagonal array of uniform mesopores. The pore sizes can be varied, but are usually in the range of 20-50 Å.

This successful application of the liquid crystal templating technique was the catalyst for exponential growth in the field of mesoporous silicas. The synthesis of two other well-studied mesoporous silicate materials soon followed: MSU-X (synthesized at Michigan State University) in 1995 and SBA-15 (synthesized at the University of Santa Barbara) in 1998.[6,7]

These materials have found a wide range of applications in chemistry, including being used as polymer reinforcement, as stationary phases for high performance liquid chromatograpy and in the field of catalysis.[8] The good thermal stability, variable pore sizes, large surface areas and ease of functionalization of the surface of these materials make them attractive candidates for use as catalyst supports.[9]

A recent report by Joo *et al* demonstrates the versatility of mesoporous silica materials when it comes to their application in catalysis.[10] The group wanted to use platinum nanoparticles in order to investigate atomic-scale properties affecting catalytic activity and selectivity. These nanoparticles would usually be stabilized by organic capping agents; however, this limits the use of the nanoparticles in high-temperature applications. Platinum atoms were therefore coated with mesoporous silica. The coated nanoparticles were prepared by using tetradecyldrimethylammonium bromide (TTAB) as capping agent, adding tetraethylorthosilicate and subsequent calcination (shown in Scheme 3.1). This yielded stabilized platinum nanoparticles designated Pt-*m*SiO_2 that were stable in air at temperatures of up to 750°C, while the mesopores in the silica provided direct access to the platinum core.

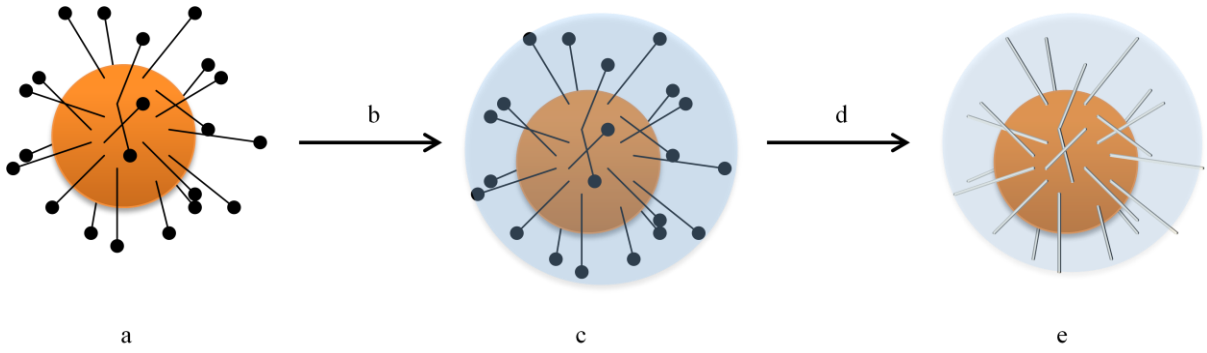

Scheme 3.1 Synthesis of Si-coated Pt-nanoparticales a) TTBA-capped Pt; b) TEOS and NaOH added, stirred at toom temperature; c) As-synthesized Pt-SiO_2; d) TTAB removed by calcination; e) Pt-*m*SiO_2

These catalysts were then applied in ethylene hydrogenation at temperatures of up to 350°C as a test reaction. The turnover frequencies and activation energies that were determined for these silica supported systems were comparable to that of platinum single crystals and colloidal platinum nanoparticle-loaded SBA-15 model catalysts.

Another example of mesoporous silica used in catalysis is found in a report by Hussein *et al*.[11] They employed the incipient wetness method using a rhodium nitrate precursor to prepare rhodium impregnated MCM-41, SBA-15-C, SBA-15-S and KIT-6. The impregnated silicas were then calcined to obtain the supported rhodium oxide catalysts. These catalysts were then tested in the decomposition of N_2O, a harmful greenhouse gas.

The Rh/SBA-15-S system showed the highest activity for N_2O decomposition and also exhibited the best strength against aging impact. The Rh/SBA-15 showed better metal dispersion and higher formation of Rh^{1+} species than Rh^{3+} or Rh^0 species when compared to the other supports. The MCM-41 showed the lowest activity, possibly due to rhodium sintering causing a blockage of the pores. The larger pore size of SBA-15-S – 180 Å vs 32 Å, 53 Å and 48 Å for MCM-41, SBA-15-C and KIT- 6 respectively - favours Rh access and leads to better diffusion and dispersion of the particles.

Another type of silica support that has received attention recently is sol-gel silica.[12,13] Sol-gel silicas are synthesized by a three-step process: The hydrolysis of an alkoxysilane, the condensation of the hydrated silica to form siloxane bonds between the molecules and the polycondensation of these dimers to form cyclic oligomers.[14] This process is illustrated in Scheme 3.2. A number of factors, including reaction time, pH, reaction solvent and drying method can influence the type of silica that is formed. Two commonly used drying methods are oven-drying and spray-drying.[15]

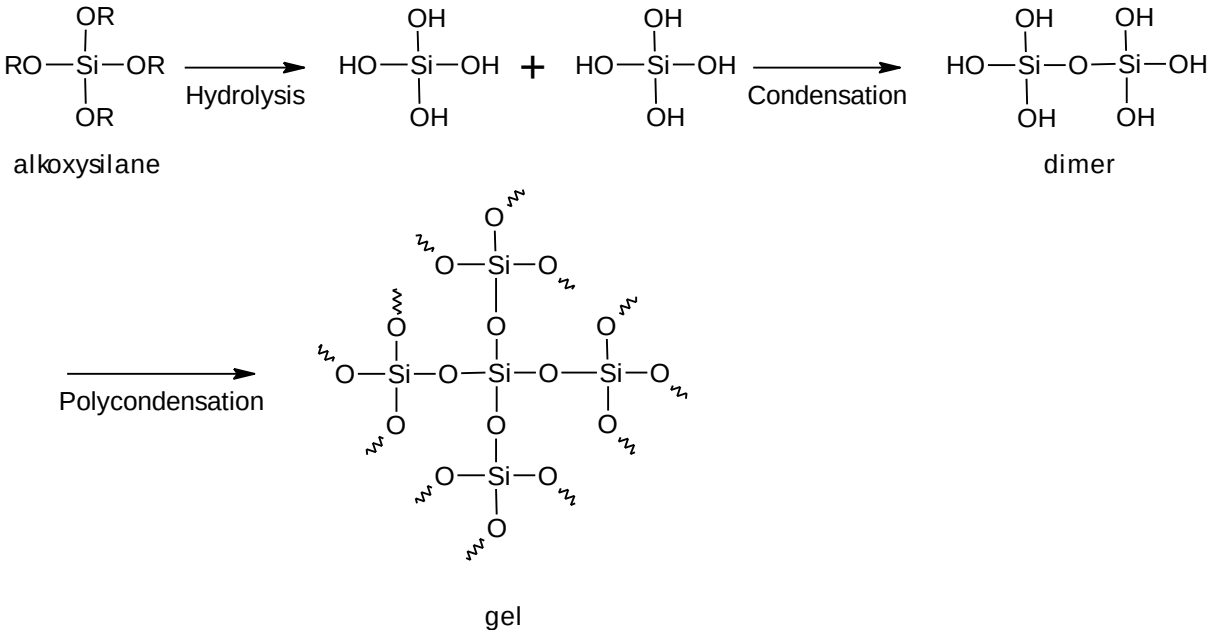

Scheme 3.2 Sol-gel formation

Zhao *et al.* compared encapsulated and covalently anchored Schiff-base manganese complexes as catalysts for cyclohexene epoxidation.[16] Figure 3.1 shows the two salicylaldehyde-alanine complexes used in the study. The complex on the left was encapsulated in silica by stirring it in a mixture of tetraethylorthosilicate and methanol and subsequent gelation. The complex on the right contains siloxane functionalities and was bonded to the sol-gel matrix by co-condensation of these groups with the tetraethylorthosilicate.

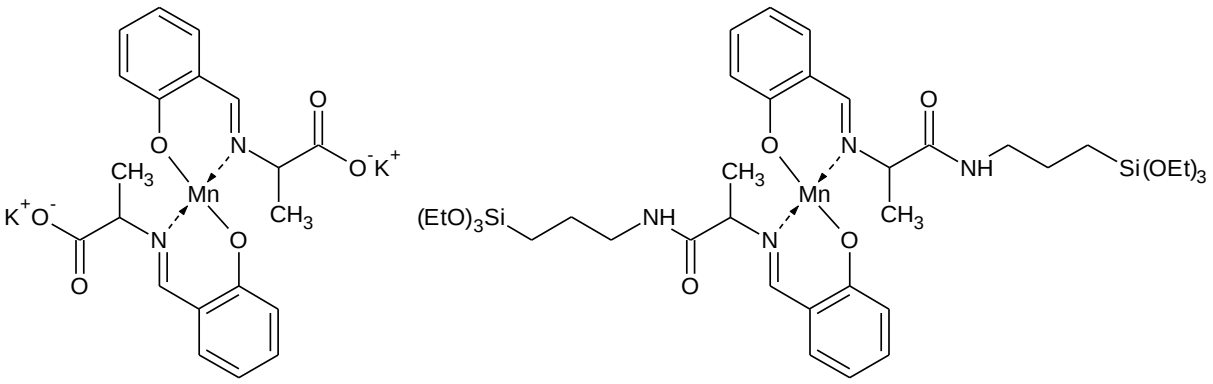

Figure 3.1 Encapsulated Sal-Ala-Mn complex (left) and anchored Sal-Ala-Mn complex (right)

The complexes were then tested in the epoxidation of cyclohexene along with an analogous homogeneous catalyst. The anchored catalyst outperformed both the encapsulated and homogeneous catalyst, with a conversion of 99.6% and selectivity of 88.2 after 6 hours. The homogeneous catalyst gave a conversion and selectivity of 89.3% and 73.2% respectively, while the encapsulated complex showed 87.8% conversion with a 80.5% selectivity. The anchored complex was also shown to be less prone to leaching, with the manganese content staying constant at 0.33% even after six catalytic runs. Over the same usage period the content in the encapsulated catalyst decreased from 0.25% to 0.16%.

The synthesis of mesoporous silicas formed by the liquid crystal templating method such as MCM-41 and SBA-15 has been well studied and is well documented in the literature. [17, 6] A simplified reaction scheme for this type of synthesis is shown in Scheme 3.3. An inorganic silicate precursor is added to a solution of a certain pH containing an appropriate surfactant molecule. Condensation of the silicate takes place around the surfactant molecules and this leads to the formation of the hexagonal array of pores.[17] The surfactant is then removed by calcination to yield the mesoporous material. The pH of the reaction solution, reaction times, and choice of surfactant influence the type of mesoporous material that is formed. Surfactants that can be used include neutral (Triton X-100), cationic (cetyl trimethylammonium bromide) and polymeric (tri-block copolymer) surfactants.[18,6,19]

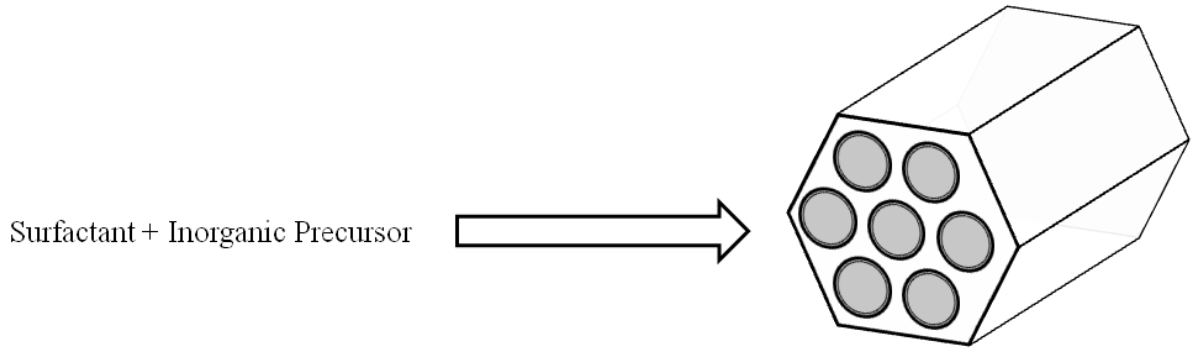

Scheme 3.3 Schematic representation of the general formation of silica by liquid crystal templating

Mesoporous silica materials are usually characterized by a wide range of solid-state analytical techniques in order to gain insight into the structure of the silica. Nitrogen adsorption analysis is done in order to determine the surface area and pore diameters of the materials. Both these properties are important when supports for catalysis are chosen. Powder X-ray diffraction analysis is used in order to determine the degree of crystallinity of the materials. The macrostructure of these materials is studied using scanning electron microscopy. Several studies have been carried out on the synthesis and characterization of mesoporous silicas and their synthesis and recommended characterization methods have been widely reported in the literature.[17,20,21]

In this chapter we report the synthesis and characterization of the mesoporous silicas MCM-41 and SBA-15 and the immobilized catalyst systems formed after copper and palladium complexes have been immobilized onto these silicas. We also report the synthesis and characterization of sol-gel silicas containing these complexes.

3.1 Synthesis and Characterization of Silica Supports MCM-41 and SBA-15

The synthetic procedure used to synthesize the MCM-41 and SBA-15 silica supports was adopted from work done by the groups of Chai and Zhao respectively.[22,6]

In order to synthesize MCM-41, cetyl trimethylammonium bromide was used as surfactant in a basic solution. Tetraethyl-orthosilicate (TEOS) was used as silica source and was added after the surfactant had dissolved completely. This resulted in a white slurry being formed.

For the synthesis of SBA-15, poly(ethyleneglycol)-*block*-poly(propyleneglycol)-*block*-poly(ethyleneglycol) (PEG) was used as surfactant in acidic conditions. Tetraethyl-orthosilicate was again used as the silica source and a white slurry formed upon the addition of TEOS.

The formed silicas were filtered and washed with water to remove any remaining surfactant and dried. The white powders were then calcined at 550°C for 8 hours to remove the respective templating molecules.

3.1.1 Characterization of MCM-41 and SBA-15

MCM-41 and SBA-15 were characterized by surface area analysis, powder X-ray diffraction and scanning electron microscopy.

3.1.1.1 Characterization of MCM-41 and SBA-15 by means of BET (Brunauer Emmett Teller) analysis

The surface area and average pore diameter of the silica supports were determined using BET analysis. The samples were degassed at 200°C for 24 hours in order to remove any solvent or moisture. The relative pressure of the environment of the silicas was increased from 0 to 1 relative pressure (P/P_0). The amount of nitrogen adsorbed was measured and used to calculate the surface area as it relates to the mass of the sample.

The change in the volume of nitrogen adsorbed onto the surface of a sample as the relative pressure changes can be illustrated as a nitrogen adsorption isotherm. According to the International Union of Pure and Applied Chemistry, there are six different types of isotherms, shown in Figure 3.2.[23] The

type of material and inner pore structure of the material determines the type of isotherm that is observed.

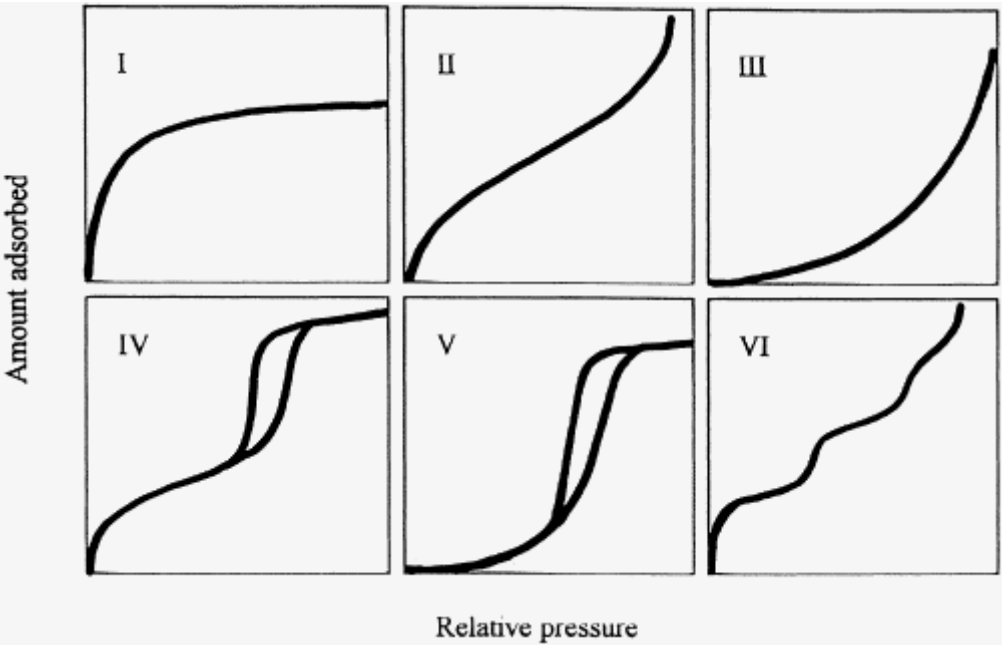

Figure 3.2 Different types of isotherm plots[23]

The isotherm plots of the native silica supports are shown in Figure 3.3. Both MCM-41 and SBA-15 show characteristic type IV isotherm plots. This is consistent with the expected mesoporous structure of the materials.[24] The adsorption-desorption curve of SBA-15 indicates that the silica contains interconnecting micropores as well as mesopores.[25]

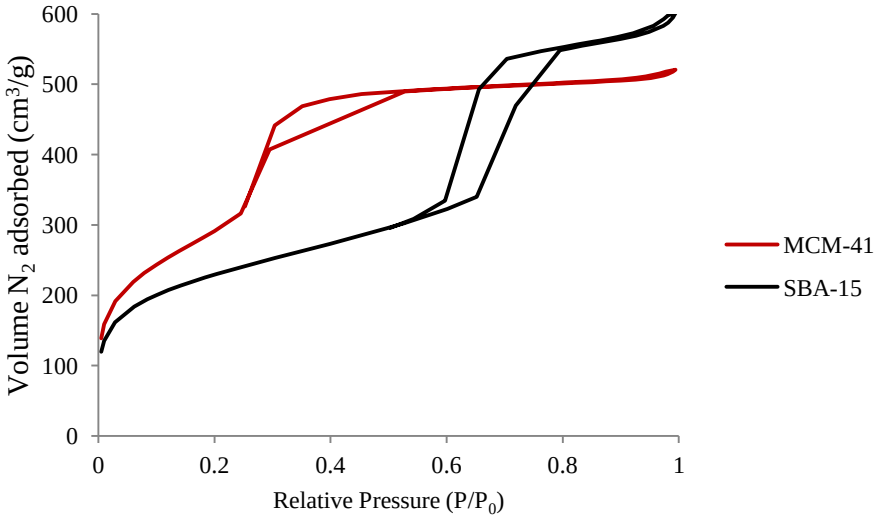

Figure 3.3 Isotherm plots for MCM-41 and SBA-15

The pore-filling step of the MCM-41 and SBA-15 occurs at P/P_0 0.30-0.53 and 0.54–0.80 relative pressures respectively. The pores of MCM-41 are filled over a slightly smaller range than that of SBA-15. This information means that MCM-41 has a narrower pore size distribution than SBA-15. Figure 3.4 shows the pore volume relative to the pore diameter for both silicas, and supports the above conclusion. The pore diameter is calculated using Barret-Joyner-Halenda (BJH) calculations and desorption data.

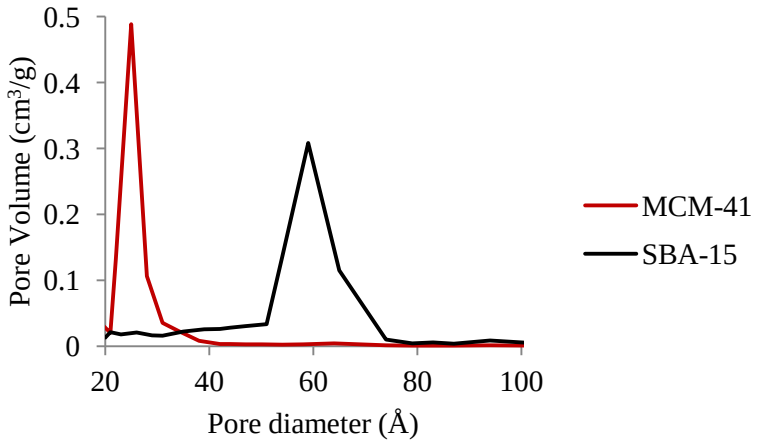

Figure 3.4 Pore size distribution plot of MCM-41 and SBA-15

Table 3.1 shows a summary of the calculated BET surface areas as well as the average pore diameters of the native MCM-41 and SBA-15 silicas. The surface area of MCM-41 is much higher than that of SBA-15, while SBA-15 has larger pore sizes. These results are consistent with results from the literature.[20]

Table 3.1 Summary of surface areas and pore diameters of native silica supports

Material	Surface area (cm^2/g)	Pore Diameter (Å)
MCM-41	1062	30.3
SBA-15	817	45.5

3.1.1.2 Characterization of MCM-41 and SBA-15 by means of Powder XRD analysis

The silica supports were also characterized by powder X-ray diffraction analysis. The diffraction patterns are shown in Figure 3.5 and 3.6 for MCM-41 and SBA-15 respectively and are typical for these types of materials.[5,26] Both supports show three well resolved peaks that can be indexed as (100), (110) and (200) diffractions that are associated with a 2-D hexagonal symmetry. This indicates

a well-ordered mesostructure. In the diffraction pattern of MCM-41, a fourth peak of low intensity can be seen and corresponds to the (210) diffraction. This indicates that the material is of a good quality.[27]

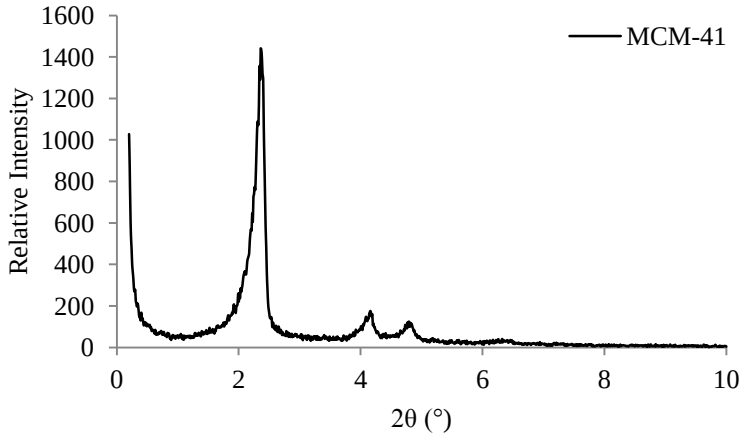

Figure 3.5 Powder XRD plot of MCM-41

The diffraction peaks for SBA-15 occur at lower angles than those of MCM-41. This is typical for SBA-15 and illustrates the influence that the synthetic method used can have on the mesostructure of the silica support. The lower reflection angles are typical of materials with larger pore diameters.[26]

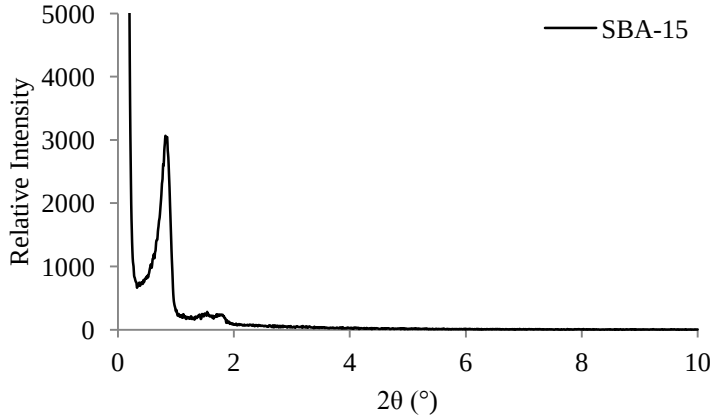

Figure 3.6 Powder XRD plot of SBA-15

A summary of the diffraction peaks is given in Table 3.2

Table 3.2 Reflection angles of diffraction planes for native MCM-41 and SBA-15

Material	(100)	(110)	(200)	(210)
MCM-41	2.35	4.15	4.73	6.32
SBA-15	0.83	1.50	1.80	n/a

The interplanar spacing of the materials for the reflection plane (100) was calculated using Bragg's equation, $n\lambda = 2d\sin\theta$, where $\lambda = 1.5401$ Å and n for $d_{100} = 1$. The d spacing for the reflection plane (100) was calculated to be 38 Å for MCM-41 and 106 Å for SBA-15. From this one can calculate the hexagonal lattice parameter a ($a = 2d_{100}/(3)^{-½}$. The hexagonal lattice parameter was then calculated to be 44 Å for MCM-41 and 122 Å for SBA-15. These values are typical for MCM-41 and SBA-15.[28- 30]

3.1.1.3 Characterization of MCM-41 and SBA-15 by means of scanning electron microscopy

The silica supports were characterized using scanning electron microscopy to verify the morphology of the materials. Figure 3.7 shows the morphology of the individual silica particles and also gives an indication of the size of the particles.

The MCM-41 particles are round or hexagonal in nature, while the SBA-15 particles are longer and form cylinders. On average, the MCM-41 particles are larger in size than the SBA-15 particles. This agrees with the known morphology of these silica supports.[5,26]

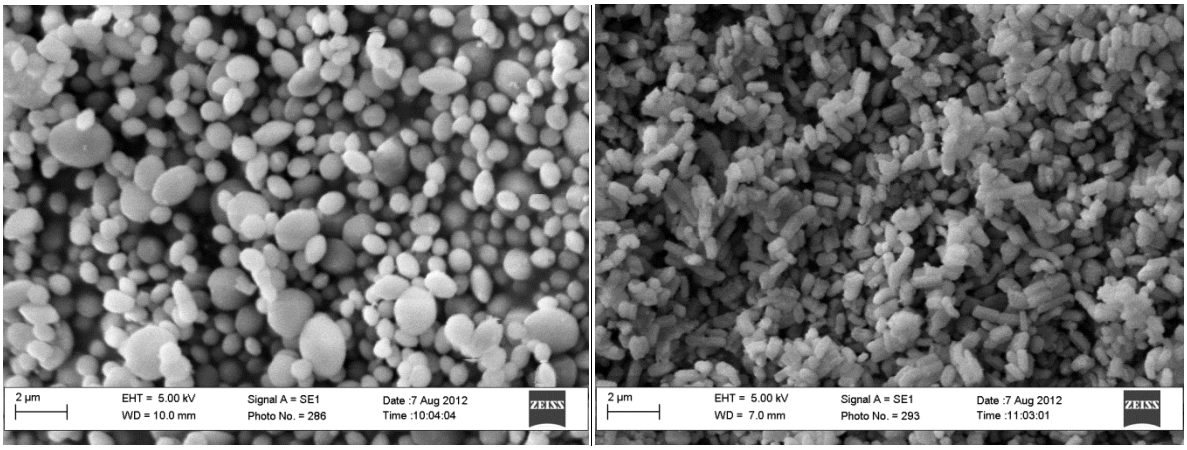

Figure 3.7 SEM micrographs of native MCM-41 (left) and SBA-15 (right)

3.2 Synthesis and Characterization of Immobilized Catalysts

In order to immobilize the siloxane-functionalized complexes onto the surface of the silica supports, a condensation reaction between the surface silanol groups of the silica and the siloxane groups has to occur. This results in the complex being covalently bonded to the silica support. Scheme 3.4 shows a general procedure for the immobilization of the complexes onto silica.

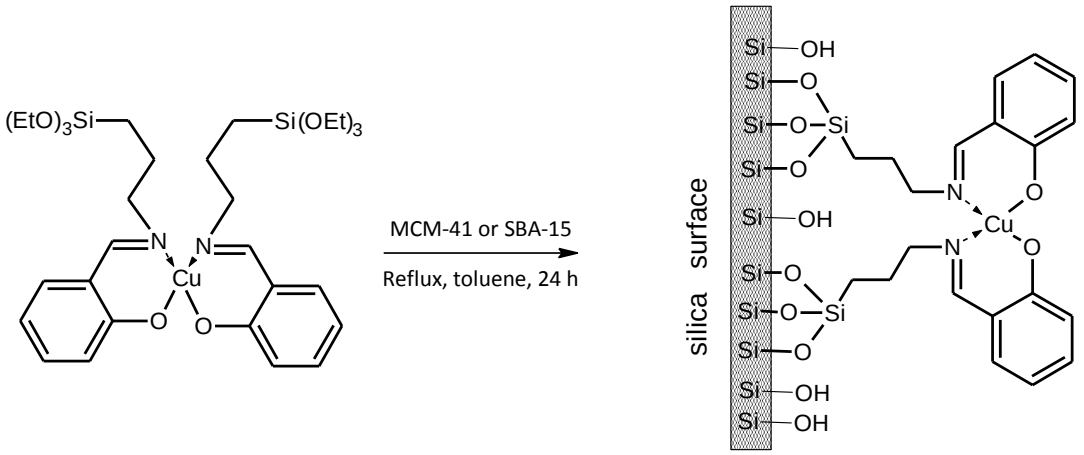

Scheme 3.4 Immobilization of functionalized complexes onto silica supports

For our study 10 weight % complex was reacted with the respective silica supports. This would lead to a 0.89 weight % of copper and a 1.40 weight % of palladium on the silica supports. The condensation reaction was carried out in toluene while being refluxed for 24 hours.

Light green powders were recovered for the immobilized copper complexes, while the immobilized palladium complexes yielded light yellow powders. The powders were extensively washed with DCM to remove any complex that was not bonded to the silica supports. The powders were then dried under vacuum to remove any residual toluene.

3.2.1 Characterization of Immobilized Catalysts

The immobilized catalysts were characterized by BET analysis, powder X-ray diffraction, thermogravimetric analysis, scanning electron microscopy and ICP-AES.

3.2.1.1 Characterization of Cu(II) and Pd(II) immobilized catalysts by means of BET (Brunauer Emmett Teller) analysis

One would expect the surface area of the supports to decrease after immobilization of the complexes onto the support, as some of the surface where the nitrogen can be adsorbed is now occupied by the complexes. BET analysis was used in order to determine whether this was indeed the case. Figure 3.8 clearly shows a decrease in the volume of nitrogen adsorbed onto the surface of the MCM-41 support after immobilization.

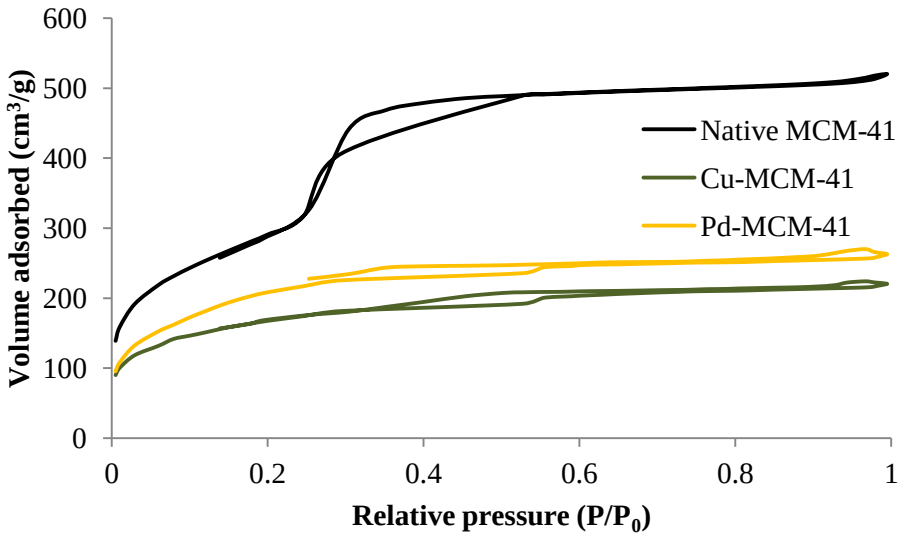

Figure 3.8 Isotherm plots for MCM-41, Cu-MCM-41 and Pd-MCM-41 (first attempt)

From Figure 3.8 one can see that the shape of the isotherm has changed as well, and almost approaches a Type I isotherm, which corresponds to a non-porous material. This indicates that the immobilization of the complexes onto the MCM-41 had an influence on the morphology of the support. The vigorous stirring of the silica slurry during immobilization could have caused the loss of crystallinity. The immobilization step was therefore repeated with a more moderate stirring rate. The BET isotherms obtained for the second group of MCM-41 immobilized catalysts, shown in Figure 3.9, are Type IV isotherms, indicating that the mesopores are still present in the material in this particular case.

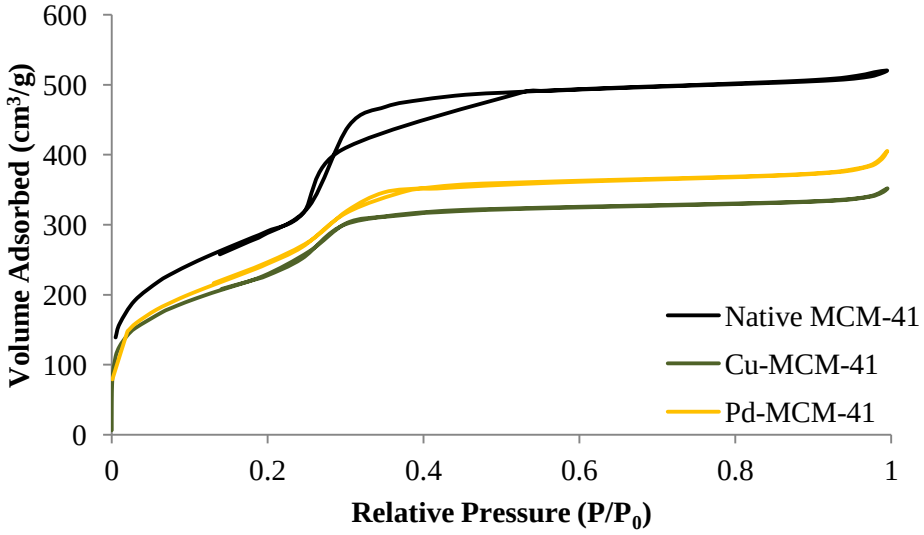

Figure 3.9 Isotherm plots for MCM-41, Cu-MCM-41 and Pd-MCM-41 (second attempt)

In the case of SBA-15, shown in Figure 3.10, the shape of the isotherms stay the same and only the volume of nitrogen adsorbed has changed.

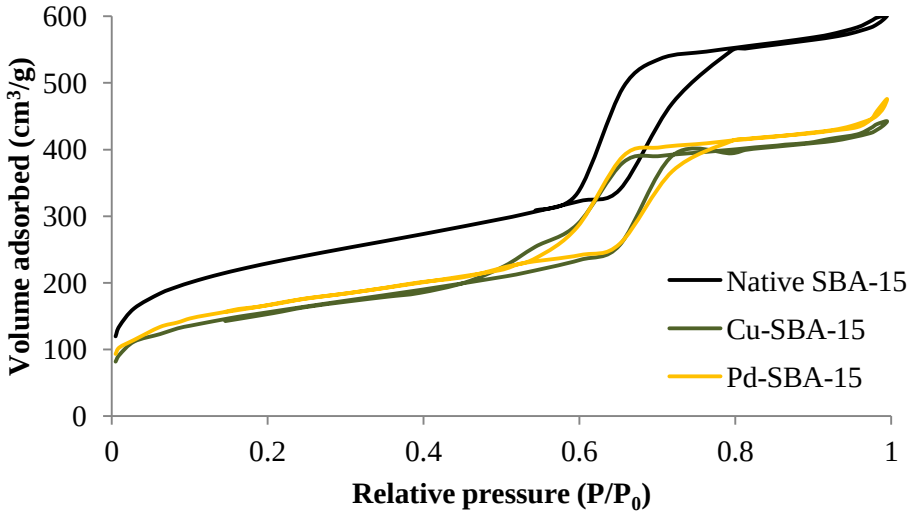

Figure 3.10 Isotherm plots for SBA-15, Cu-SBA-15 and Pd-SBA-15

A summary of the surface area and pore diameter results for MCM-41 and SBA-15 after immobilization of the catalysts is given in Table 3.3. As expected, there is a decrease in the surface areas after immobilization of the catalysts. The pore diameters of the MCM-41 after immobilization are significantly smaller, while the pore diameters of the SBA-15 after immobilization are slightly larger.

Table 3.3 Summary of surface areas and pore diameters of native silica supports and immobilized catalysts

Material	Surface area (cm^2/g)	Pore Diameter (Å)
MCM-41	1062	30.3
Cu-MCM-41	822	25.7
Pd-MCM-41	886	27.1
SBA-15	817	45.5
Cu-SBA-15	559	49.0
Pd-SBA-15	569	46.8

The change is surface area is fairly consistent, ranging from 176 cm^2/g to 258 cm^2/g.

3.2.1.2 Characterization of Cu(II) and Pd(II) immobilized catalysts by means of Powder XRD analysis

The immobilized catalysts were also characterized by means of powder X-ray diffraction. One would expect the diffraction patterns to be similar to that of the native silica supports, provided that a change in morphology has not taken place.

In the XRD plot for MCM-41 and the first batch of immobilized catalysts systems on MCM-41, shown in Figure 3.11, a change in the diffraction pattern is observed. No peaks are observed for the immobilized catalysts. A loss of crystallinity has therefore taken place. This agrees with the BET results discussed above.

After the complexes were re-immobilized on MCM-41 the powder XRD plot (Figure 3.12) shows that the crystallinity is retained. This confirms what was seen in the BET isotherm plots for the second group of catalysts immobilized on MCM-41. It is suspected that physical degradation of the silica took place during the immobilization process.

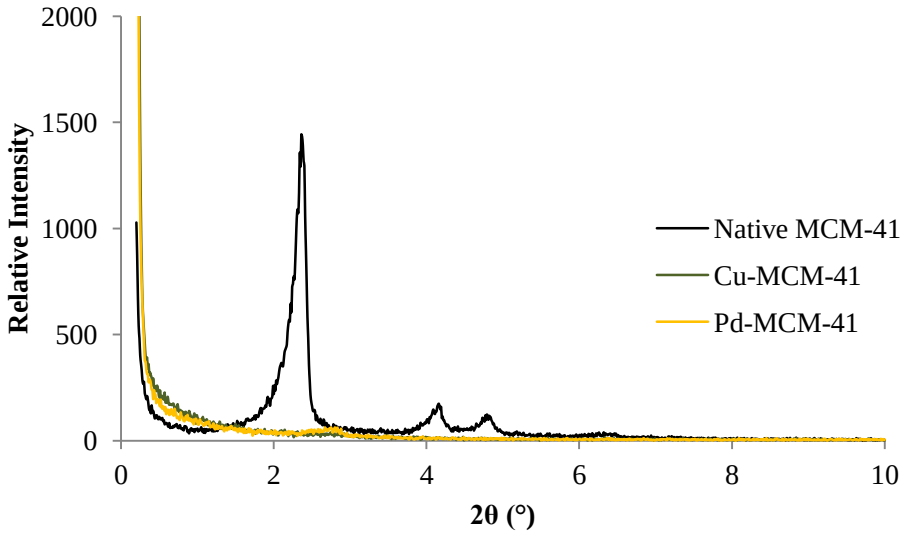

Figure 3.11 Powder XRD plots for MCM-41, Cu-MCM-41 and Pd-MCM-41 (first attempt)

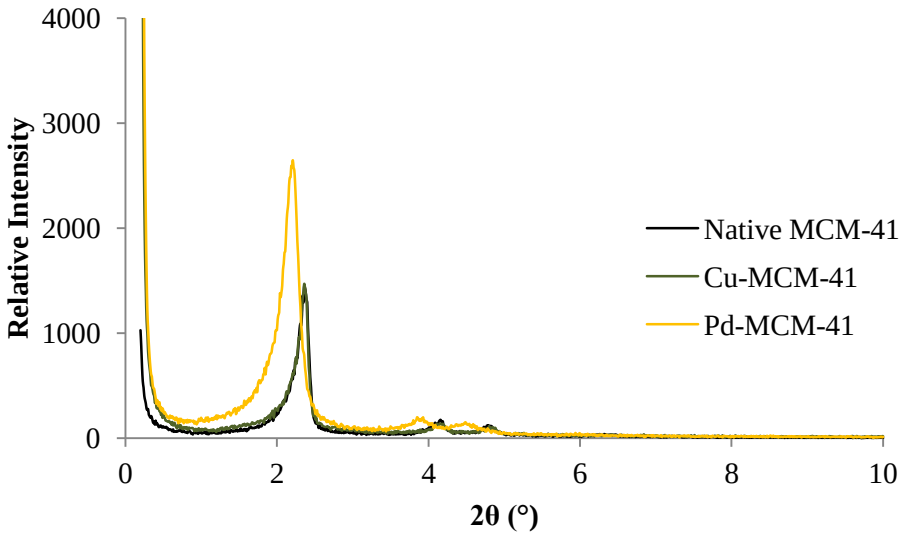

Figure 3.12 Powder XRD plots for MCM-41, Cu-MCM-41 and Pd-MCM-41 (second attempt)

For the immobilized catalysts on SBA-15, the diffraction pattern does not differ much from the native SBA-15. Figure 3.13 shows that the crystallinity has been retained after immobilization of the complexes and the structure of the support was not significantly altered during immobilization.

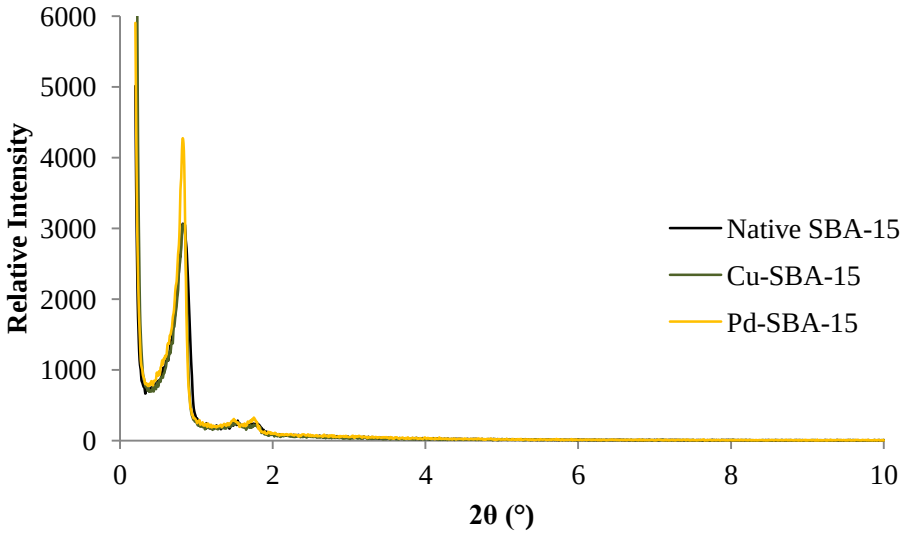

Figure 3.13 Powder XRD plots for SBA-15, Cu- SBA-15 and Pd- SBA-15

3.2.1.3 Characterization of Cu(II) and Pd(II) immobilized catalysts by means of thermogravimetric analysis

The immobilized catalysts were characterized using thermogravimetric analysis. A change in weight should occur when the immobilized complex starts to decompose and is lost from the silica supports. Figure 3.14 shows the weight loss profiles for the copper immobilized catalysts. An initial loss, corresponding to a loss of moisture that was adsorbed on the silica, is observed below 100°C. The loss is greater for Cu-MCM-41 than for Cu-SBA-15, which shows that more moisture was adsorbed onto the surface of the Cu-MCM-41. The decomposition of the copper complexes takes place between 300°C and 350°C. At this temperature, CuO is formed while the ligand decomposes. This loss is about 3% of the total weight for both the Cu-MCM-41 and Cu-SBA-15. After this loss, the weight remains stable.

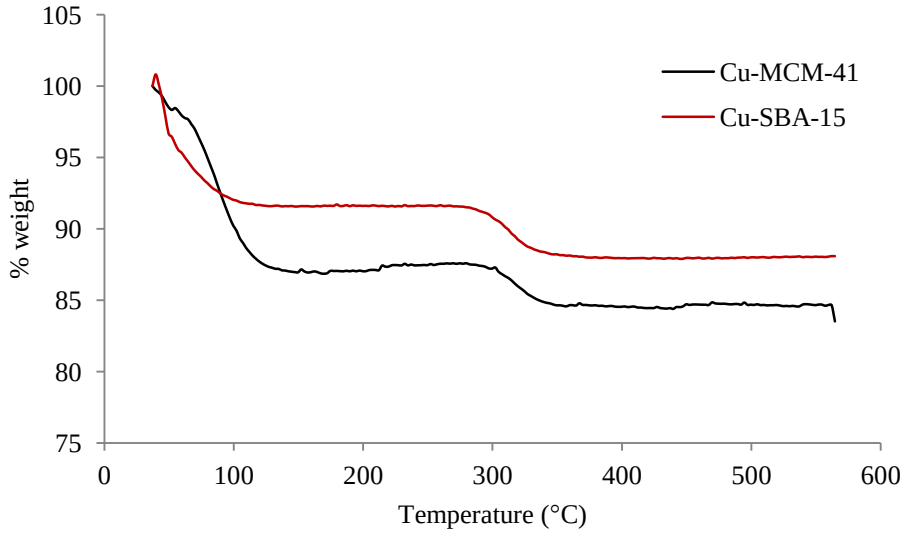

Figure 3.14 TGA plot for Cu-immobilized catalysts

For the palladium immobilized catalysts, an initial weight loss is observed as well, corresponding to moisture loss (Figure 3.15). As in the previous case, this loss is greater for MCM-41 than for SBA-15. A second loss occurs between 265°C and 400°C. At this temperature the ligand decomposes and is lost from the silica, while the palladium is oxidized to form PdO. The weight loss is again roughly 3% of the total weight.

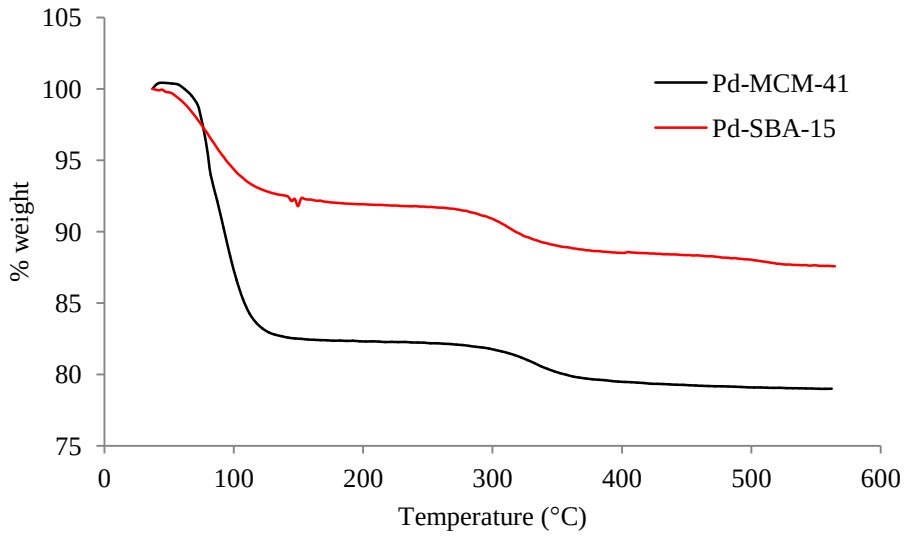

Figure 3.15 TGA plot for Pd-immobilized catalysts

3.2.1.4 Characterization of Cu(II) and Pd(II) immobilized catalysts by means of scanning electron microscopy

The immobilized catalysts were also characterized by scanning electron microscopy in order to determine whether any changes in the morphology had occurred during immobilization. Figure 3.16a shows the micrographs of native MCM-41 and Cu-MCM-41 while Figure 3.16b shows micrographs of native SBA-15 and Cu-SBA-15.

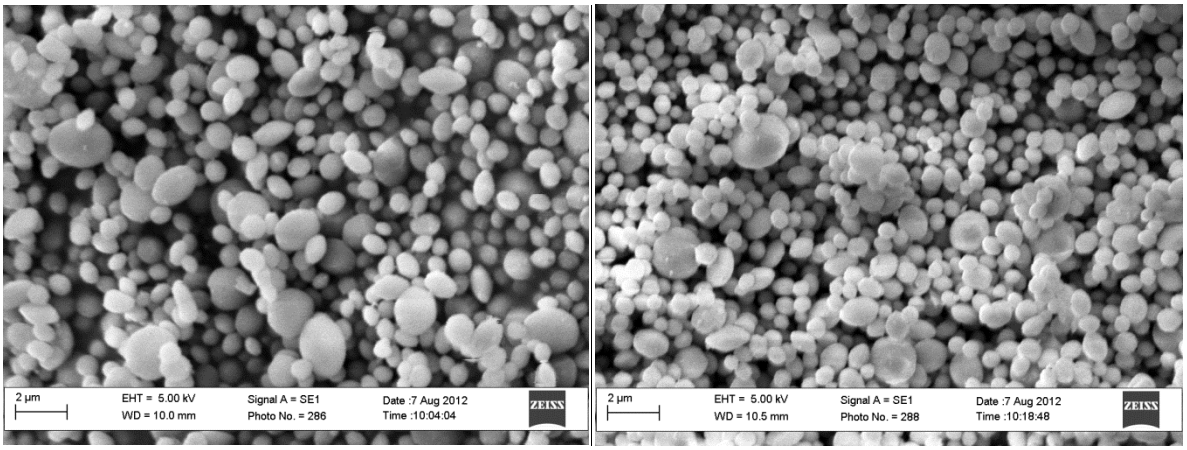

Figure 3.16a SEM micrographs of native MCM-41 (left), Cu-MCM-41 (right)

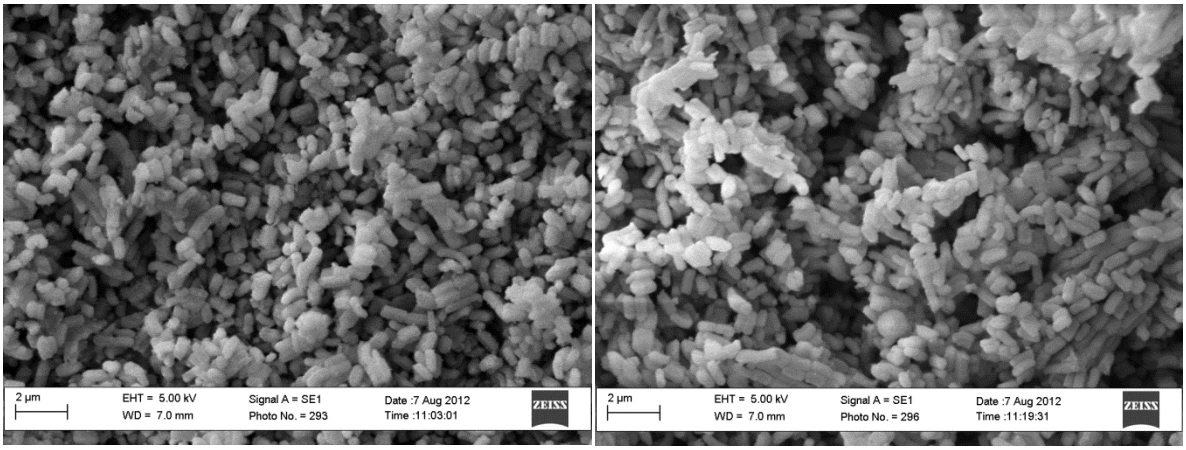

Figure 3.16b Native SBA-15 (left) and Cu-SBA-15 (right)

The micrographs showed no significant change in the microstructure after the immobilization process had taken place. Similar results were obtained for the immobilized catalysts containing palladium complexes.

3.2.1.5 Characterization of Cu(II) and Pd(II) immobilized catalysts by means of ICP-AES

Inductively coupled plasma atomic emission spectroscopy was done on the immobilized catalysts in order to determine the exact metal loading on the silica supports. The silica was digested using hot concentrated nitric acid and hot *aqua regia* for the copper and palladium immobilized complexes respectively. Any remaining solid was filtered off, and the filtrate was analyzed for the presence of metals.

A summary of the results obtained can be seen in Table 3.4. It can be seen that the metal loading on SBA-15 is higher than on MCM-41, although in the case of the copper complex the difference is very slight.

Table 3.4 Metal loading on immobilized catalysts

Material	Weight % Cu	Weight % Pd
Cu-MCM-41	0.91	n/a
Pd-MCM-41	n/a	1.00
Cu-SBA-15	0.92	n/a
Pd-SBA-15	n/a	1.30

The copper loading on the supports is slightly higher than expected (0.91 and 0.92 weight % vs 0.89 weight %). This can be attributed to weighing errors. The palladium loading on the supports is lower

than the expected loading (1.00 and 1.30 weight % vs 1.40 weight %). The loss of support integrity during the immobilization of the palladium complex onto the MCM-41 might explain the lower metal loading.

3.3 Synthesis and Characterization of Sol-gel Silicas

Two types of catalyst systems were prepared using the sol-gel technique – one where the catalysts were physically encapsulated, and the other with the catalysts being covalently anchored to the silica matrix. For the physically encapsulated systems, the model complexes were used, and the functionalized complexes were used for the anchored systems. Silica containing no catalyst were prepared as well and is referred to as native silica.

TEOS (7.36 mL) was added to a 1:6 mole ratio mixture of THF (10.70 mL) and water (3.57 mL). The pH of the mixture was adjusted to 1.5 using hydrochloric acid. The mixture was stirred for 18 hours while the hydrolysis reaction took place. The pH of the mixture was raised to 5.8 using an ammonia solution, after which the appropriate complex was added. Gelation of the silica took place over a 30 minute time period. The silica was then dried using either the spray-drying or oven-drying method. Spray-dried silicas were obtained as powders. In the case of oven-drying, the formed gel was dried at 70°C for five days and then ball-milled in order to obtain the silica as a powder.

Four sol-gel catalyst systems were obtained (Table 3.5).

Table 3.5 Sol-gel catalysts

	Complex	Method of drying
SG1	Model Cu(II)	Spray-dried
SG2	Functionalized Cu(II)	Spray-dried
SG3	Model Cu(II)	Oven-dried
SG4	Functionalized Cu(II)	Oven-dried

3.3.1 Characterization of sol-gel silicas

The immobilized catalysts were characterized by thermogravimetric analysis, scanning electron microscopy and ICP-AES.

3.3.1.1 Characterization of sol-gel silicas by means of thermogravimetric analysis

Thermogravimetric analysis was used to analyze the sol-gel systems. As stated in Section 3.2.1.3, a change in weight should occur when the complex starts to decompose and is lost from the silica supports. Figure 3.17 shows the weight loss profiles for the spray-dried sol-gel silica catalyst systems.

An initial loss, corresponding to a loss of moisture that was adsorbed on the silica, is observed below 100°C for the native silica as well as the silica containing the complexes. The rate of weight loss decreases at 140°C for all three systems. The silica containing the metal complex shows and extra weight loss step at 360°C. This corresponds to the decomposition of the ligand and the formation of CuO. Similar weight loss profiles were observed for the oven-dried sol-gel silica catalyst systems and these are shown in Figure 3.18.

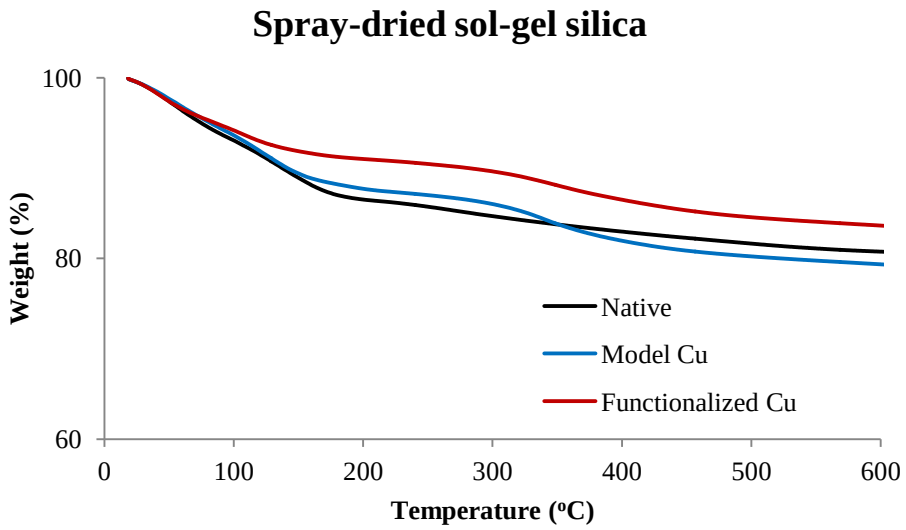

Figure 3.17 TGA plot for spray-dried sol-gel catalyst systems

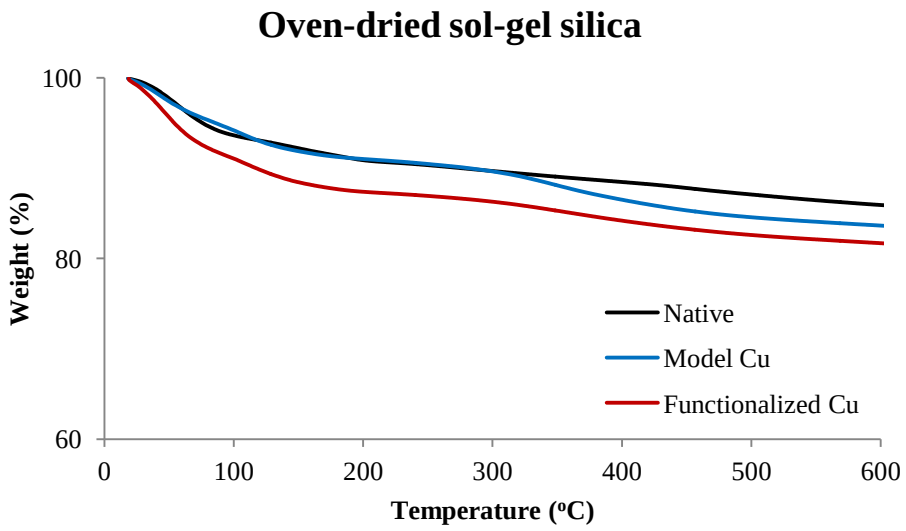

Figure 3.18 TGA plot for oven-dried sol-gel catalyst systems

3.3.1.2 Characterization of sol-gel silicas by means of scanning electron microscopy

The SEM micrographs of the sol-gel silicas are shown in Figure 3.19. In the case of the native spray-dried silica, spherical particles of varying sizes are observed. Some of the particles have a dimpled appearance due to buckling of the shell during formation.[31] In the micrograph of **SG2**, almost all of the particles contain dimples or cavities. According to Iskandar *et al.*, there are four main factors that can influence the morphology of the particles: droplet size, mass fraction of the particles within the droplet, gas flow rate during evaporation and temperature of evaporation.[32] In our case, the change in morphology is due to the difference in mass fraction of the particles. After the addition of the copper complex, the mass fraction of the particles in the droplet is higher, and the surface tension forces that keep the droplets in a spherical shape are overcome by inertial effects.

The micrographs of the oven-dried silicas show uneven particles with a wide range of shapes and sizes. This is due to the way the glassy precursor to the silica is shattered during the ball-milling process. There is no significant difference in morphology between the native oven-dried silica and **SG4**.

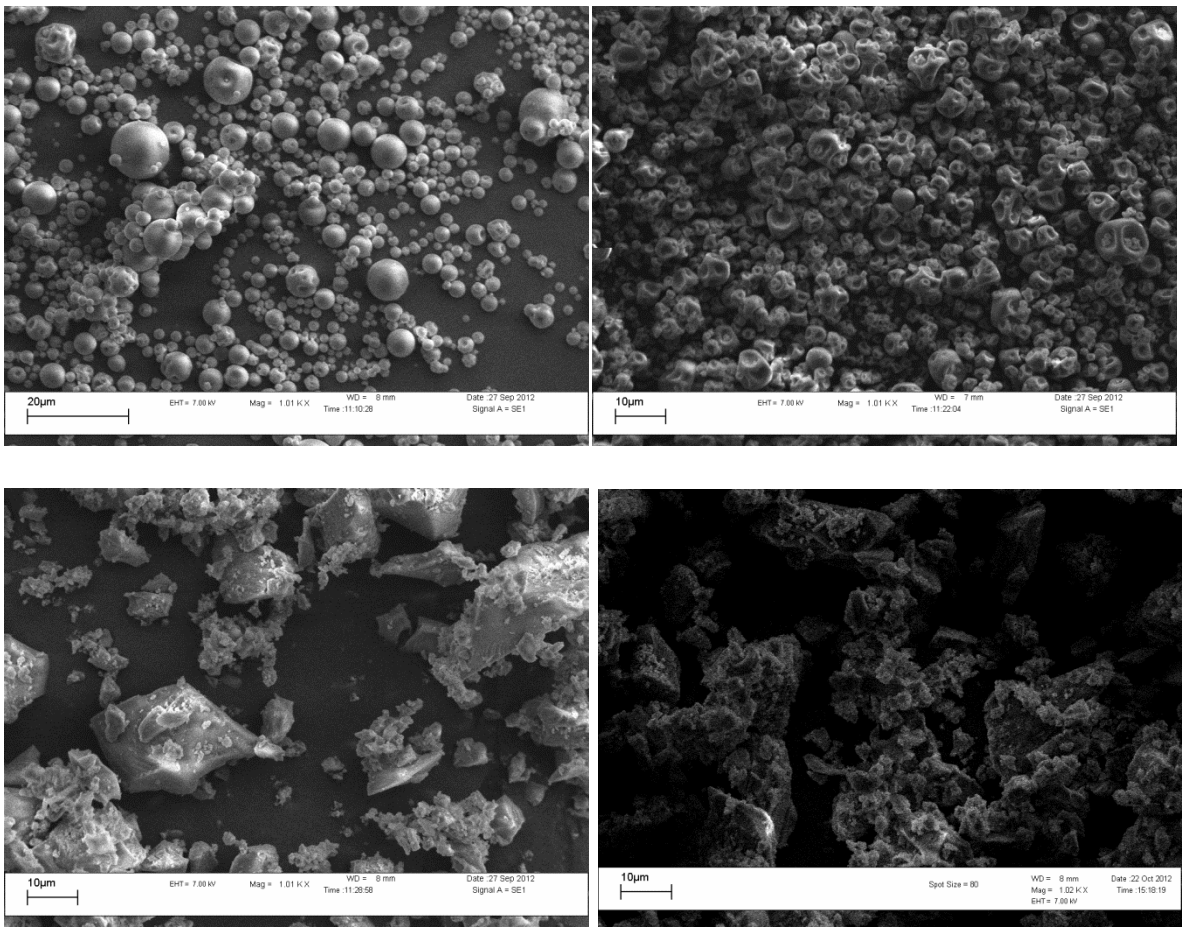

Figure 3.19 SEM micrographs of native spray-dried silica (top left), SG2 (top right), native oven-dried silica (bottom left) and SG4 (bottom right)

3.3.1.3 Characterization of sol-gel silicas by means of ICP-AES

Inductively coupled plasma atomic emission spectroscopy was done on the immobilized sol-gel catalysts in order to determine the exact metal loading achieved. The silica was digested using hot concentrated nitric acid and hot *aqua regia* for the copper and palladium immobilized complexes respectively. Any remaining solid was filtered off, and the filtrate was analyzed for the presence of metals. A summary of the results obtained can be seen in Table 3.6.

Table 3.6 Metal loading on sol-gel catalysts

Material	Weight % Cu
SG1	0.61
SG2	0.36
SG3	0.54
SG4	0.37

The metal loading is higher for both the physically encapsulated systems than for the corresponding anchored systems. The copper content by mass of the model complex, used to make the physically encapsulated systems, is 16% while for the functionalized complex it is 9%. Since the mass of the complexes added to the hydrolyzed TEOS systems was kept constant, one would expect that the physically encapsulated systems would exhibit a higher metal loading.

3.4 Concluding remarks

Two types of mesoporous silica, MCM-41 and SBA-15 have been successfully synthesized and characterized using a wide range of solid-state techniques. The Cu(II) and Pd(II) functionalized complexes described in Chapter 2 have been immobilized on these silicas to yield four different catalyst systems. These catalyst systems have been characterized as well and data obtained from BET measurements, TGA analysis and ICP analysis indicates that the metal complexes have been immobilized onto the silica supports.

Sol-gel techniques were used to prepare four additional catalyst systems. The Cu(II) complexes were physically entrapped (model complexes) or covalently anchored (functionalized complexes) in the sol-gel silica matrix. ICP analysis indicates that the complexes are incorporated into the silica.

3.5 Experimental section

3.5.1 General remarks and instrumentation

The synthesis of and immobilization of complexes onto mesoporous silicas were carried out under nitrogen using standard Schlenk techniques. A Buchi Mini Spray Dryer B-290 was used to synthesize the spray-dried silica. Ball-milling was carried out using a Fritsch Planetary Mono Mill Pulverisette 6 instrument.

Powder XRD analysis was done on an X'Pert Pro Multi Purpose Diffractometer with a Reflection Transmission Spinner. Nitrogen adsorption/desorption analysis was done on an ASAP 2010 (Accelerated Surface Area end Porosimetry System) instrument. The samples were degassed at 250°C for 24 hours prior to analysis. SEM micrographs were recorded on a LEO 1430VP microscope.

ICP-AES analysis was done on the immobilized catalysts to quantify the amount of metal that is present in the catalyst. The samples were prepared by digesting 40 mg of the immobilized catalyst in hot nitric acid (copper complexes) or hot *aqua regia* (palladium complexes). The sample was then filtered and the filtrate made up to a known volume and analyzed on a Spectro Arcos ICP-OES with a Burgener T2100 and cyclonic spray chamber as nebulizer.

3.5.2 Materials

Reagents were purchased from Sigma-Aldrich and used as recieved. These include tetraethylorthosilicate, cetyl trimethylammonium bromide and poly(ethyleneglycol)-block-poly(propyleneglycol)-block-poly(ethyleneglycol) block copolymer. Solvents were purchased from Sigma-Aldrich and Kimix Chemicals. Toluene was dried over sodium wire with added benzophenone.

3.5.3. Synthesis of native supports

3.5.3.1 Mesoporous silica MCM-41

An ammonium solution (410 ml, 25% wt) was added to distilled water (540 ml) (pH 12.3). Whilst stirring the solution, the surfactant (cetyltrimethylammonium bromide) (3.994 g) was added. The solution was heated at 50°C while being stirred. Tetraethoxysilane (TEOS) (20 ml) was added after the solution became homogeneous. A white slurry soon formed and the mixture was stirred for a further 2 hours at 50°C. The mixture was left to cool to room temperature and was filtered and washed with 1100 ml distilled water and left to dry. The white solid obtained was calcined at 550°C (temperature slowly increased). The calcination process was kept running for 8 hours. 3.800 g of MCM-41 was obtained.

3.5.3.2 Mesoporous silica SBA-15

Poly(ethylene)-*block*-poly(propylene)-*block*-poly(ethylene) (8.050 g) was dissolved in 60 ml of distilled water and 2 M HCl solution (360 ml) while being stirred at 35°C. TEOS (18.2 ml) was added to this stirred solution (after everything dissolved) and was stirred at 35°C for 20 hours. The temperature of the mixture was then increased to 80°C and aged for 24 hours without being stirred. A solid product formed and it was filtered off and washed with 1800 ml of distilled water and dried at room temperature. The white product was then calcined at 550°C for 8 hours. 5.976 g of SBA-15 was obtained.

3.5.4 Synthesis of immobilized catalysts

3.5.4.1 Cu(II) salicylaldimine immobilized catalysts

The procedure followed for immobilization of the metal complexes onto MCM-41 and SBA-15 was exactly the same. Cu-MCM-41 is used as an example. Complex **C2** (0.102 g, 0.143 mmol) was added to a slurry of MCM-41 (1.005 g in 10 ml dry toluene) in a 50 ml round bottom flask. The slurry was refluxed at 110°C for 24 hours and gave a dark green mixture. The solid was filtered off and was then washed with dry dichloromethane (5 x 10 ml) to remove any unreacted complex. The light green product obtained was dried under vacuum to remove any residual toluene. 1.100 g of Cu-MCM-41 and 1.107 g of Cu-SBA-15 was obtained.

3.5.4.2 Pd(II) salicylaldimine immobilized catalysts

The procedure followed for immobilization onto MCM-41 and SBA-15 was exactly the same. Pd-MCM-41 is used as an example. Complex **C4** (0.099 g, 0.131 mmol) was added to a slurry of MCM-41 (1.015 g in 10 ml dry toluene) in a 50 ml round bottom flask. The slurry was refluxed at 110°C for 24 hours and gave a dark green mixture. The solid was filtered off and was then washed with dry dichloromethane (5 x 10 ml) to remove any unreacted complex. The light yellow product obtained was dried under vacuum to remove any residual toluene. 1.106 g of Pd-MCM-41 and 1.110 g of Pd-SBA-15 was obtained.

3.5.5 Synthesis of sol-gel silicas

3.5.5.1 Synthesis of native spray-dried silica

Tetraethylorthosilicate (7.36 mL, 32.96 mmol) was dissolved in a mixture of tetrahydrofuran (10.70 mL) and distilled water (3.57 mL) and stirred at room temperature. The pH was adjusted to 1.5 by the addition of hydrochloric acid (0.13 mL). The solution was stirred for 18 hours. Ammonia solution (0.30 mL) was added to raise the pH to 6. After 30 minutes the mixture was dried by spray-drying. A white powder (1.426 g) was obtained.

3.5.5.2 Synthesis of spray-dried silica with physically encapsulated Cu(II) complex SG1

Tetraethylorthosilicate (7.36 mL, 32.96 mmol) was dissolved in a mixture of tetrahydrofuran (10.70 mL) and distilled water (3.57 mL) and stirred at room temperature. The pH was adjusted to 1.5 by the addition of hydrochloric acid (0.13 mL). The solution was stirred for 18 hours. Ammonia solution (0.30 mL) was added to raise the pH to 6. Immediately after the addition of the ammonia, **C1** (0.100 g) was added and the solution turned a dark green colour. After 30 minutes the mixture was dried by spray-drying. A light green powder (1.548 g) was obtained.

3.5.5.3 Synthesis of spray-dried silica with anchored Cu(II) complex SG2

Tetraethylorthosilicate (7.36 mL, 32.96 mmol) was dissolved in a mixture of tetrahydrofuran (10.70 mL) and distilled water (3.57 mL) and stirred at room temperature. The pH was adjusted to 1.5 by the addition of hydrochloric acid (0.13 mL). The solution was stirred for 18 hours. Ammonia solution (0.30 mL) was added to raise the pH to 6. Immediately after the addition of the ammonia, **C2** (0.100 g) was added and the solution turned a dark green colour. After 30 minutes the mixture was dried by spray-drying. A light green powder (1.604 g) was obtained.

3.5.5.4 Synthesis of native oven-dried silica

Tetraethylorthosilicate (7.36 mL, 32.96 mmol) was dissolved in a mixture of tetrahydrofuran (10.70 mL) and distilled water (3.57 mL) and stirred at room temperature. The pH was adjusted to 1.5 by the addition of hydrochloric acid (0.13 mL). The solution was stirred for 18 hours. Ammonia solution (0.30 mL) was added to raise the pH to 6. After 30 minutes the mixture was placed in an oven at 70°C where it was dried for 5 days. A clear glass-type material was obtained which was ball-milled for 6 minutes to yield a white powder (1.385 g).

3.5.5.5 Synthesis of oven-dried silica with physically encapsulated Cu(II) complex SG3

Tetraethylorthosilicate (7.36 mL, 32.96 mmol) was dissolved in a mixture of tetrahydrofuran (10.70 mL) and distilled water (3.57 mL) and stirred at room temperature. The pH was adjusted to 1.5 by the addition of hydrochloric acid (0.13 mL). The solution was stirred for 18 hours. Ammonia solution (0.30 mL) was added to raise the pH to 6. Immediately after the addition of the ammonia, **C1** (0.100 g) was added and the solution turned a dark green colour. After 30 minutes the mixture was placed in an oven at 70°C where it was dried for 5 days. A dark green glass-type material was obtained which was ball-milled for 6 minutes to yield a light green powder (1.954 g).

3.5.5.6 Synthesis of oven-dried silica with anchored Cu(II) complex SG4

Tetraethylorthosilicate (7.36 mL, 32.96 mmol) was dissolved in a mixture of tetrahydrofuran (10.70 mL) and distilled water (3.57 mL) and stirred at room temperature. The pH was adjusted to 1.5 by the

addition of hydrochloric acid (0.13 mL). The solution was stirred for 18 hours. Ammonia solution (0.30 mL) was added to raise the pH to 6. Immediately after the addition of the ammonia, **C2** (0.100 g) was added and the solution turned a dark green colour. After 30 minutes the mixture was placed in an oven at 70°C where it was dried for 5 days. A dark green glass-type material was obtained which was ball-milled for 6 minutes to yield a light green powder (1.978 g).

3.6 References

1. Breck, D. W. *Zeolite Molecular Sieves;* Wiley: New York, 1974.

2. Flanigan, E. M.; Bennett, J. M.; Grose, R. W.; Cohen, J. P.; Patton, R. L.; Kirchner, R. M.; Smith, J. V. *Nature* **1978,** *271,* 512.

3. Davis, M. E.; Saldarriaga, C.; Montes, C.; Garces, J.; Crowder, C. *Zeolites* **1988,** *8,* 362.

4. Dessau, R. M.; Schlenker, J. L.; Higgins, J. B. *Zeolites* **1990,** *10,* 522.

5. Beck, J. S.; Vartuli, J. C.; Roth, W. J.; Leonowicz, M. E.; Kresge, C. T.; Schmitt, K. D. . C. C. T.-W.; Olson, D. H.; Sheppard, E. W.; McCullen, S. B.; Higgins, J. B.; Schlenker, J. L. *J. Am. Chem. Soc* **1992,** *114,* 10834.

6. Zhao, D.; Huo, Q.; Feng, J.; Chmelka, B. F.; Stucky, G. D. *J. Am. Chem. Soc.* **1998,** *120,* 6024.

7. Bagshaw, S. A.; Prouzet, E.; Pinnavaia, T. J. *Science* **1995,** *269,* 1242.

8. Giraldo, L. F.; Lopez, B.; Perez, L.; Urrego, S.; Sierra, L.; Mesa, M. *Macromol. Symp.* **2007,** *258,* 129.

9. Lee, I.; Albiter, M. A.; Zhang, Q.; Ge, J.; Yin, Z.; Zaera, F. *Phys. Chem. Chem. Phys.* **2011,** *13,* 2449.

10. Joo, S. H.; Park, J. Y.; Tsung, C.; Yamada, Y.; Yang, P.; Somorjai, G. A. *Nature Materials* **2009,** *8,* 126.

11. Hussain, M.; Fino, D.; Russo, N. *J. Hazard. Mater.* **2012,** *211,* 255.

12. Kholdeeva, O. A.; Maksimchuk, N. V.; Maksimov, G. M. *Catal. Today* **2010,** *157,* 107.

13. Monge-Marcet, A.; Pleixats, R.; Cattoen, X.; Man, M. W. C. *Catal. Sci. Technol.* **2011,** *1,* 1544.

14. Kato, M.; Sakai-Kato, K.; Toyo'oka, T. *J. Sep. Sci.* **2005,** *28,* 1893.

15. Wang, B.; Zhang, W.; Zhang, W.; Mujumdar, A. S.; Huang, L. *Dry. Technol.* **2005,** *23,* 7.

16. Zhao, J.; Han, J.; Zhang, Y. *J. Mol. Cat. A-Chem.* **2005,** *231,* 129.

17. Ying, J. Y.; Mehnert, C. P.; Wong, M. S. *Angew. Chem. Int. Ed.* **1999,** *38,* 56.

18. Sierra, L.; Guth, J.-L. *Micropor. Mesopor. Mater.* **1999,** *27,* 243.

19. Mesa, M.; Sierra, L.; Lopez, B.; Ramirez, A.; Guth, J.-L. *Solid State Sci.* **2003,** *5,* 1303.

20. de Oliveira, E. C.; Pires, C. T.; Pastore, H. O. *J. Braz. Chem. Soc.* **2006,** *17,* 16.

21. Slowing, I. I.; Vivero-Escoto, J. L.; Trewyn, B. G.; Lin, V. S.-Y. *J. Mater. Chem.* **2010,** *20,* 792.

22. Cai, Q.; Lin, W. Y.; Xiao, F.; Pang, W.; Zhou, B.; Chen, X. *Micropor. Mesopor. Mater.* **1999,** *32*, 1.

23. Donohue, M. D.; Aranovich, G. L. *Adv. Colloid Interface Sci.* **1998,** *137*, 76.

24. Cychosz, K. A.; Guo, X.; Fan, W.; Cimini, R.; Gor, G. Y.; Tsapatsis, M.; Neimark, A. V.; Thommes, M. *Langmuir* **2012,** *28*, 12647.

25. Esparza, J. M.; Ojeda, M. L.; Campero, A.; Hernandez, G.; Felipe, C.; Asomoza, M.; Cordero, S.; Kornhauser, I.; Rojas, F. *J. Mol. Cat. A* **2005,** *228*, 97.

26. Zhang, H.; Sun, J.; Ding, M.; Bao, X.; Klein-Hoffmann, A.; Weinberg, G.; Sy, D.; Schlogl, R. *J. Am. Chem. Soc.* **2004,** *126*, 7440.

27. Huo, Q.; Margolese, D. I.; Stucky, G. D. *Chem. Mater.* **1996,** *8*, 1147.

28. Grünberg, B.; Emmler, T.; Gedat, E.; Shenderovic, I.; Findenegg, G. H.; Limbach, H.; Buntkowsky, G. *Chem. Eur. J.* **2004,** *10*, 5689.

29. Zhu, J.; Konya, Z.; Puntes, V. F.; Kiricsi, I.; Miao, C. X.; Ager, J. W.; Alivisatos, A. P. S. G. A. *Langmuir* **2003,** *19*, 4396.

30. Manzano, M.; Aina, V.; Arean, C. O.; Balas, F.; Cauda, V.; Colilla, M.; Delgado, M. R.; Vallet-Regi, M. *Chem. Eng. J.* **2008,** *137*, 30.

31. Paul, G.; Heimink, J.; Koller, H. *Chem. Mater.* **2008,** *20*, 5083.

32. Iskandar, F.; Gradon, L.; Okuyama, K. *J. Colloid. Interf. Sci.* **2003,** *265*, 296.

Chapter 4: Preliminary studies on the catalytic oxidation of benzyl alcohol

4. Introduction

The oxidation of alcohols to carbonyl compounds is one of the most widely employed reactions in organic chemistry.[1] Currently, potassium permanganate and potassium dichromate are used in industry as oxidants, but their toxicity, corrosive properties and the fact that stoichiometric amounts of these chemicals are needed have motivated research into cheaper and more environmentally friendly processes, preferably using recyclable catalysts.[2,3] Air, molecular oxygen and hydrogen peroxide are considered clean oxidants and various catalysts using these compounds as oxidants have been developed.[4]

Hanson *et al*. reported the synthesis and application of an 8-quinolinate vanadium complex for the oxidation of various alcohols under mild conditions, using air as oxidant and triethylamine as base.[5] While reaction temperatures were as low as 60°C, the reaction times were typically long, and the solvent that was used, dichloroethane, is not considered environmentally friendly.[6]

Villa *et al*. reported the use of palladium nanoparticles supported on carbon nanotubes for benzyl alcohol oxidation.[7] These catalysts showed high conversion of benzyl alcohol to benzaldehyde at 80°C. The reactions were carried out in a mixture of water and cyclohexane. The catalysts could also be recycled up to seven times without a significant loss in selectivity to benzaldehyde. In contrast to the previously mentioned vanadium catalysts, which used air at ambient pressure as oxidant, the palladium catalysts required molecular oxygen at a pressure of 2 bar in order to obtain good results.

In general, stoichiometric amounts of an appropriate metal are needed for the transformation of an alcohol to its corresponding aldehyde or ketone. The metal is reduced by two oxidative units in the process. Various co-oxidants such as oxygen, hydrogen peroxide and nitroxyl radicals can be used to regenerate the metal to its oxidized state. It is therefore possible to use catalytic amounts of the metal if appropriate co-oxidants are employed. A general overview of this process is shown in Figure 4.1.

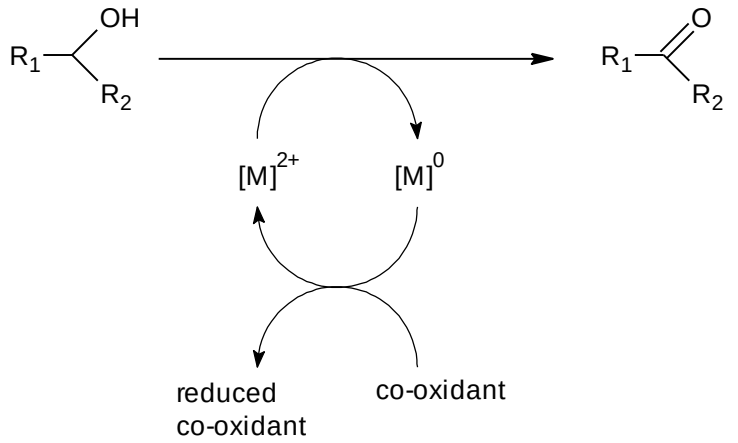

Figure 4.1 General mechanism for the oxidation of an alcohol

4.1 Application of Cu(II) and Pd(II) in oxidation

4.1.1 Application of Cu(II) in oxidation

Copper complexes are commonly used together with stable nitroxyl radicals in alcohol oxidation reactions. This system was first reported by Brackman and Gaasbeek in 1966 who used di-*tert*-butylnitroxyl and a copper(II) phenanthroline complex for the aerobic oxidation of methanol to formaldehyde.[8] In 1984, Semmelhack *et al.* used the radical (2,2,6,6-tetramethylpiperidin-1-yl)oxyl (TEMPO) in combination with cuprous chloride for alcohol oxidation.[9] The exact reaction mechanism of this reaction has been the matter of debate in the literature, with valuable contributions coming from the groups of Semmelhack, Neumann and Stack.[10,11]

Recently, a catalytic cycle based on data available in the literature has been proposed by Sheldon and Arends.[12] The key step in the cycle involves intramolecular hydrogen abstraction within an alkoxycopper(II)/TEMPO complex and is shown in Figure 4.2. The TEMPO is coordinated to the copper in a η^2 fashion. Hydrogen abstraction generates a coordinated ketyl radical anion as well as TEMPOH. Inner-sphere electron transfer then affords Cu(I) and the carbonyl product. Half a mole equivalent of a molecule of oxygen is used to oxidize two molecules of TEMPOH to TEMPO. TEMPO in turn oxidizes Cu(I) back to Cu(II). The full catalytic cycle is shown in Scheme 4.1.

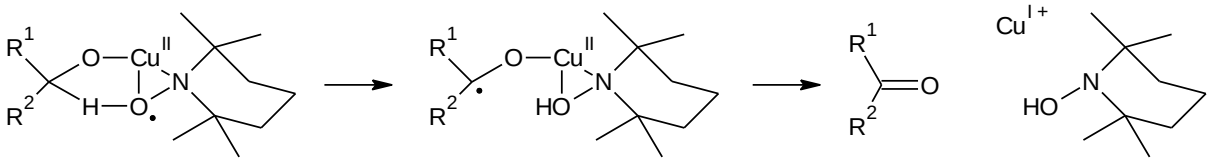

Figure 4.2 Intramolecular hydrogen transfer followed by oxidative elimination

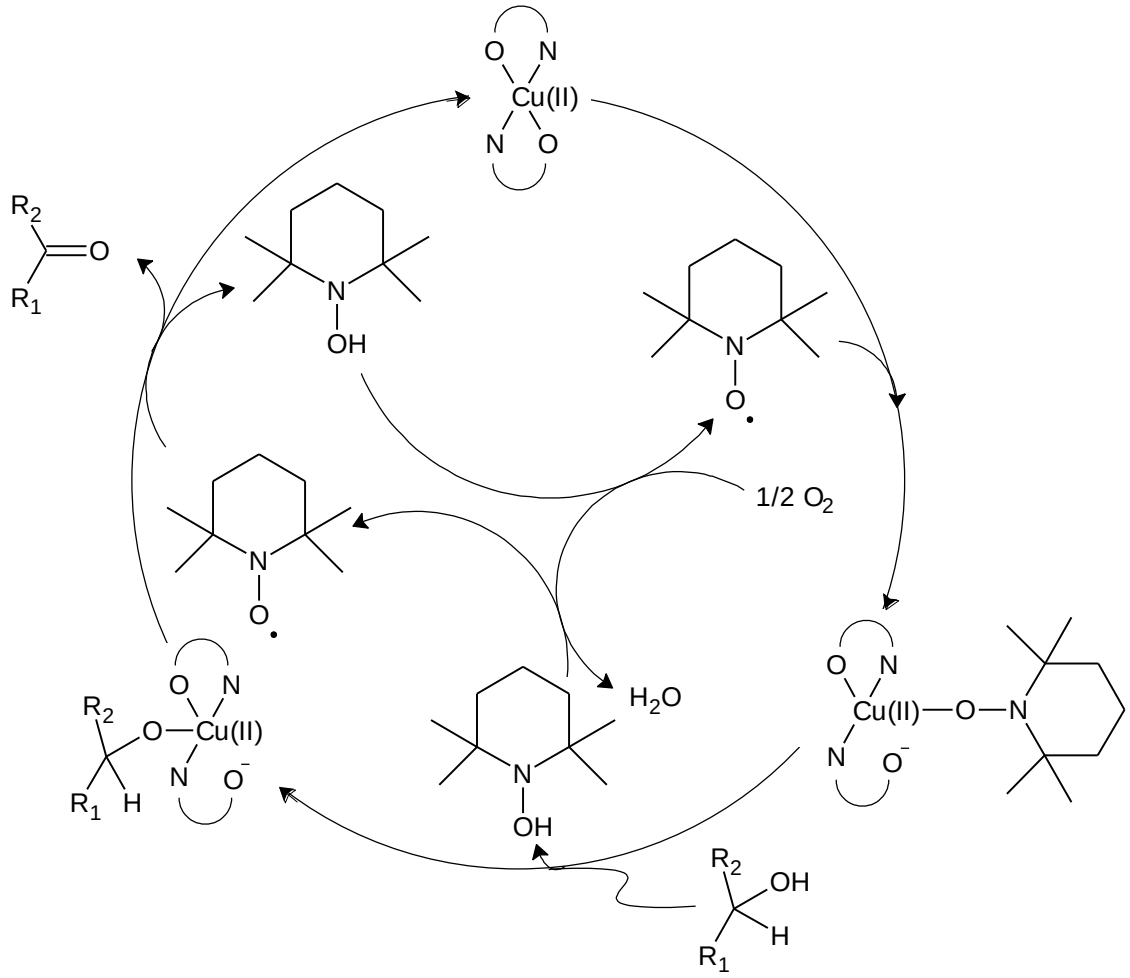

Scheme 4.1 Proposed Cu/TEMPO oxidation mechanism[12, 13]

4.1.2 Application of Pd(II) in oxidation

The groups of Stahl and Muzart have extensively studied the mechanism of alcohol oxidation catalyzed by palladium.[14,15] Schultz *et al*. have studied the effect of different ligands on the mechanism and concluded that the rate-limiting step of the reaction might be altered from β-hydride elimination to deprotonation of the coordinated alcohol by changing the ligand system from $Pd(OAc)_2$/pyridine to $Pd(OAc)_2$/triethylamine.[16] This leads to a catalyst that is active at room temperature.

Oxidation reactions catalyzed by palladium usually contain a dehydrogenation step. Palladium hydride intermediates are formed and are reactivated by H-acceptors. It is not always possible to distinguish between an H-acceptor and a co-oxidant – many co-oxidants such as oxygen and allyl halogens can act as H-acceptors as well. Scheme 4.2 shows a situation where the H-acceptor is situated on the active catalyst. HX is eliminated to form the Pd^0 species, which is again oxidized by the appropriate oxidant to regenerate the active catalyst.

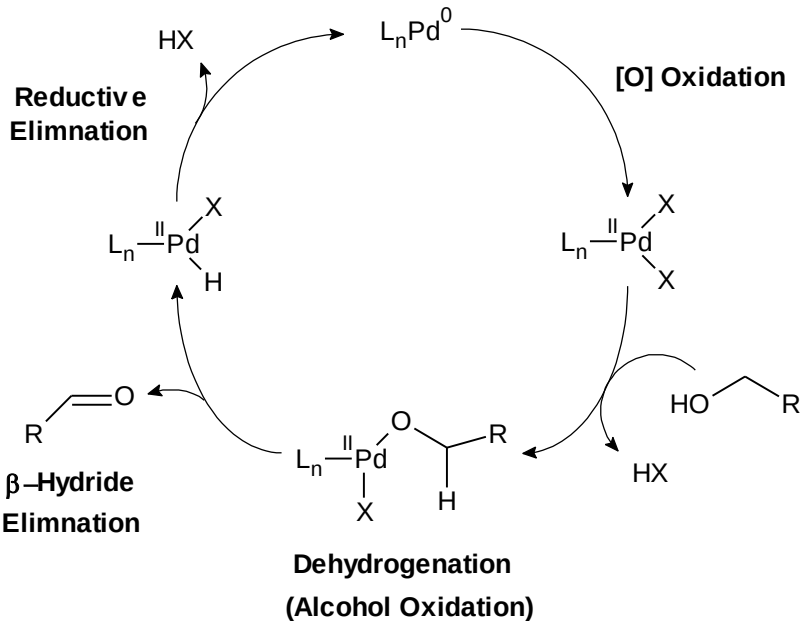

Scheme 4.2 Catalytic cycle for the oxidation of a primary oxygen to its aldehyde by a Pd(II) catalyst[17]

4.2 Complexes used as catalysts

The synthesis and characterization of the model complexes and immobilized catalysts were discussed in Chapter 2 and 3 respectively. Their catalytic activity in the oxidation of benzyl alcohol is evaluated in this chapter.

This preliminary study focuses on the oxidation of benzyl alcohol to benzaldehyde, as it serves as a model reaction for the oxidation for alcohols in general. The complexes shown in Figure 4.3 were evaluated as catalysts. Subsequently, immobilized analogues of these catalysts were evaluated as well and the results were compared to that of their homogeneous counterparts.

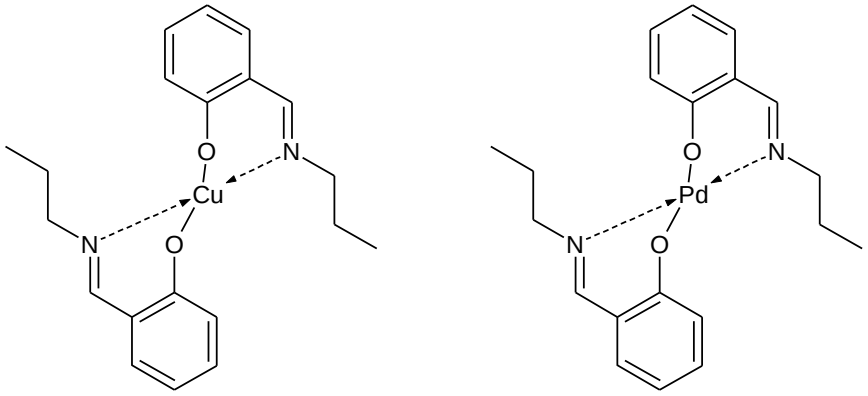

C1 **C3**

Figure 4.3 Model complexes employed in catalysis reactions

4.3 Oxidation of benzyl alcohol by Cu(II) catalyst systems

4.3.1 Oxidation of benzyl alcohol

C1 was used to determine the optimum conditions for the oxidation of benzyl alcohol to benzaldehyde. The procedure followed was adapted from Ahmad *et al.*[13] A generalized reaction scheme is shown in Scheme 4.3. The effects of metal loading, temperature, reaction time and substrate concentration were evaluated by testing complex **C1** under a range of conditions.

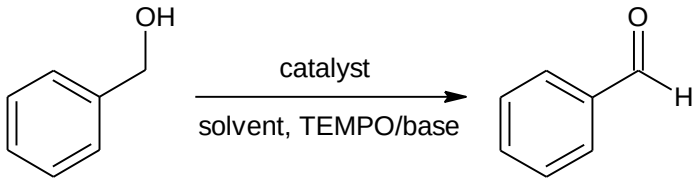

Scheme 4.3 Benzyl alcohol oxidation

4.3.2 Influence of different reaction conditions on catalyst activity

Typical reaction conditions were: 0.996 mmol benzyl alcohol, 0.3 mol% metal, 2 mol% TEMPO, toluene as solvent, 1.5 ml total reaction volume, 100°C, 3 hours under 1 bar oxygen pressure. The catalyst and TEMPO were added from 5 mg/ml solutions in toluene. All solutions and solvents were saturated with oxygen before use. Typically, the catalyst, TEMPO and solvent were added to a reactor tube at room temperature. The reaction was then heated to the appropriate temperature under 1 bar oxygen pressure. The substrate was injected once the appropriate temperature had been reached, and the reaction allowed to continue for the appropriate time.

4.3.2.1 Effect of catalyst system components on conversion

The complete catalyst system consists of three components: the complex, TEMPO, and an oxidant (in this case molecular oxygen). The effect of each of these on the reaction was investigated. A reaction done in the absence of the complex showed 3% conversion after three hours, while the conversion in the absence of TEMPO showed no conversion after three hours. Both these components are therefore essential in the reaction. A reaction was done in the absence of oxygen but in the presence of catalyst, and showed 12% conversion after three hours. This indicates that TEMPO can act as a weak oxidant in the absence of oxygen. A summary of these reactions is shown in Figure 4.4.

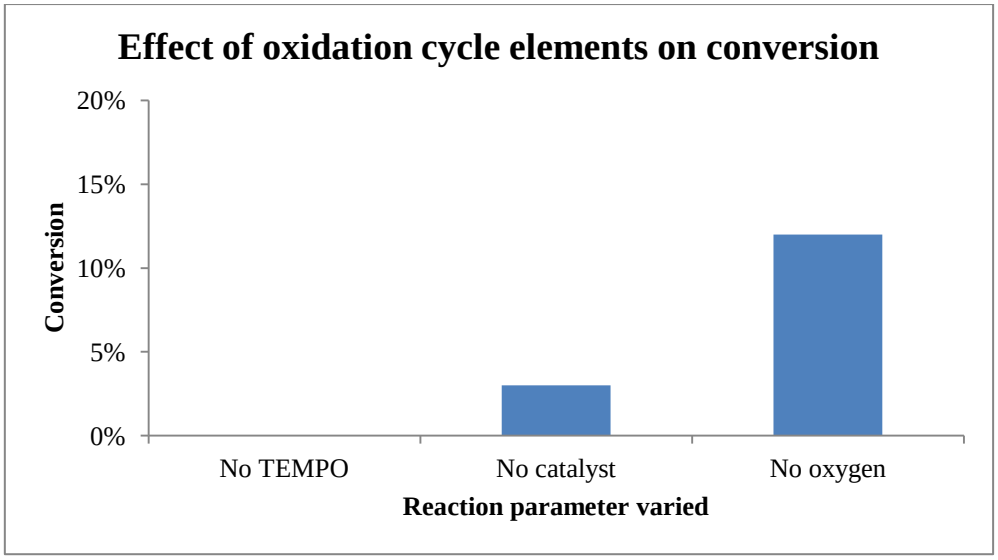

Figure 4.4 Effect of oxidation cycle components on conversion

4.3.2.2 Effect of metal loading on conversion

After it was established that the catalyst, TEMPO and oxygen play a role in the oxidation reaction, the effect of metal loading on the reaction was investigated. Three reactions were set up containing 0.0015, 0.003 and 0.005 mmol Cu(II) respectively (0996 mmol benzaldehyde, 1.5 ml toluene, 0.02 mmol TEMPO, 100°C, 3 hours, 1 bar oxygen pressure).

An increase in the conversion of benzyl alcohol to benzaldehyde was observed as the metal loading was increased, with a reasonable conversion of 68% seen with 0.3 mol%. When 0.5 mol% metal is used, the conversion increases to 86%, as shown in Figure 4.5.

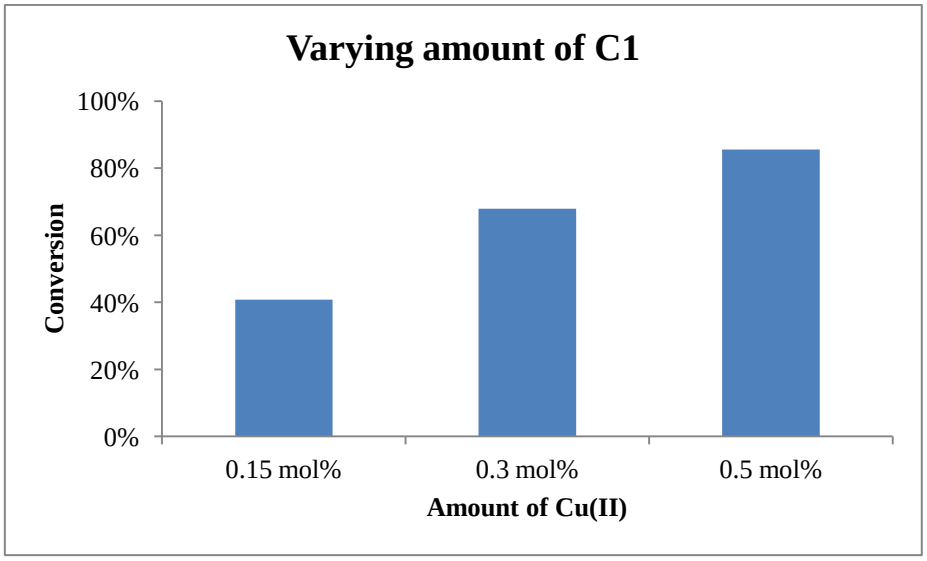

Figure 4.5 Effect of metal loading on conversion

4.3.2.3 Effect of co-oxidant loading on conversion

The amount of co-oxidant in the reaction was varied from 2 mol% as reported by Ahmad *et al*.[13] Three reactions, containing 1 mol%, 2 mol% and 4 mol% respectively, were set up (0.996 mmol benzaldehyde, 1.5 ml toluene, 0.3 mol% catalyst, 100°C, 3 hours, 1 bar oxygen pressure).

The conversion increased slightly as the amount of TEMPO in the reaction increased, although there was not a large difference in the conversion. At 1 mol% TEMPO, the conversion after three hours was 62% and this increased to 67% for 2 mol% and 71% for 4 mol% TEMPO. It was decided that the 4% increase of conversion after doubling the amount of catalyst from 2 mol% was not enough to justify the use of 4 mol%, and the TEMPO loading was kept at 2 mol% for the subsequent reactions. A summary of the results is shown in Figure 4.6.

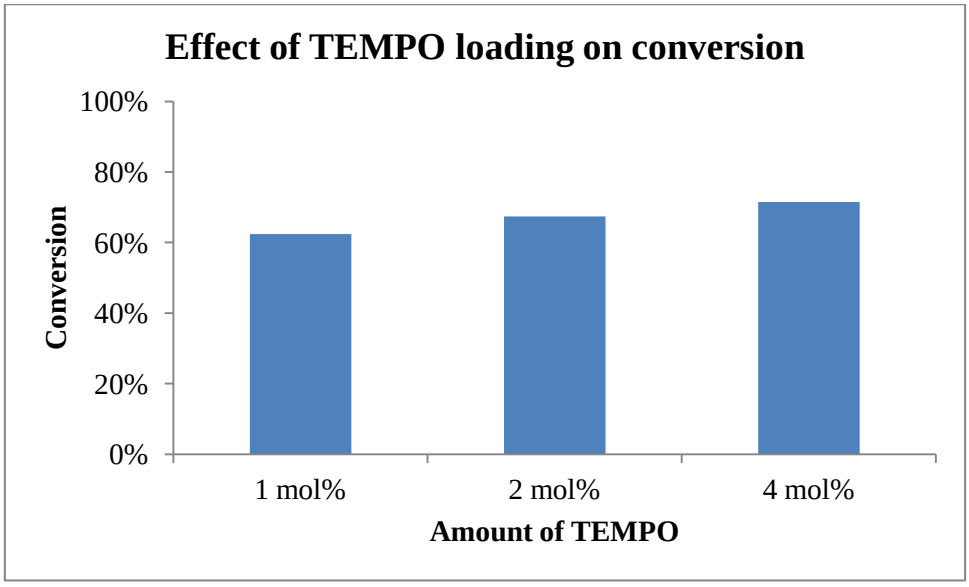

Figure 4.6 Effect of co-oxidant loading on conversion

4.3.2.4 Effect of substrate concentration on conversion

The effect of varying the substrate concentration was studied by keeping the molar amounts of the substrate, catalyst and co-oxidant the same and varying the total solvent volume. Total solvent volumes of 1.5 mL, 5 mL and 10 mL were employed (0.996 mmol benzaldehyde, toluene, 0.3 mol% catalyst, 2 mol% TEMPO, 100°C, 3 hours, 1 bar oxygen pressure). It is known from previous experience that it can be difficult to get the immobilized catalyst into a slurry if the solvent volume is very low, and this experiment was performed to see how higher solvent volumes would influence the reaction.

The conversion rapidly decreased with a decrease in substrate concentration. A conversion of 70% was seen with a solvent volume of 1.5 mL ([substrate] = 0.067 M). This decreased by almost half to 36% when the solvent volume was increased to 5 mL ([substrate] = 0.020 M). For a total solvent volume of 10 mL ([substrate] =0.010 M), the conversion was only 12%. The results for this experiment are summarized in Figure 4.7.

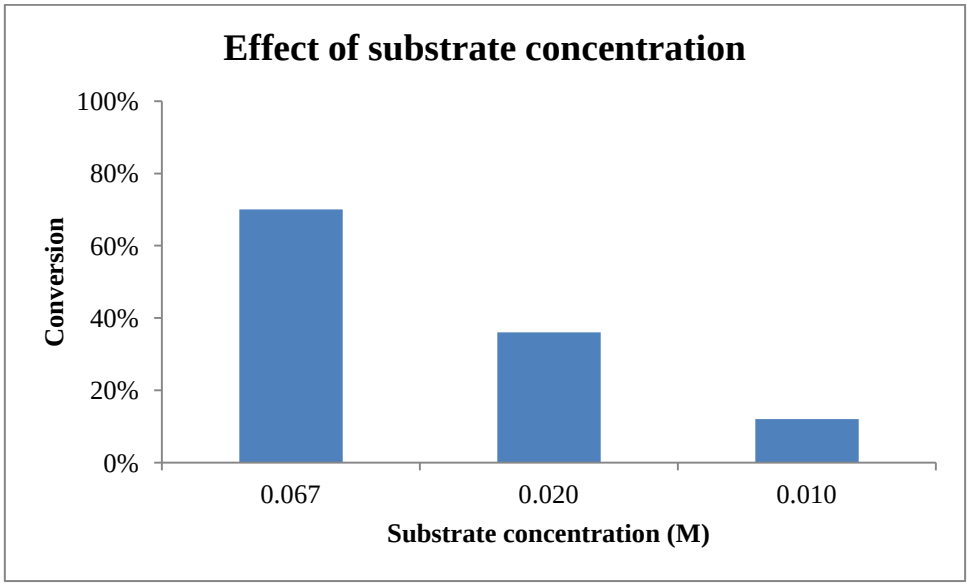

Figure 4.7 Effect of substrate concentration on conversion

Taking these results into account, it was decided that, for the immobilized systems, the substrate concentration should be kept at 0.067 M. The molar amounts of the substrate, catalyst and co-oxidant would be increased along with the solvent volume if necessary.

4.3.2.5 Effect of temperature on conversion

The effect of varying the temperature of the reaction was investigated, since using lower temperatures could be advantageous from an energy point of view. Three different metal loadings (0.0015, 0.003 and 0.005 mmol metal) were used in reactions at temperatures of 50°C, 75°C and 100°C (0.996 mmol benzaldehyde, 1.5 ml toluene, 0.02 mmol TEMPO, 3 hours, 1 bar oxygen pressure).

It was found that conversion at 50°C was very low for all three metal loadings, with only a slight increase with higher metal loading. The conversion increased for all three metal loadings at 75°C, with the conversion for 0.3 mol% and 0.5 mol% being almost similar. At 100°C there was a clear difference between 0.3 mol% and 0.5 mol%, with the highest conversion observed being 86%. These results are summarized in Figure 4.8.

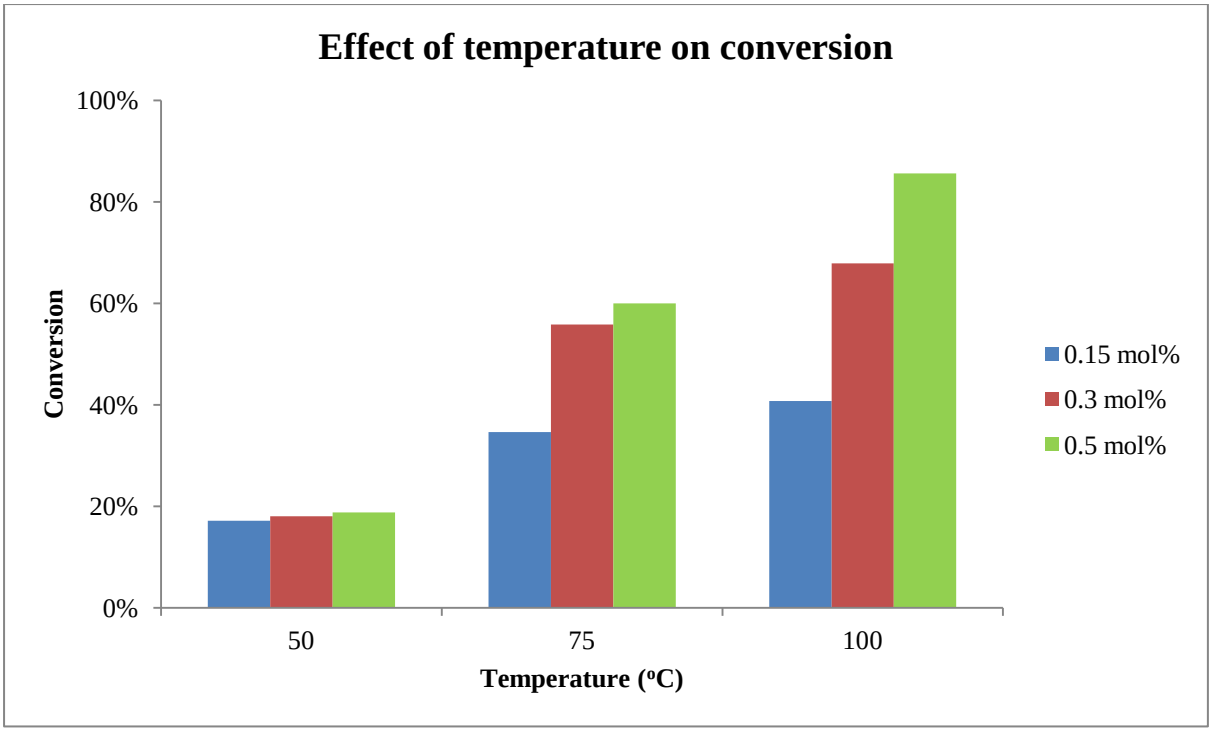

Figure 4.8 Effect of temperature on conversion at different metal loadings

4.3.2.6 Effect of reaction time on conversion

The effect of time on the catalysis reactions was investigated. Three reactions containing different metal loadings were set up (0.15 mol%, 0.3 mol% and 0.5 mol%). Since samples were taken periodically from these reactions, a larger total reaction volume was used. The relative concentrations of all elements of the reaction were kept the same as for the previous reactions. The conditions therefore were: 9.96 mmol benzaldehyde, 15 ml toluene, 2 mol% TEMPO, 100°C, 1 bar oxygen pressure. The results of this reaction are shown in Figure 4.9.

After 20 minutes, the conversion is below 20% for all three metal loadings. After an hour, the conversion for the reactions containing 0.3 mol% and 0.5 mol% increased to almost 40%, while for 0.15 mol% it was just above 20%. After a three-hour period there was a clear difference between the conversions for the three metal loadings, with the conversion for 0.5 mol% being almost 80%. After nine hours, the rate of the conversion starts slowing down for all three metal loadings. The reaction containing 0.5 mol% metal shows complete conversion of benzyl alcohol to benzaldehyde after 30 hours. At this stage the conversion is still increasing for the other two metal loadings.

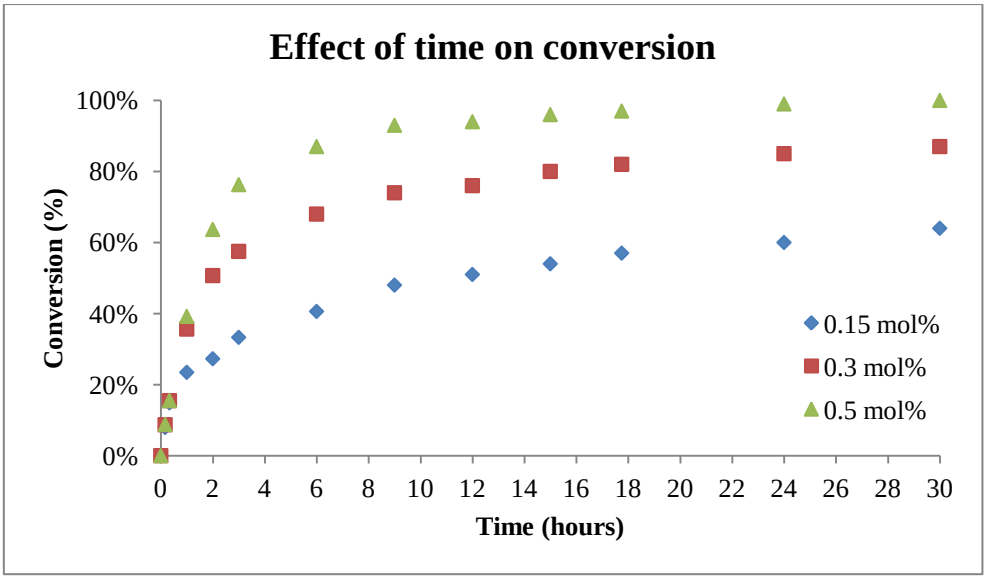

Figure 4.9 Effect of time on conversion at different metal loadings

The activity expressed as turnover frequency (TOF) of these catalysts was calculated in terms of mol product formed per mol catalyst per hour. As expected, the activity is higher when a lower catalyst loading is employed over a short reaction time, with 0.15 mol% metal loading having a TOF of 155 after one hour, compared to a TOF of 78 for 0.5 mol% metal loading. The activity decreases rapidly over time. For a metal loading of 0.15 mol% the TOF after three hours is 75, which is half of the TOF after one hour. After 24 hours the activity is very low with TOFs of under 20, no matter which metal loading is used. This would seem to indicate that catalyst deactivation is occurring over time. A summary of these results is shown in Figure 4.10.

Taking both the conversion and TOF values into account, it was decided that employing 0.3 mol% catalyst in a three hour reaction would be suitable for testing the immobilized catalyst systems.

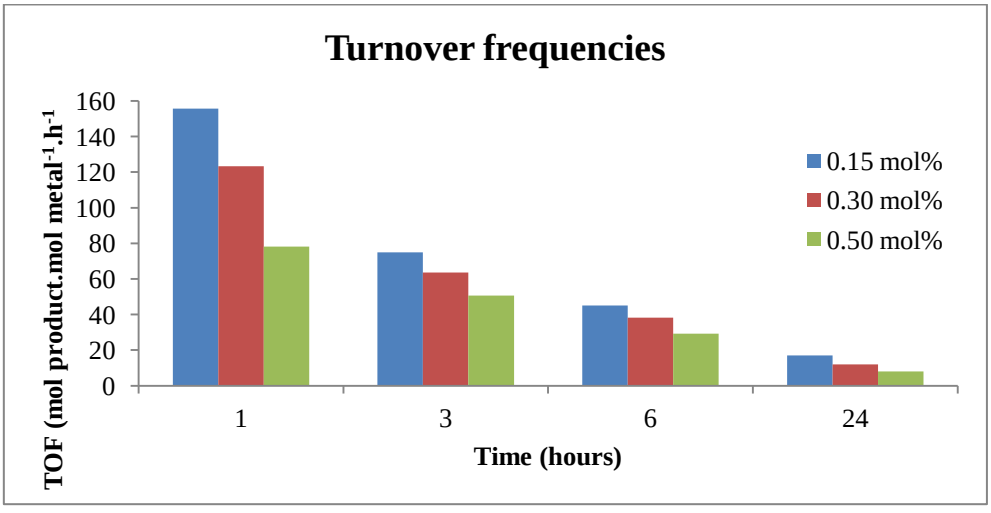

Figure 4.10 Turnover frequencies for different metal loadings at various time periods

4.3.3 Oxidation of benzyl alcohol by immobilized Cu(II) systems

The immobilized catalyst systems were employed as catalysts using the optimum conditions established for the homogeneous system in the previous section. The conditions were: 0.996 mmol benzaldehyde, 1.5 mL toluene, 0.3 mol% metal, 2 mol% TEMPO, 100°C, 3 hours, 1 bar oxygen pressure. The results for the mesoporous silica as well as a control reaction with the model complex can be seen in Figure 4.11.

The immobilized catalyst systems showed no activity when compared to the model complex. The conversion drops from 60% to 3% - as shown in Section 4.3.2.1, the co-catalyst on its own is capable of achieving 3% conversion. A second reaction was done with a higher solvent volume, since it was quite difficult to get all of the immobilized catalyst into a slurry with the solvent volume being 1.5 mL. The total solvent volume for the second reaction was 5 mL. The concentrations of substrate, catalyst and co-oxidant were kept the same as for the previous reaction. Similar results were observed to that obtained in the previous reaction, with the conversion dropping from 55% for the model catalyst to 2% for the reactions containing immobilized catalysts. Again, this is most likely due to the activity of the co-oxidant on its own.

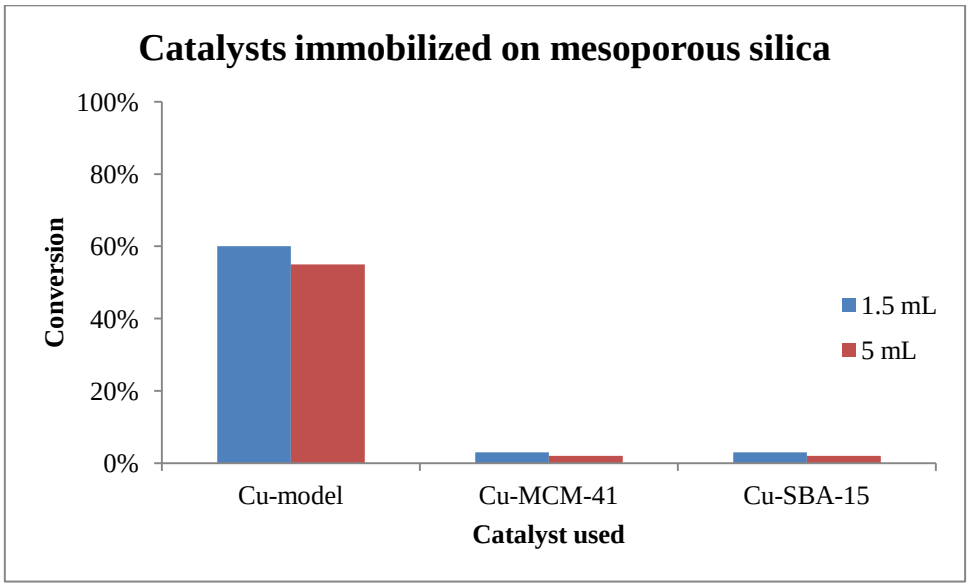

Figure 4.11 Mesoporous catalyst systems tested in benzyl alcohol oxidation

The sol-gel catalyst systems were then tested under conditions similar to those used for the second reaction done with the mesoporous catalyst systems. Two of the sol-gel catalyst systems contain physically encapsulated model copper complexes, with the other two containing functionalized copper complexes where the siloxane functionalities were co-condensed with the silica matrix. One model and one functionalized system was dried using spray-drying in which the solvent is instantly

evaporated. The other two catalyst systems were prepared by drying the silica gel in an oven for a long period of time.

As Figure 4.12 shows, as decrease in conversion is again observed when the sol-gel catalyst systems are compared with the model complex. The sol-gel catalyst systems containing the physically encapsulated model complex shows higher conversion than those where the functionalized complex was incorporated into the silica matrix. This is most likely due to the model complex leaching from the silica. The catalysis observed is therefore most likely as a result of leached metal complex leading to a homogeneous catalyst system instead of catalysis being driven by an immobilized catalyst.

ICP-AES was done to confirm that leaching had taken place. The results show that, for the physically encapsulated systems (M-Cu-spray and M-Cu-oven) between 2 ppm and 5 ppm copper was present in the reaction solution after the silica was filtered off. This represents metal leaching of between 20% and 40%. For the catalysts containing the functionalized complex (F-Cu-spray and F-Cu-oven), the amount of copper present in the reaction solution is much lower – less than 0.7 ppm. These results indicate that it is the homogeneous catalyst that is responsible for the benzyl alcohol oxidation in these systems. The results also show that the functionalized complex is less prone to leaching and is most likely bound to the silica support.

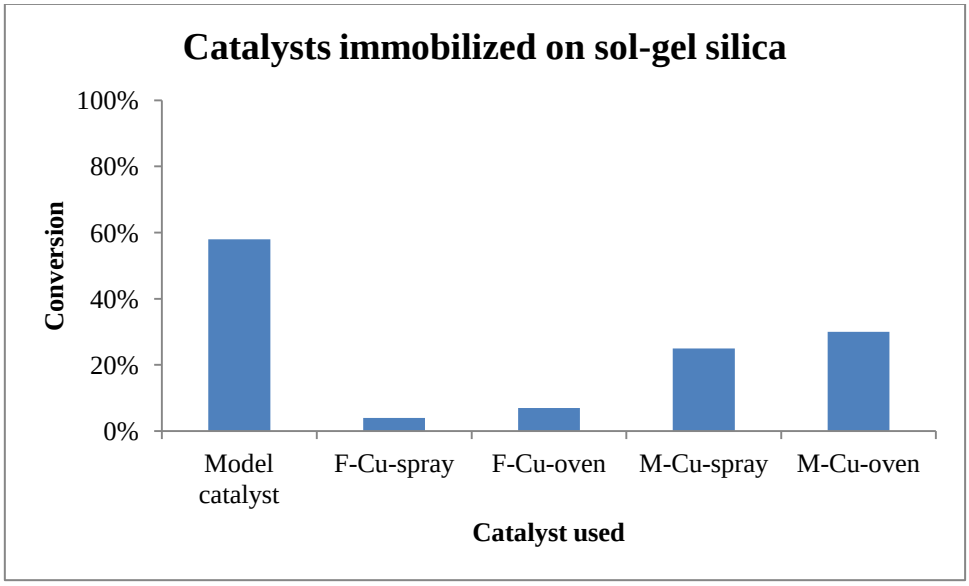

Figure 4.12 Sol-gel catalyst systems tested in benzyl alcohol oxidation

The sol-gel catalysts were filtered off and re-used in the oxidation reaction. The reaction conditions were kept exactly the same. No conversion was seen for this second reaction. It is likely that the metal remaining in the catalyst is encapsulated within the silica and is not accessible for catalysis. These

results, along with the ICP data, indicate that it is indeed the leached metal complex that was responsible for the formation of benzaldehyde in the previous reaction.

There are two possible explanations for the lack of catalytic activity of the heterogenized catalyst systems: The catalyst systems are defective due to changes in the catalyst structure that took place during immobilization which were not observed during characterization, or the reaction mechanism of the alcohol oxidation is impacted negatively as a result of the immobilization. Figure 4.13 shows a key step in the oxidation catalytic cycle of the oxidation reaction which requires both the co-oxidant, TEMPO, and the substrate to be simultaneously coordinated to the metal centre. Given the fact that the metal complex is entrapped in a constrained environment within the silica matrix, it might be difficult for both the substrate and the sterically encumbered TEMPO to effectively coordinate to the metal centre simultaneously. It is assumed that a large portion of the complex is encapsulated within the pores of the mesoporous support and that in this case the metal centre is not accessible to the relatively large TEMPO molecule. The net result of this would be the inability of the reaction to proceed via the accepted mechanism. This hypothesis could possibly be confirmed by surface modelling studies but due to time constraints these studies were not carried out.

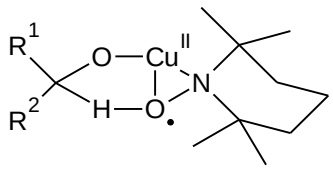

Figure 4.13 Alkoxycopper(II)/TEMPO complex

In order to establish whether the encapsulated complexes maintained their integrity and whether they were able to act as precatalysts, it was decided to test them in phenol hydroxylation using a previously reported procedure for such immobilized catalysts.[18] This was to probe whether the inactivity observed in the TEMPO mediated reactions were due to the process under investigation or catalyst deactivation under the reaction conditions employed. In phenol hydroxylation the co-catalyst is H_2O_2, a much smaller molecule than TEMPO with the result that steric crowding around the active site is expected to be far less.

4.3.3.1 Phenol hydroxylation by immobilized Cu(II) systems

The experimental procedure described by Ray *et al*. was followed, and thus phenol (1 mmol) was added to a parallel reactor tube along with either model or immobilized catalyst (0.01 mmol), and 10 mL of water buffered at a pH of 6.[18] The reaction mixture was heated to 110°C under 1 bar oxygen and 6% H_2O_2 (1 mmol) was added. The reaction was stirred for 6 hours. The results of this reaction is shown in Figure 4.14.

When the model copper complex is employed as catalyst, the phenol conversion is 63%. When the immobilized catalyst systems are used, conversions of 60% and 64% for Cu-MCM-41 and Cu-SBA-15 respectively are obtained. These results correlate well with those reported previously.[18]

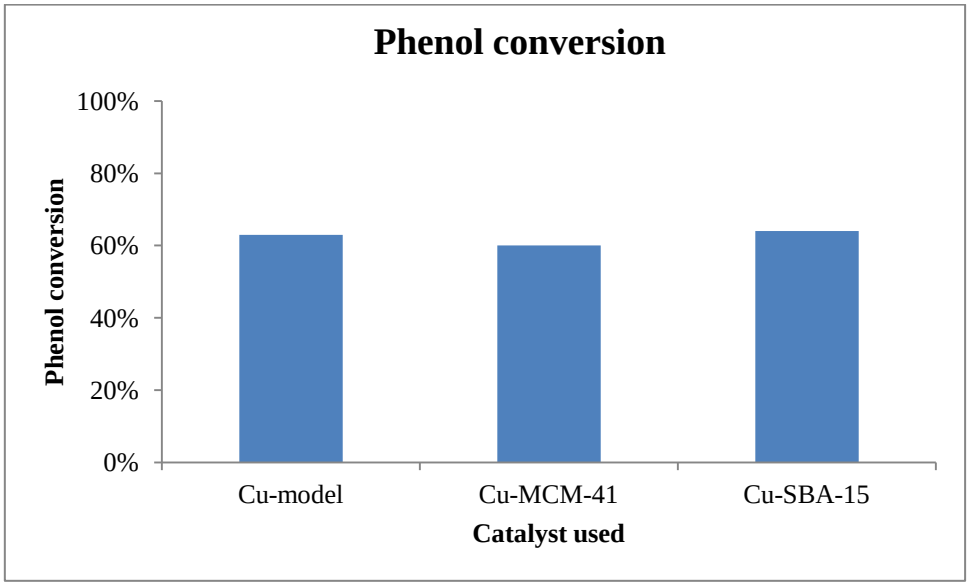

Figure 4.14 Phenol conversion

The results of the phenol hydrogenation reaction show that our heterogenized copper catalyst system is still intact and had not deactivated during the immobilization process. The low conversions obtained for the immobilized catalysts in the benzyl alcohol oxidation reaction are thus most likely due to steric crowding at the support surface.

4.4 Attempted Oxidation of benzyl alcohol by Pd(II) catalyst systems

In order to investigate the activity of the palladium model catalyst for benzyl alcohol oxidation, reaction conditions similar those reported by Choudhary *et al.* for alcohol oxidation by Schiff base palladium complexes were used.[19] K_2CO_3 was employed as base in a 1:1 ratio to the substrate.

Typically, the palladium model complex (0.002 mmol) was added to a reactor tube along with K_2CO_3 (0.996 mmol). Toluene was added to give a total solvent volume of 1.5 mL. The reaction mixture was stirred under 1 bar of oxygen while being heated to 100°C. Once the appropriate temperature was reached, benzyl alcohol (0.996 mmol) was added to the reactor tube and the reaction was left to proceed for 3 hours.

A control reaction without any base showed no conversion of benzyl alcohol to benzaldehyde. When the appropriate amount of base was added, only 2% conversion was observed. An attempt was made to improve the conversion by using a longer reaction time, but the conversion remained at 2%. The metal loading was then increased to 2 mol% to see if this would improve the conversion, as the copper systems showed great sensitivity to metal loading. In the palladium system, however, no improvement was seen, even after 24 hours. A summary of these reactions is given in Figure 4.15.

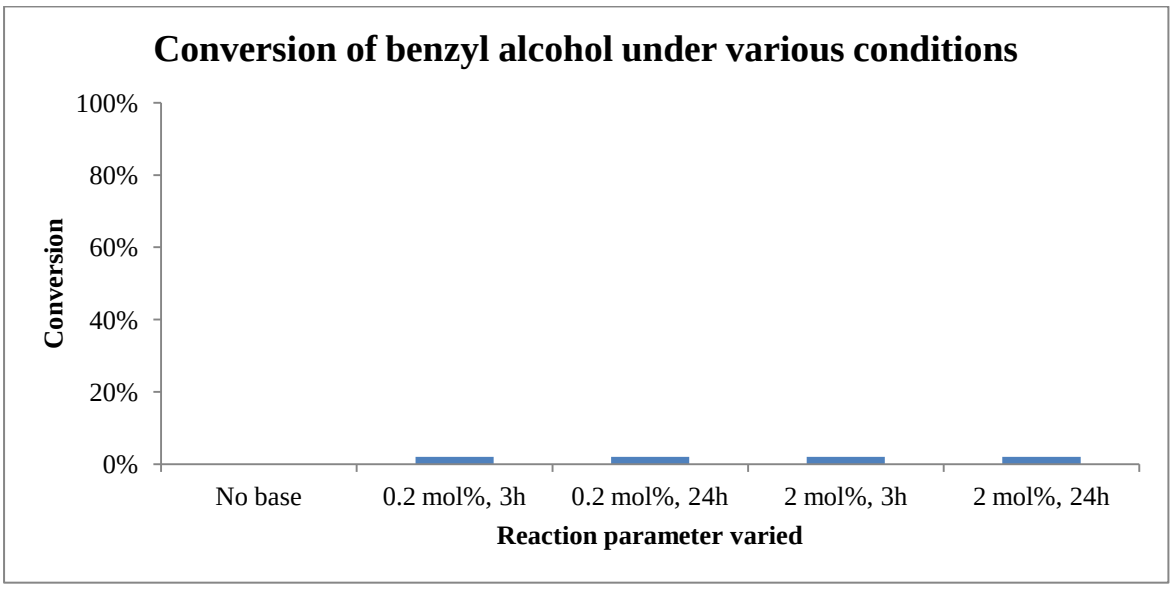

Figure 4.15 Conversion of benzyl alcohol when using palladium model catalyst

Due to time constraints, no further investigation into the palladium catalyst systems was done. The immobilized palladium catalysts were also not investigated. It must be mentioned that most of the palladium complexes used for oxidation in the literature have one or more labile ligands such as chloride or acetate. As shown in Scheme 4.2, one of these ligands undergoes reductive elimination in order to complete the catalytic cycle. The lack of labile ligands in our system might be the cause of the low conversion observed.

4.5 Hydrogen peroxide as oxidant in benzyl alcohol oxidation

Hydrogen peroxide is considered a mild oxidant, along with molecular oxygen and air.[4] We therefore tested our model complex systems using hydrogen peroxide as oxidant. The reactions were carried out at 80°C in 3 mL of acetonitrile under aerobic conditions. Benzyl alcohol (0.996 mmol) was used as substrate and 6% H_2O_2 as oxidant. For the copper complex, metal loadings of 0.15 mol% and 0.30 mol% was used while 0.30 mol% metal loading was employed for the palladium complex.

Initially, 2 mole equivalents of hydrogen peroxide were used per mole substrate. After three hours both copper-containing reactions showed a conversion to benzaldehyde of 18% while the reaction containing the palladium catalyst showed 8% conversion. A further two mole equivalents of hydrogen peroxide was added and after three more hours (six hours in total) the conversion had increased to 42% for the copper-containing reactions and 18% for the palladium-containing reaction. The results are summarized in Figure 4.16.

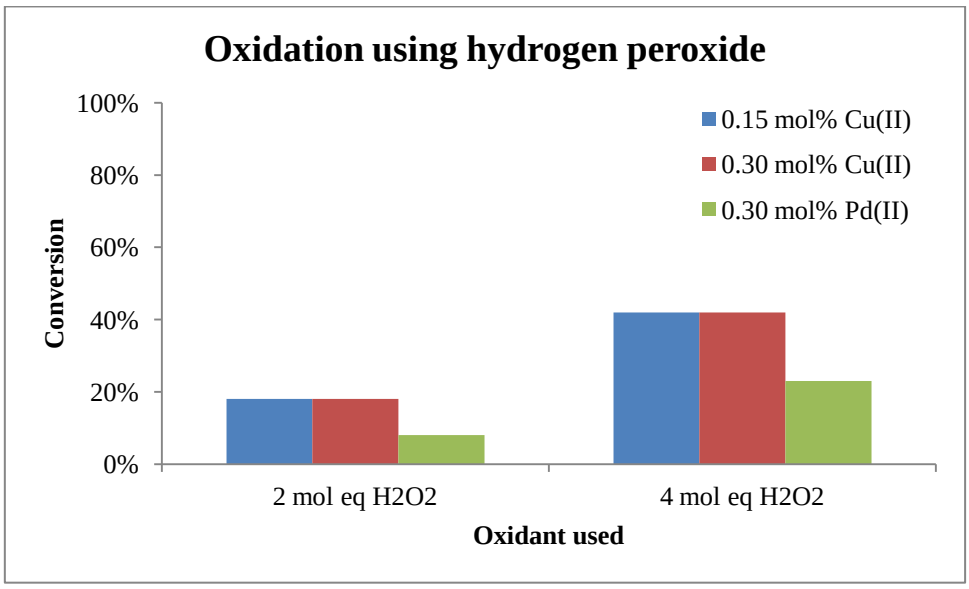

Figure 4.16 Oxidation of benzyl alcohol using hydrogen peroxide as oxidant

Our results show that, for the model copper complex, oxygen is a better oxidant than hydrogen peroxide. The fact that the conversion is the same for the two different metal loadings seems to indicate that the catalyst does not play that big a role in the oxidation reaction. It is also possible that the complex was destroyed during the addition of the hydrogen peroxide. For the palladium complex, hydrogen peroxide is a more promising oxidant than oxygen.

4.6 Concluding remarks

Preliminary studies showed that the Cu(II) complex was quite active for benzyl alcohol under our chosen conditions. The presence of a co-catalyst, TEMPO, was vital for the reaction to occur. Quantitative conversion was observed at 0.5 mol% metal loading after 30 hours.

A dramatic decrease in conversion was observed for the immobilized systems. The mesoporous catalyst systems showed almost no conversion. The conversion for the sol-gel systems was slightly higher; however, this was largely attributed to leaching of the complex.

The Pd(II) complexes showed almost no conversion of benzyl alcohol to benzaldehyde, even at high metal loadings. This was attributed to the lack of labile ligands on the metal centre.

4.7 Experimental section

4.7.1 Methods and instrumentation

All reactions were carried out using a Radley's parallel reactor with a gas distribution system, with the exception of the reaction done in the absence of oxygen described in Section 4.3.2.1 which was carried out under Schlenk conditions. Apart from this reaction, all reactions were carried out under an oxygen atmosphere. Acetonitrile and toluene were dried over 0.3 nm and 0.4 nm molecular sieves respectively. Chemicals were purchased from Sigma-Aldrich and used as received. Oxidation reactions were analyzed on Varian 3900 gas chromatograph with a HP Innowax column. Phenol hydroxylation reactions were analyzed on a Waters 600E HPLC instrument with a 5µ Luna C18 column with dimensions 250 x 4.60 mm. Acetonitrile and water in a 1:1 ratio were used as mobile phase. The filtrate metal content was determined using a Spectro Arcos ICP-OES with a Burgener T2100 and cyclonic spray chamber as nebulizer.

4.7.2 Typical procedure for benzyl alcohol oxidation

4.7.2.1 Cu(II) systems

In a typical oxidation reaction, the required amount of model complex or immobilized catalyst and TEMPO was added to the reaction vessel, followed by the solvent. The model complex and TEMPO were added using 5 mg/mL stock solutions in toluene. All solvents and solutions were saturated with oxygen. The mixture was then stirred under 1 bar oxygen while being heated to the appropriate temperature. Once the temperature was reached, the substrate was added. The reaction was then left to proceed under 1 bar oxygen for the appropriate period of time. After the allotted time, 0.05 mL samples were taken for analysis by gas chromatography. In the case of the immobilized catalyst systems, the reaction mixture was filtered through a 0.45 µm syringe filter before sampling. *p*-Xylene was used as internal standard.

4.7.2.2 Pd(II) systems

In a typical oxidation reaction, the required amount of model complex and K_2CO_3 was added to the reaction vessel, followed by the solvent. The model complex was added using 1 mg/mL stock solutions in toluene. All solvents and solutions were saturated with oxygen. The mixture was then stirred under 1 atm oxygen while being heated to the appropriate temperature. Once the temperature was reached, the substrate was added. The reaction was then left to proceed under 1 atm oxygen for

the appropriate period of time. After the allotted time, 0.05 mL samples were taken for analysis by gas chromatography. *p*-Xylene was used as internal standard.

4.7.2.3 Hydrogen peroxide as oxidant

In a typical oxidation reaction, the required amount of model Cu(II) or Pd(II) complex and benzyl alcohol (0.996 mmol) were added to the reaction vessel, followed by the solvent. The model complexes were added using 5 mg/mL stock solution in acetonitrile. All solvents and solutions were saturated with oxygen. The mixture was then stirred under aerobic conditions while being heated to the appropriate temperature. Once the temperature was reached, the hydrogen peroxide was added. The reaction was then left to proceed for the appropriate period of time. After the allotted time, 0.05 mL samples were taken for analysis by gas chromatography. *p*-Xylene was used as internal standard.

4.7.3 Typical procedure for phenol hydroxylation

In a typical phenol hydroxylation reaction, the required amount of phenol (1 mmol) and catalyst (0.01 mmol metal) was added to the reaction vessel, followed by 10 mL of water buffered at a pH of 6 (K_2HPO_4/NaOH buffer). The reaction was then stirred under 1 bar oxygen while being heated to 110°C. Once the temperature was reached, 6% H_2O_2 (1 mmol) was added. The reaction was then left to proceed for 6 hours. After the allotted time, the sample was filtered through a 0.45 µm syringe filter, diluted 100 times with acetonitrile and analyzed by HPLC. Acetonitrile and water in a 1:1 ratio were used as mobile phase. External calibration curves were used to calculate the conversion.

4.8 References

1. Hudlicky, M. *Oxidations in Organic Chemistry;* American Chemical Society: Washington, DC, 1990.

2. Figiel, P. J.; Kopylovich, M. N.; Lasri, J.; da Silva, M. F. C. G.; da Silva, J. J. R. F.; Pombeiro, A. J. L. *Chem. Commun.* **2012,** *46,* 2766.

3. Sheldon, R. A.; Arends, I. W. C. E.; ten Brink, G.; Dijksman, A. *Acc. Chem. Res.* **2002,** *35,* 774.

4. Matsumoto, T.; Ueno, M.; Wang, N.; Kobayashi, S. *Chem. Asian. J.* **2008,** *3,* 196.

5. Hanson, S. K.; Wu, R.; Silks, L. A. *Org. Let.* **2011,** *13,* 1908.

6. Alfonsi, K.; Collberg, J.; Dunn, P. J.; Fevig, T.; Jennings, S.; Johnson, T. A.; Kleine, H. P.; Knight, C.; Nagy, M. A.; Perry, D. A.; Stefaniak, M. *Green Chem.* **2008,** *10,* 31.

7. Villa, A.; Wang, D.; Dimitratos, N.; Su, D.; Trevisan, V.; Prati, L. *Catal. Today* **2010,** *150,* 8.

8. Brackman, W.; Gaasbeek, C. J. *Recl. Trav. Chim. Pays-Bas* **1966,** *85,* 257.

9. Semmelhack, M. F.; Schmid, C. R.; Cortes, D. A.; Chou, S. C. *J. Am. Chem. Soc.* **1984,** *106,* 3374.

10. Semmelhack, M. F.; Schmid, C. R. . C. D. A. *Tetrahedon Lett.* **1986,** *27,* 1119.

11. Wang, Y.; DuBois, J. L.; Hedman, B.; Hodgson, K. O.; Stack, T. D. P. *Science* **1998,** *279,* 537.

12. Sheldon, R. A.; Arends, I. W. C. E. *Adv. Synth. Catal.* **2004,** *346,* 1051.

13. Ahmad, J. U.; Figel, P. J.; Raisanen, M. T.; Leskela, M.; Repo, T. *Appl. Catal. A-Gen.* **2009,** *371,* 17.

14. Stahl, S. S. *Angew. Chem. Int. Ed.* **2004,** *43,* 3400.

15. Muzart, J. *Tetrahedron* **2003,** *59,* 5789.

16. Schultz, M. J.; Adler, R. S.; Zierkiewicz, W.; Privalov, T.; Sigman, M. S. *J. Am. Chem. Soc.* **2005,** *127,* 8499.

17. Sigman, M. S.; Schultz, M. *J. Org. Biomol. Chem.* **2004,** *2,* 2551.

18. Ray, S.; Mapolie, S. F.; Darkwa, J. *J. Mol. Catal. A-Chem.* **2007,** *267,* 143.

19. Choudhary, D.; Paul, S.; Gupta, R.; Clark, J. H. *Green Chem.* **2006,** *8,* 479.

Chapter 5: Concluding Remarks and Suggestions for Future Work

5.1 Concluding remarks

Chapter one of this thesis provides an overview on the process of heterogenization of catalysts onto solid supports. The focus is on the covalent bonding of metal complexes to mesoporous silica. MCM-41 and SBA-15 are identified as excellent support materials due to their high surface area, pore sizes, regular arrangement of pores and high concentration of silanol groups on the silica surface. The oxidation of alcohol with mild oxidants such as hydrogen peroxide and molecular oxygen is identified as our target reaction. Various metal complexes that have been used for alcohol oxidation are discussed. Copper and palladium complexes with Schiff base ligands are well suited for our purpose as these ligands can be easily modified to include an ethoxysilane group which can bind the complexes covalently to the silica supports.

In **Chapter two** the synthesis of two different model and functionalized ligands is described. These ligands were characterized using FT-IR and ^{1}H-NMR. Cu(II) and Pd(II) complexes of these ligands were then prepared. The Cu(II) salicylaldimine complexes were characterized using FT-IR, EPR and UV-VIS spectroscopy while the Pd(II) salicylaldimine complexes were characterized using FT-IR, ^{1}H-NMR and ^{13}C-NMR spectroscopy. The characterization data proved that these complexes were successfully synthesized. The Cu(II) complexes of the diimine ligands were characterized using FT-IR spectroscopy and it was found that binding to the metal took place only through the nitrogen atom on the pyridine rings. A variety of copper salts were tested in this reaction, but the diimine Cu(II) complexes could not be isolated.

The synthesis of two different silica supports, MCM-41 and SBA-15 is discussed in **Chapter three**. These materials were synthesized using literature methods and characterized by a variety of solid-state techniques. The functionalized complexes were then immobilized onto the supports and the heterogenized catalyst systems were characterized using nitrogen adsorption analysis, powder X-ray diffraction, thermogravimetric analysis, scanning electron microscopy and ICP-AES analysis. Through these techniques we were able to establish that the complexes had been immobilized onto the silica without destabilizing the supports. Sol-gel catalyst systems were also prepared making use of two different drying methods. The model copper complexes were physically encapsulated within the silica matrix while the functionalized complexes were co-condensed with the silica. These catalyst systems were characterized using scanning electron microscopy and ICP-AES.

In **Chapter four** the use of the complexes as benzyl alcohol oxidation catalysts is disucssed. The model Cu(II) compound was found to be an active catalyst at reasonably low metal loadings, using molecular oxygen as oxidant and (2,2,6,6-Tetramethylpiperidin-1-yl)oxyl as co-oxidant. The immobilized catalyst systems were not active for the benzyl alcohol oxidation reaction, but were found to catalyse the hydroxylation of phenol. The lack of activity in the alcohol oxidation reaction was attributed to steric hindrance around the active site due to the entrapment of the complex within the silica matrix. This may have hindered the formation of a key intermediate in the Cu(II)/TEMPO oxidation cycle. The model Pd(II) complexes were found to be not active in the oxidation of benzyl alcohol with oxygen as oxidant, but shows some promise when hydrogen peroxide is employed as oxidant.

5.2 Suggestions for future work

In Chapter one, it was briefly mentioned that our current approach to tethering the complex to the silica surface imposes some limits on the nitrogen donor ligands that can be used. Different approaches to tethering should be explored. One system that looks promising is the formation of a macrocyclic tetradentate ligand (N,N,O,O) with a free hydroxyl group. This ligand could then be further functionalized via the hydroxyl group to incorporate a siloxane functionality.

As mentioned in Chapter four, the reason for the low activity of the immobilized catalysts may be steric crowding on the surface of silica. Surface modelling studies could be carried out in order to gain better insight into what exactly is happening at the silica surface during the oxidation reaction. Surface modelling can also be used to determine whether the complexes are immobilized on the outer surface of the silica or inside of the pores.

Different ligands systems for the palladium complexes should be explored. Instead of using a N,O chelating ligand, a N,N chelating ligand systems could be employed. The steric bulk of the ligands could also be varied and substituents with different electronic effects could be studied.